Aalto University
School of Engineering

Aalto University
School of Engineering
Department of Applied Mechanics
Nordic Master Programme in Maritime Engineering

Zheng Xing

RESPONSE AND STRUCTURAL ANALYSIS OF A FLAP-TYPE WAVE ENERGY CONVERTER IN A COMBINED WIND AND WAVE CONCEPT

Master's thesis for the degree of Master of Science in Technology submitted for inspection, Espoo, 2 September, 2014.

Supervisor **Professor Pentti Kujala**

Instructors **Professor Jerzy Matusiak**
Adjunct Associate Professor Zhen Gao (NTNU)

Aalto University
School of Engineering

Aalto University, P.O. BOX 11000, 00076
AALTO
www.aalto.fi

Abstract of master's thesis

Author Zheng Xing

Title of thesis Response and Structural Analysis of a Flap-type Wave Energy Converter in a Combined Wind and Wave Concept

Department Department of Applied Mechanics

Professorship Maritime Engineering **Code of professorship** Kul-24

Thesis supervisor Professor Pentti Kujala

Thesis advisors Professor Jerzy Matusiak, Adjunct Associate Professor Zhen Gao

Date 02.09.2014 **Number of pages** 17+90+51 **Language** English

Abstract

In this thesis, the novel combined wind turbine and wave energy device, named Semi-submersible Flap Combination (SFC), is studied in terms of supporting arm strength of Wave Energy Converters (WECs) and produced power by WECs.

Currently most offshore wind turbines are installed in shallow water up to 50-meter's water depth. However more steady and higher density wind is found in far offshores. In this case, floating platforms have to be used. But there are a lot of problems in designing, constructions and installations. More importantly, the cost is very high for commercialization. On the other hand, projects of WECs have been carried out around the world in the last decade in order to make use of wave energy. The combined concept is come up with in order to produce more power in one single production tool, or multi-use platform to be more cost effective. So the SFC concept has been developed under this background.

The SFC consists of one Semi-submersible and three WECs. A comprehensive time domain simulations considering representative stochastic wind-sea states are carried out for both the SFC model and the Bottom-Fixed Wave Energy Converters (BFWEC) in the simulation tool SIMO/RIFLEX/AeroDyn. Some theories behind the simulation tool are reviewed before going into simulations. The pitching natural period of BFWEC is evaluated in Worksheet and decay curve simulation in SIMO/RIFLEX. Natural periods between 14s and 15s are got. The Ultimate Limite States (ULS) strength check is made for the supporting arms of WECs in both operational condition and survival condition according to the NORSOK Standard N004. Utility Factor (UF) is introduced to give a consistent and intuitive result. Comparisons between BFWEC and WECs of SFC are made in terms of UFs. The design for supporting arms are safe and reliable in terms of the design given in this thesis. The last part is calculating produced power by WECs. There are some differences between the BFWEC and WECs of SFC in producing power. Some conclusions are made in the end.

Keywords Semi-submersible Flap Combination (SFC), Wave Energy Converters (WECs), SIMO/RIFLEX/AeroDyn , Strength check, Utility Factor (UF), Produced power

Preface

This thesis presents the work done for the Master Thesis in the Nordic Master Programme in Maritime Enegineering, Ocean Structure track. The first year of my master study was spent in AALTO University, Finland. I spent the second year in Norwegian University of Science and Technology (NTNU), Norway. This thesis has been carried out individually in the Spring of 2014, lasting to the end of August of 2014 in NTNU. My supervisors are Prof. Torgeir Moan from NTNU, Prof. Jerzy Matusiak from AALTO University, and my co-supervisors are Adjunct Associate Professor Zhen Gao from NTNU and Post Doc. Constantine Michailides from NTNU.

The novel concept of Semi-submersible Flap Combination (SFC) combines a floating wind turbine and Wave Energy Converters (WECs) to produce more power and be more cost effective. Comprehensive simulations are carried out for the SFC model and Bottom-Fixed Wave Energy Converter (BFWEC) model in SIMO/RIFLEX/AeroDyn. The main aims are to make Ultimate Limit States (ULS) strength check for supporting arms of WECs according to the NORSOK Standard N004 and calculate produced power by WECs.

In the fall of 2013, ULS strength check is carried out to the BFWEC in operational condition. The following work extends to this thesis's contents. It gives me a very complete study and recognization on WECs used for new ocean structures.

Otaniemi, Finland
2014-08-29

Zheng Xing

Acknowledgment

With this thesis done, it means I am going to end with a new start in my life. There are so many great people giving me help during these years, I would like to thank them all sincerely and gratefully.

First of all, I would like to thank Prof. Torgeir Moan for giving me this opportunity to finish my master thesis under his supervision. This topic is very exciting and challenging, it drives me to learn a lot. Secondly I would like to give my thanks to my co-supervisor Adjunct Associate Professor Zhen Gao, he gives me many helps and suggestions on my topic. His smartness and erudition give me much impression. My co-supervisor Post Doc. Constantine Michailides, who is always with me helping me from the beginning to the end of my thesis, has given me many detailed comments and instructions, I am so grateful for his time, patience and kindliness. I want to say thank you so much. Dr. Luan Chengyu has helped me a lot on my modelling and analysis, I am so thankful for all the help from him. Besides, I want to express my gratitude and thanks to my supervisor in AALTO University, Prof. Jerzy Matusiak. He is so benevolent and always caring about my thesis process and my study. His comments polish this thesis to much extent. His lectures are so interesting and vivid. Thank you all my supervisors and co-supervisors.

I have to give my special thanks to Prof. Pentti Kujala from AALTO University for giving me opportunites to do researching in ship laboratory. He is so humorous and kind. Also I would like to thank our Project Manager Jakub Montewka and Dr. Floris Goerlandt. I have had a very nice time with them and learn a lot, I feel very honoured to be a member of our team. I also want to give my thanks to all the LRK's fellows, they are so gorgeous and nice.

In Finland and Norway, I have met many good friends and great people. They help me a lot in my study and life, and we have had a very wonderful time together. I also want to express my thanks to my old good friends who are millions of miles away from me. Thank them for all these years' accompanying and encouragement.

In the end, I want to thank my families. Gratitude is given to my uncles Li Zhongqiang and Tang Bing, my aunts Zheng Shifei , Zheng Shishu and Luo Yingquan, my grandmother Lin Wenchao, my brothers Li Xianhua and Zheng Xinghua, my sister Luo Shijiao. Much tearful gratitude and love are given to my beloved father Zheng Shiguo and mother Li

Shizhen, thank my parents for their love and sacrifice.

There are many people that I don't mention, but I am so grateful and thankful to all of them. Thank all the good people for their kindliness, love, care.

Contents

Acronyms

BBDB	Backward Bent Duct Buoy
BFWEC	Bottom-Fixed Wave Energy Converter
FMUF	Final Maximum Utility Factor
MARINA	Marine Renewable Integrated Application
MRE	Marine Renewable Energy
MUF	Maximum Utility Factor
OWC	Oscillating Water Column
PTO	Power Take-Off
SFC	Semi-submersible Flap Combination
SSG	Sea Slot-cone Generator
UF	Utility Factor
ULS	Ultimate Limit States
WEC	Wave Energy Converter
WWEA	World Wind Association

List of Symbols

C	Damping coefficient
C_M	Frequency-dependent mass matrix
D	Cylinder diameter
D_1	Linear damping matrix
D_2	Quadratic damping matrix
E	Wave energy stored in a horizontal square meter of wave
H	Wave height
Hs	Wave significant height
K	Hydrostatic stiffness matrix
M	Frequency-dependent mass matrix
M_{Rd}	Limited bending moment
M_{Sd}	Design bending moment
$M_{T,Rd}$	Limited torsional moment
$M_{T,Sd}$	Design torsional moment
N_{Sd}	Design tensile force
$N_{t,Rd}$	Limited axial strength
P	Produced power by WEC
P_T	Transported energy per meter width of wave front
R^D	Damping force
R^E	External force
R^I	Inertia force

R^S	Internal structural reaction force
T_E	Wave energy period
T_d	Damped natural period
T_n	Pitching natural period of BFWEC
Tz	Zero crossing wave period
V	Wind velocity
V_B	Body velocity
V_{Rd}	Limited shear force
V_{Sd}	Design shear force
V_w	Wave velocity
β	Form parameter
$\ddot{r}$	Structural acceleration
δ	Logarithmic decrement
$\dot{r}$	Structural velocity
γ	Peakedness parameter
λ	Wave length
ω	Wave frequency
ω_R	Rotational velocity
ω_d	Damped natural frequency
ω_n	Pitching natural frequency of BFWEC
ω_p	Peak frequency
ϕ	Wave velocity potential
ρ	Water density
σ	Spectral parameter
θ	Wave direction
ζ	Wave elevation, damping ration
ζ_a	Wave amplitude
a_1	Horizontal undisturbed fluid acceleration
c_g	Velocity of wave front
f	Vector function

g	Acceleration of gravity
k	Wave number, stiffness
m	Mass
p	Water pressure
p_a	Atmospheric pressure
q	Exciting force vector
$q^{(1)}_{(WA)}$	First-order wave excitation force
$q^{(2)}_{(WA)}$	Second-order wave excitation force
q_{CU}	Current drag force
q_{WI}	Wind drag force
q_{ext}	Other wave excitation forces
r	Structural displacement
u	Horizontal undisturbed fluid velocity
x	Position vector
z	Water depth

List of Figures

List of Tables

Chapter 1

Introduction

1.1 Background

Energy is always a big issue for human society. Traditionally oil and gas play a dominant role in energy consumption. Since they are non-renewable and many environmental problems arise, such as water pollution and greenhouse effects, much attention has been drawn to renewable energy and oceans just have abundant sources of it, majority of which still remains to be explored and utilized. Energies of winds, waves and currents come from the broad oceans. They are renewable, clean and abundant. According to World Wind Energy Association (WWEA, 2014) , world wind energy capacity has increased from 280000 MW in 2012 to 32000 MW by the end of 2013. It almost equals 4% of the global electricity power consumption. Waves are caused by winds when blowing along the water surface. The global wave energy is about 100 EJ/yr, that is 32,000 TWh theoretically, but only less than 20% can be made use of because of efficiency and technology. The average energy for a sinusoidal wave with height H stored in a horizontal square meter can be expressed as

$$E = \frac{1}{8}\rho g H^2, \tag{1.1}$$

where

ρ is water density,

g the acceleration of gravity,

H wave height.

The transported energy per meter width of wave front is measured by

$$P_T = c_g E = \frac{1}{32\pi}\rho g^2 H^2 T_E, \tag{1.2}$$

where

c_g is velocity of wave front,

T_E wave energy period.

It can be simplified in deep water by

$$P_T \approx H^2 T_E. \tag{1.3}$$

So a power of 450 kW/m is expected in the wave with a significant height $H = 6m$ and wave energy period $T_E = 12.6s$. The wave energy density is evaluated to be five times of the wind energy density. Although it cannot compete with wind energy now, it has a great market potential for future energy demand and more and more industries and governments are interested in it. Offshore wind and wave energies are widely recognized as sources of replacements for oil and gas.

Nowadays many offshore wind turbines are designed to withstand large loads from winds and waves, and corrosive problems are also in consideration for dozens of years' service period. Most of them are installed in a relatively shallow water depth, ranging from 10 meters to 50 meters. These water areas are very limited for some coastal countries, like China, Norway, US, Japan and so on. However, wind energy is more intensive and steady in deep water. More and more attention has been drawn to far offshore districts. Explorations of deep water have come up with new challenges for designs, installations and maintenances which lead to a significant higher cost. One potential solution is to develop large rated wind turbines and another one is to combine wind energy and wave energy in a single production tool—multi-use combined floating platform.

Varieties of offshore wind turbines are being designed to adapt to different sea depths and the characteristics of them are various. The sea depth is divided into three distinct zones (Roddier et al., 2011): shallow water (less than 20 meters), transitional zone (be-

tween 20 meters and 50 meters) and deep water (more than 50 meters) as shown in Figure 1.1. Fixed-bottom structures are economically suitable for shallow and transitional zones. Currently most offshore wind turbines are based on bottom-mounted substructures in shallow water depth. Jackets and tripod structures are suitable for deeper water depths, even up to 50 – 60 meters. Floating wind turbines are emerging for the demand of going into deep seas. Three floating support platforms for wind turbines, including tension leg platform, spar buoy and barge, have been investigated by Jonkman and Matha (2011) and the following dynamic responses are discussed: impacts from the dynamic coupling effects between the turbine and floating hull, the platform motions, stability, ultimate and fatigue loads. These aspects are all the important factors that have to be considered and designed in very careful manners. For water depth larger than 100 meters, floating wind turbines will be the most economical type to utilize. Semi-submersible wind turbine is the one that will be investigated in this thesis, it is the hull that is used to install WECs on for the Semi-submersible Flap Combination (SFC) (Luan et al., 2014a), but the focus will be on the Wave Energy Converters (WECs) .

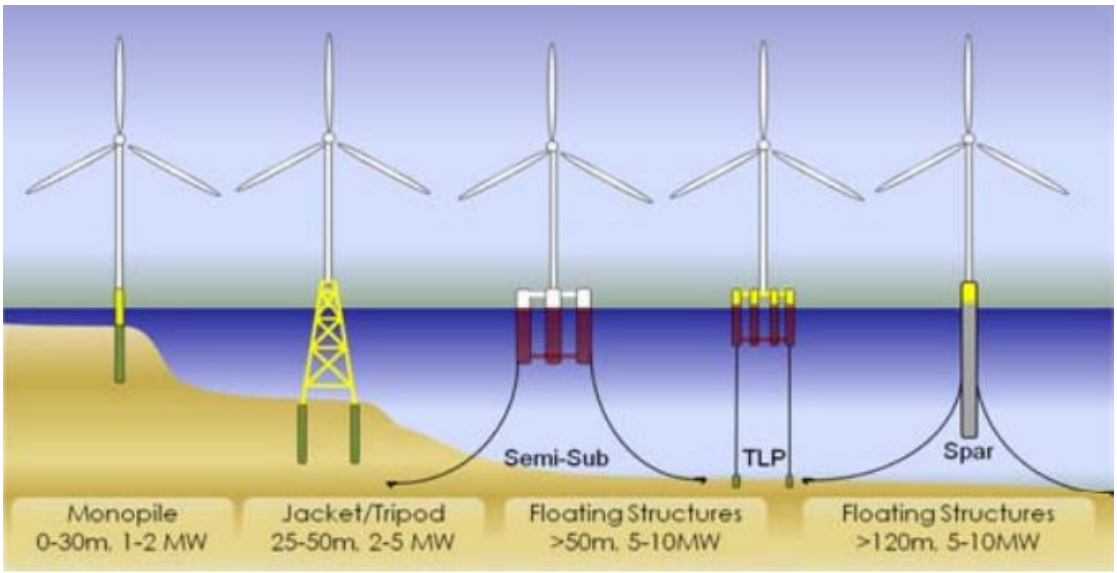

Figure 1.1: Different offshore wind turbines used according to water depth.

The idea of converting wave energy can be traced back to 200 years ago. But it is not until 1970s that wave energy drawn much attention and several models of wave energy converters had been tested by Palme (1920), Scott (1965), Masuda (1972) and Bott

et al. (1978). In 1974, S.H. Salter, from University of Edinburgh, has published the famous "Salter Duck" design and showed the possibility to get large portion of energy from waves (Salter, 1974). The fundamental research of wave energy has begun in the physics department of NTH (now NTNU) in 1973. Budar and Falnes (1975), from NTH, came up with the " point absorber" term meaning a device whose horizontal dimension is much smaller than wavelength and " absorption length" (now knows as "capture length") defined as " the width of a wavefront across which passes an average amount of power equal to that converted by the point absorber". They got a remarkable conclusion that an absorption length can be greater than the dimension of a point absorber. In the past decade, many research institutions have involved in the study of wave energy in Europe and other parts of the world. The European Commission has supported a lot of international conferences focusing on wave energy since 1986 (Clément et al., 2002). The wave energy research has been carried out by Centre for Ships and Ocean Structures (CeSOS) and other departments in NTNU since 2003. A lot of productive works have been achieved (Taghipour et al., 2008) (Lopes et al., 2009) (Yang et al., 2010) (Hals et al., 2011) (Kurniawan,A. and Moan,T., 2012) (Kurniawan,A. and Moan,T., 2013) (Luan et al., 2014b) (Michailides et al., 2014).

1.2 Floating Wind Turbines and Wave Energy Converters

1.2.1 Floating Wind Turbines

Wind and wave power is more steady and of a higher density far away from offshores, where water depth goes into deep zones. Floating wind turbines are deployed in deep water up to 300 meters for the purpose of cost-effective generation of electricity.

The Hywind, with 5-MW, is a deep water floating wind turbine proposed by Norsk Hydro in 2006. The hull is concrete and a steel tower is mounted on the top of it. It is moored by three mooring steel wires with clump weights as shown in Figure 1.2 (Nielsen et al., 2006). HywindSim and SIMO/RIFLEX are presented in their study to predict the dynamics of the Hywind concept. SIMO/RIFLEX is a code for the analysis of coupled floating bodies, which is developed by Marintek [1], and it is also the main tool for simulation of

[1]Link: http://www.sintef.no/home/MARINTEK/

Semi-submersible Flap Combination (SFC) studied in this thesis. In 2009, Norway has installed the first floating wind turbine with 3-MW in the offshore of Karmøy by using this Hywind concept in the water depth of around 120 meters. Phase IV of the IEA Annex XXIII Offshore Code Comparison Collaboration (OC3) chose the Hywind concept to do further research because of its simplicity of design, suitability for modeling and probability to commercialization (Jonkman, 2010). Some modifications have been made in the tower, substructures and control systems. In OC4 Phase II, a semi-submersible wind turbine with 5-MW (Robertson et al., 2012) has been developed in 2012. Roddier et al. have

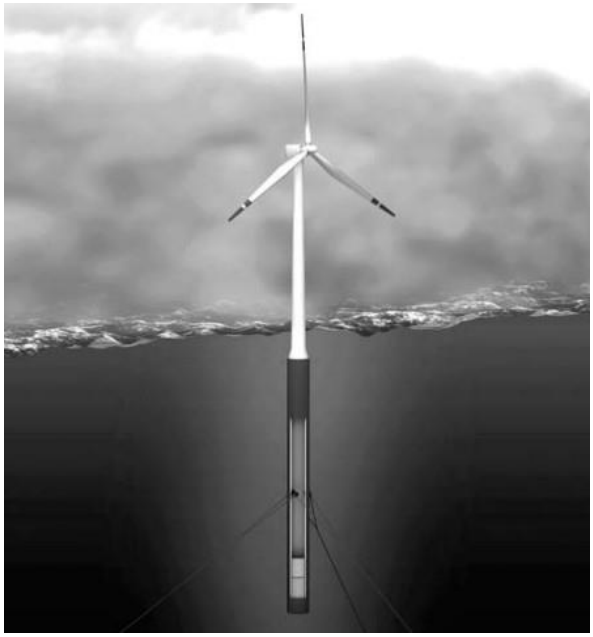

Figure 1.2: The Hywind floating wind turbine.

designed a generic 5 MW-WindFloat based on the experience of designing a 2 MW WindFloat demonstration project in Portugal. Three columns connected by braces are used to support the wind turbine (Figure 1.3) (Roddier et al., 2011). In the end of 2013, the largest offshore 6-MW wind turbine produced by Alstom, has been installed off the Ostend harbor in Belgium. In 2014, Luan et al. (2014a) from CeSOS of NTNU [2] come up with the 5-MW Semi-submersible wind turbine which is the floating hull for the later SFC concept discussed in this thesis.

[2]Link: http://www.cesos.ntnu.no/

Figure 1.3: WindFloat wind turbine.

1.2.2 Wave Energy Converters

WECs are utilized to absorb energy from waves and transfer it into the energy human can make use of, for instance, the electricity power. A WEC typically can be divided into the following subsystems (Salter et al., 2002; Kurniawan et al., 2012):

1. A primary interface, such as a float, flap or column of water, where hydrodynamic interactions happen with surrounding waves, thus motions of waves transmit to interface's motions.

2. A power take-off (PTO) mechanism, which could be mechanical, hydraulic, pneumatic, electrical subsystems or their combinations.

3. Means for keeping the primary interface at sea, such as cables or struts.

4. A control subsystem which can increase relative velocity and rectify the primary interface direction, for instance, in order to maximize power capture.

5. An electrical network of cables, transformers and switchgear for combining and

transmitting the power to electricity grid.

Projects of WECs have been carried out all around the world, especially in Europe in the last decade. A variety of wave energy technologies have been discussed depending on water depths and locations. A classification of wave energy systems is given by Falcão (2010) mostly based on working principles, as shown in Figure 1.4.

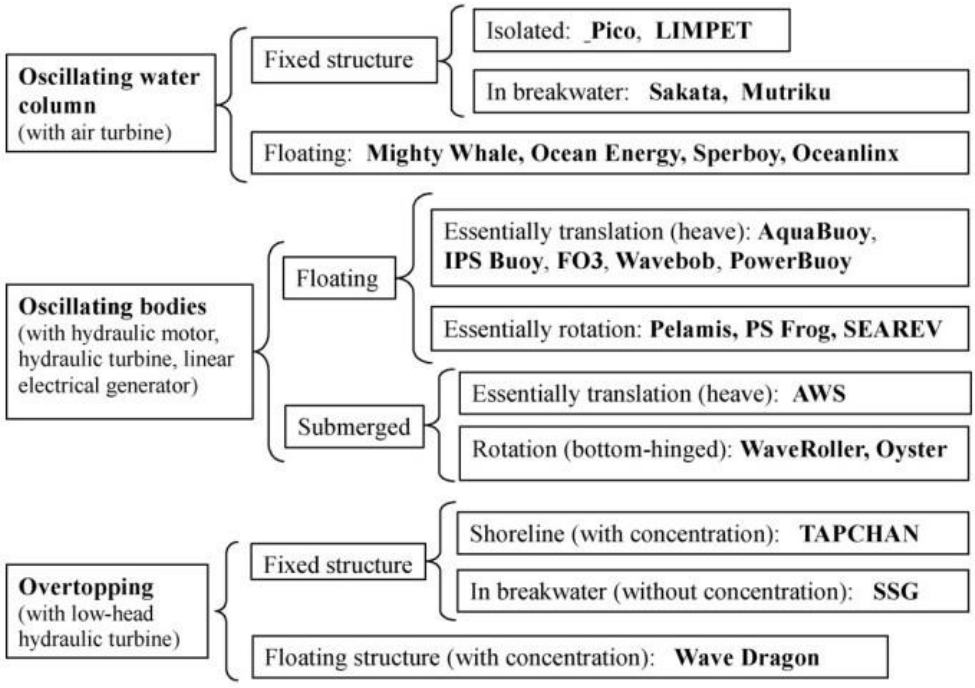

Figure 1.4: Classification of wave energy systems.

Oscillating Water Columns (OWCs) are partly submerged and the main working principle is to make the air trapped in the column to flow by waves and then an electric generator is driven by the air. A sketch of an OWC is shown in Figure 1.5 (Falcão, 2010). In 1978, Masuda came up with the Backward Bent Duct Buoy (BBDB) , a new geometry of a gloating OWC ,as shown in Figure 1.6 (Masuda and McCormick, 1986; Babarit et al., 2012). It can move in six degrees of freedom and the water column length is made larger compared to former OWCs, so that resonance can be generated by waves. The conclusion that "the addition of projecting sidewalls will increase the energy capture of a wave-energy device" made by Ambli et al. (1982) is confirmed by Count and Evans (1984). This result has been applied in many OWCs. In 1985, a full sized prototype of OWC is built in Norway (Bønke

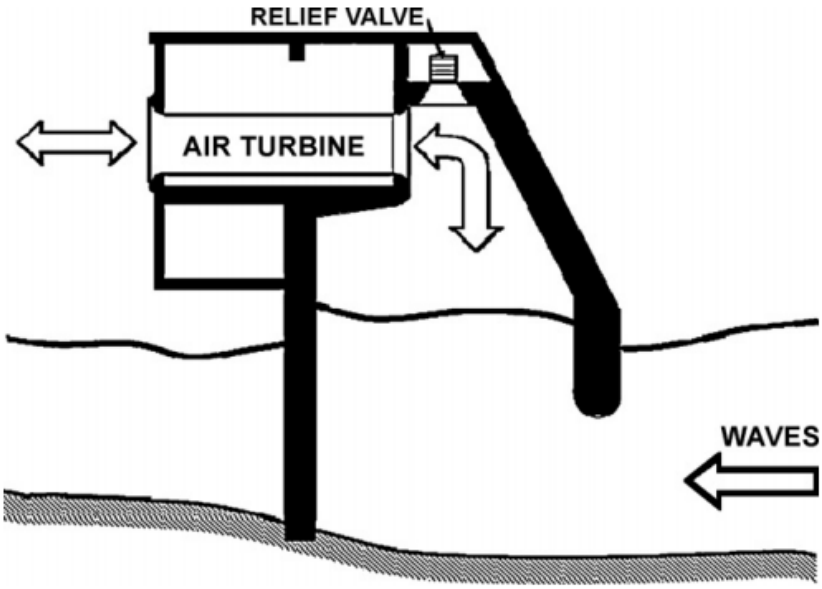

Figure 1.5: Cross sectional view of a bottom-fixed OWC.

and Ambli, 1986).

Oscillating bodies are conceived to exploit much powerful waves and they can go into deep water. The simplest one can be single-body heaving buoy. The idea is transforming the wave motions into buoy's heaving, the Norwegian buoy investigated by Budal et al. (1982) is such an example that its spherical floater can oscillate in heaving. The buoy can also be connected to a bottom fixed structure and the heaving motion between the sea surface and seabed is driven by waves. Floating heaving buoy array is used in order to get more power as shown in Figure 1.7 (Babarit et al., 2012). All WECs are connected to a submerged structure, which are moored by tension wires. A single-body heaving buoy will encounter problems if there is a large distance between free surface and sea bottom or when tides happen. So two-body heaving systems are come up with and energy is generated by the relative motion of these two bodies. In 1999, Falnes has studied its hydrodynamics theoretically in detail (Falnes, 1999).

The overtopping WECs will capture mostly the waves close to crest and store them in a reservoir where height is above surrounding sea surface. The potiential energy of stored water can be converted into other energy. The Tapered Channel Wave Power Device is developed and built based on this principle in Norway from 1980 to 1985. It consists of a

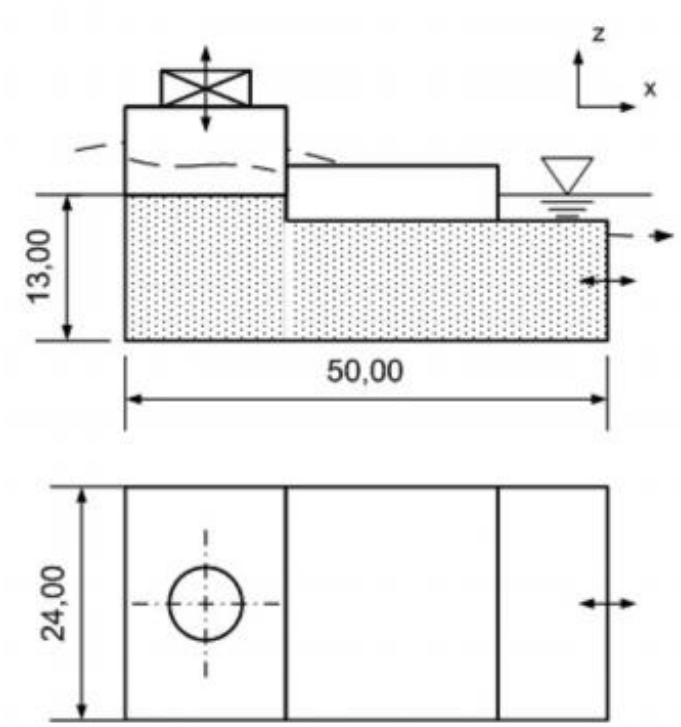

Figure 1.6: Sketches of Backward Bent Duct Buoy.

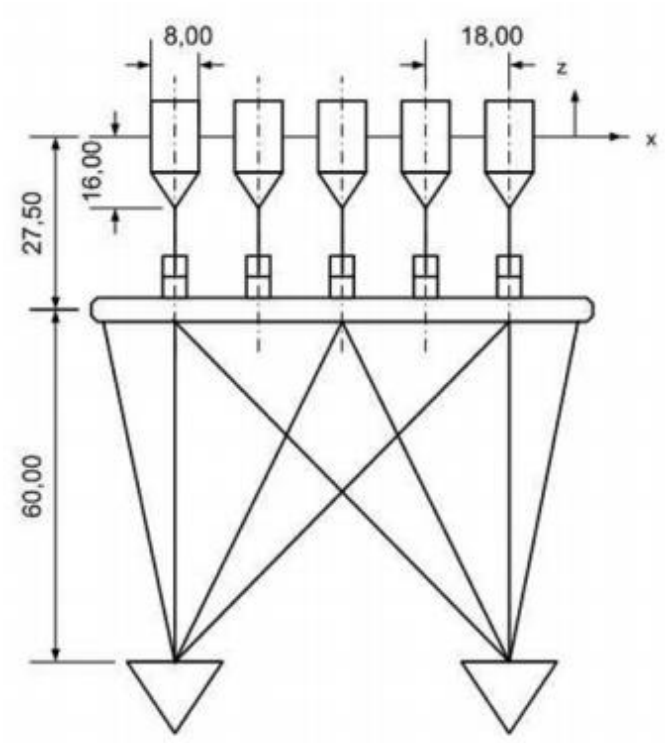

Figure 1.7: Floating heaving buoy array.

collector for concentrating waves, a converter, a reservoir for storing water and a water-turbine. This converter has no moving parts and is entirely passive. It is suitable for a broad range of wave heights, frequencies and directions with high energy conversion efficiency (Mehlum, 1986). Kofoed et al. (2006) developed the converter Wave Dragon with two wave reflectors concentrating on waves to a ramp for capturing overtopping water in Denmark. A Sea Slot-cone Generator (SSG) is developed by Margheritini et al. (2009) based on the slopping wall concept. It comprises a number of reservoirs on the top of each other and the low cost of structure and robustnes are keys to success.

WECs can also convert wave motions into power by pitching instead of translation. Devices will rotate around an axis of a structure, primarily fixed on sea bottom. An early and famous example is the nodding Duck by Salter (Salter, 1974). A string of Ducks are arranged aligned with wave crest direction as shown in Figure 1.8. The bottom-hinged devices are proposed on the basis of pendulum hinged at sea bottom. An early example is the mace conceived by Slater (Salter, 1992). The reciprocating pitching motion is converted into power by a Power Take-off (PTO) mechanism. The principle of this idea is applied to the WECs investigated in this paper, but the WECs are hinged on the PTO systems which are mounted on the pontoons of a semisubmersible.

Figure 1.8: A string of Ducks with gyroscopes.

Many sketches, designs, and animations have been announced publicly, also measurements for estimation of wave energy are invesitgated. Eigth wave energy converters with different principles are estimated in terms of annual power absorption by Babarit et al. (2012). The WECs investigated in this thesis is based on the study results of Kurniawan,A. and Moan,T. (2013). In their paper, study results show that for most of the WEC optimal geometries, their rotation axes are close to the sea bottom and bodies close to the free surface. One stressed conclusion is that the optimal cross sectional dimensions are generally less than one third of the water depth when wave frequencies are from 0.4 to 1.3 rad/s, which can be verified in the dimension of our flap. An elliptical flap supported by two arms is investigated in the paper of Babarit et al. (2012). They have summarized the characteristics of the pitching wave absorber with rotatable flap as: the resonant characteristics of the absorber may be altered by changing the flap angle, and it can be utilized properly to broaden the absorption bandwidth; a low reaction force is experienced when having the flap aligned perpendicularly to the arm, it can be a method to avoid large forces associated with large waves.

1.2.3 MARINA Platform Project

Based on the former works of floating wind turbines and WECs, a natural thinking comes out: how to combine wind and wave energy together? How can a floating wind turbine combine with WECs in order to obtain more power and reduce costs? The Marine Renewable Integrated Application (MARINA) Platform Project [3] is a European project aimed to establish a set of criteria for evaluation of multi-purpose platforms for marine renewable energy(MRE) . Two or three realisations of multi-purpose renewable energy platforms for offshore wind and ocean energies will be produced. The SFC model discussed in this thesis is a combined concept studied in the framework of this project.

Before going into that, Li Lin has made a comparison between five European offshore sites on the wind and wave energy conditions for the MARINA Platform Project, and there are eighteen sites in North Sea and the Atlantic Ocean considered to be potential sites as shown in Figure 1.9 (Li et al., 2013). The five sites for comparisons circled in the map are

[3] Link: http://www.marina-platform.info/

selected based on the geographic conditions, average wind and wave energy storage and extreme conditions. The detailed information of these eighteen sites can be found in the paper (Li et al., 2013) and a simplified one is presented in Table 1.1. The selected sea states (discussed in Chapter 4) in this thesis's simulations are based on the work of Li et al. (2013).

Figure 1.9: Maps for the eighteen potential sites of MARINA Project.

1.2.4 Semi-submersible Flap Combination

Luan et al. (2014b) have come up with a concept of a semi-submersible with a 5MW horizontal axis wind turbine with three flap-type WECs, this concept is named as Semi-submersible Flap Combination(SFC). It consists of one semi-submersible wind turbine and three WECs so that wind and wave energies can be made use of in this multi-use platform. The total power production will increase and cost of unit power will be reduced. Descriptions of the SFC concept and WECs will be illustrated in Chapter 3. The

Table 1.1: Wind and wave energy distribution

(a) Wind and wave energy distribution and magnitudes.

Site No.	Area	Name	Average Wind Power Density at 80m height (W/m^2)	Average Wave Power Density (kW/m)
1	Atlantic	Sem Rev	530	17
2	Atlantic	Buoy Estaca de Bares	690	47
3	Atlantic	Buoy Cabo Silleiro	650	43
4	Atlantic	Sao Pedro Pilot Zone	360	32
5	Atlantic	Wave Hub	620	32
6	Atlantic	Lewis West	1120	65
7	Atlantic	Ireland,Sybil Head,Co.Kerry	950	70
8	Atlantic	BIMEP	190	37
9	Atlantic	EMEC Wave West Buoy	650	38
10	Enlish Channel	Marwick Head	660	28
11	Mediterranean	Marwick Head	740	13
12	North Sea	Horn Sea West	810	9
13	North Sea	Belwind 1	750	6
14	North Sea	Norway 5	1100	46
15	North Sea	Denmark,North Sea Center	870	14
16	North Sea	Usira II	910	29
17	North Sea	FINO 3	850	13
18	North Sea	Moray Firth	660	6

(b) Power values of different colours.

Colour	Wind Power (W/m^2)	Wave Power (kW/m)
White	<500	<15
Yellow	500-900	15-25
Red	>900	>25

flap-type WECs will be discussed in details in this thesis, especially the WECs responses in the SFC concept, which can be compared with the response of a single Bottom-Fixed WEC (BFWEC) .

1.3 Contexts and Objectives

The combined wind and wave energy platform, SFC, is designed to make use of wind energy and wave energy at the same time. In this thesis, the concentration is put on the WECs of SFC. A single WEC hinged at sea bottom is investigated in terms of wave-induced motions and Ultimate Limit States (ULS) design check of the structural arms according to NORSOK Standard N004 in a previous project thesis. This work extents to study a global and comprehensive analysis model of SFC in SIMO/RIFLEX/AeroDyn and output the responses of WECs when both wind and wave loads are considered. Two majored aspects are investigated: the produced power by WECs and structural responses of the arms. Then comparisons are made between the BFWEC and WECs of SFC in terms of these two aspects. The main objectives are listed as following:

1. Carry out the global response analysis for the single BFWEC in survival wave conditions and make the ULS design check based on NORSOK Standard N004.

2. Calculate produced power of the BFWEC in operational condition.

3. Carry out an extensive time-domain simulations for SFC considering representative stochastic wind and wave conditions. Investigate the effects of wind and wave induced Semi-submersible motions on the power absorption and structural response of the WECs and its arms.

4. Make comparisons between the BFWEC and the three WECs of SFC.

1.4 Studying Method

Generally analysis of ocean structures is frequency and time dependent. Frequency and time can be separated on the basis of some assumptions and simplifications. Thus

solutions can be got in frequency domain regardless of time, which is much convenient. Even some analytical solutions can be derived. Linear models are dominant when going into dynamics of ocean structures. Forces and displacements are able to be calculated in frequency domain, the former can be evaluated by some frequency dependent coefficients (Jefferys, 1984). By contrast, time domain method is very time consuming and only numerical solutions are obtained, it is heavily dependent on software and hardware of computers until now. Time-domain method is always presented because of substantial degrees of nonlinearities in WECs modeling, which mainly due to control mechanisms and PTO systems. It is the studying method that used in this thesis.

Majority of offshore wind turbines have been installed in shallow water until now. Steadier wind and higher wind velocity, which means more wind energy, are measured at a farther distance away from offshores. Sophisticated aero-elastic simulations tools, which can analyze onshore wind turbines well enough, can not be used directly in offshore wind turbines, especially in farther offshores. The key issue is the wave-induced motion of floating wind turbines. Aerodynamics of wind turbines and hydrodynamics of floating supporting structures have to be considered and analyzed in one simulation tool. SIMO/RIFLEX/AeroDyn is a code published in the series paper by Ormberg et al. (2011) and Luxcey et al. (2011). It is a well proven simulation tool for coupled floating structures and adopted in this thesis' study.

Forces and displacements of WECs of SFC are generated from simulations of different sea states in SIMO/RIFLEX/AeroDyn. Simulation results are presented according to time series. Forces will be checked according to the NORSOK Standard N004 (Standards Norway, 2004) which have been coded in Matlab. Displacements are used for calculation of produced power by WECs. This is implemented in Matlab as well.

1.5 Thesis Overview

In this Chapter, some backgrounds of wind turbines and WECs are introduced. In Chapter 2, the simulation tool SIMO/RIFLEX/AeroDyn is discussed in terms of the theories behind them. Potential wave theory and Morison equation are reviewed as well. Then

descriptions of simulation models, including BFWEC and SFC, are described in detail in Chapter 3. The numerical model of WEC is explained in simulation tool as well. In Chapter 4, wind-sea states are defined before simulation process. Wind loads are considered for the SFC model. Simulation process is illustrated and examples of results are plotted in terms of forces and displacements. Chapter 5 presents two methods to get the pitching natural period of BFWEC, quite a good agreement is got between these two methods. In Chapter 6, ULS strength check of supporting arms of WECs is carried out according to the NORSOK Standard N004 (Standards Norway, 2004) in operational condition and survival condition. In Chapter 7, produced power by WECs is calculated and compared. In the last Chapter, conclusions are summarized and some recommendations for future work are come up with. A chart flow of this thesis is presented in Figure 1.10.

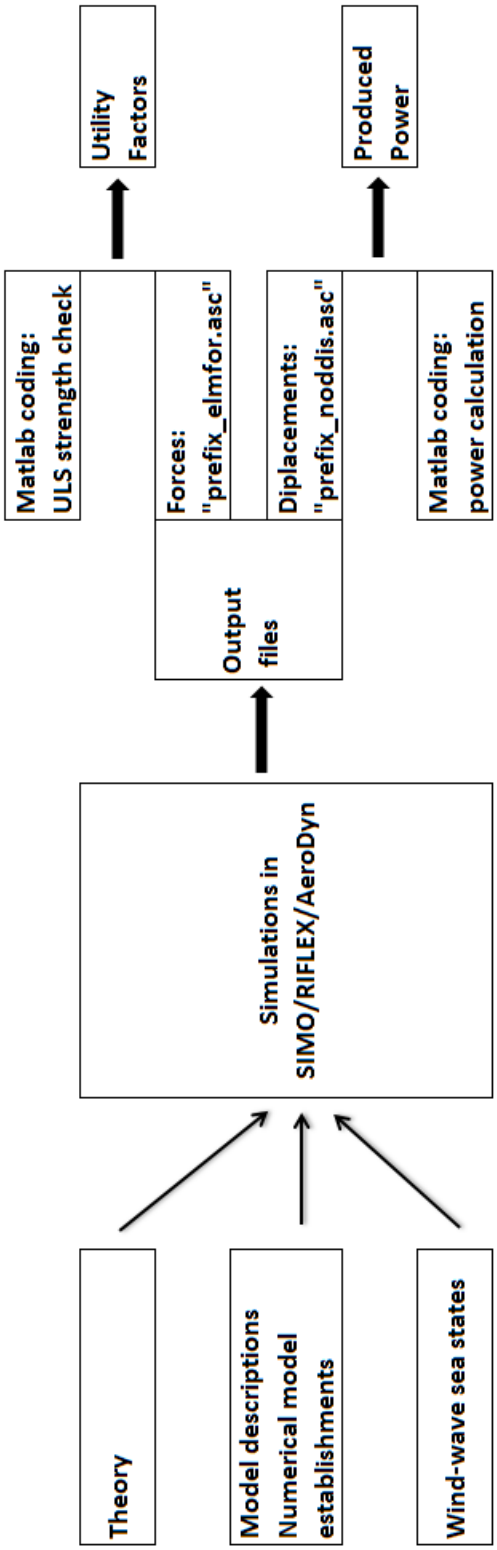

Figure 1.10: Thesis flow chart.

Chapter 2

Theory Review and Introduction of Simulation Tool

In the papers of Ormberg et al. (2011) and Luxcey et al. (2011), they developed the code SIMO/RIFLEX/AeroDyn, in order to solve the problem of the wave-induced motions of floating wind turbines. It is a well proven simulation tool for coupled ocean structures. All the structural parts, such as nacelle, blades, Semi-submersible and WECs are included in this finite element model of SFC. Time domain numerical analysis of the single bottom-fixed WEC and SFC model have been carried out in this simulation tool. The basic theories will be reviewed in three parts: AeroDyn, SIMO, and RIFLEX.

2.1 Introduction to AeroDyn

AeroDyn calculates the aerodynamic loads on wind turbine blade elements based on velocities and positions provided by dynamics analysis routines and simulated wind inputs. It is not a stand-alone programme, but a plug-in type code for interfacing with a number of dynamics programs. Here the interactions with SIMO/RIFLEX are utilized to analysis the SFC model. The primary data input file is called 'AERODYN.IPT', which is a text data file that describes blades. The hub-height(HH) wind files are used for the wind input files, which allows several different parameters to be updated throughout the simulation. The airfoil data files represent the aerodynamic properties of AeroDyn model

elements. The flow chart of aerodynamic calculations is presented in Figure 2.1.(David J. Laino and A. Craig Hansen, 2002)

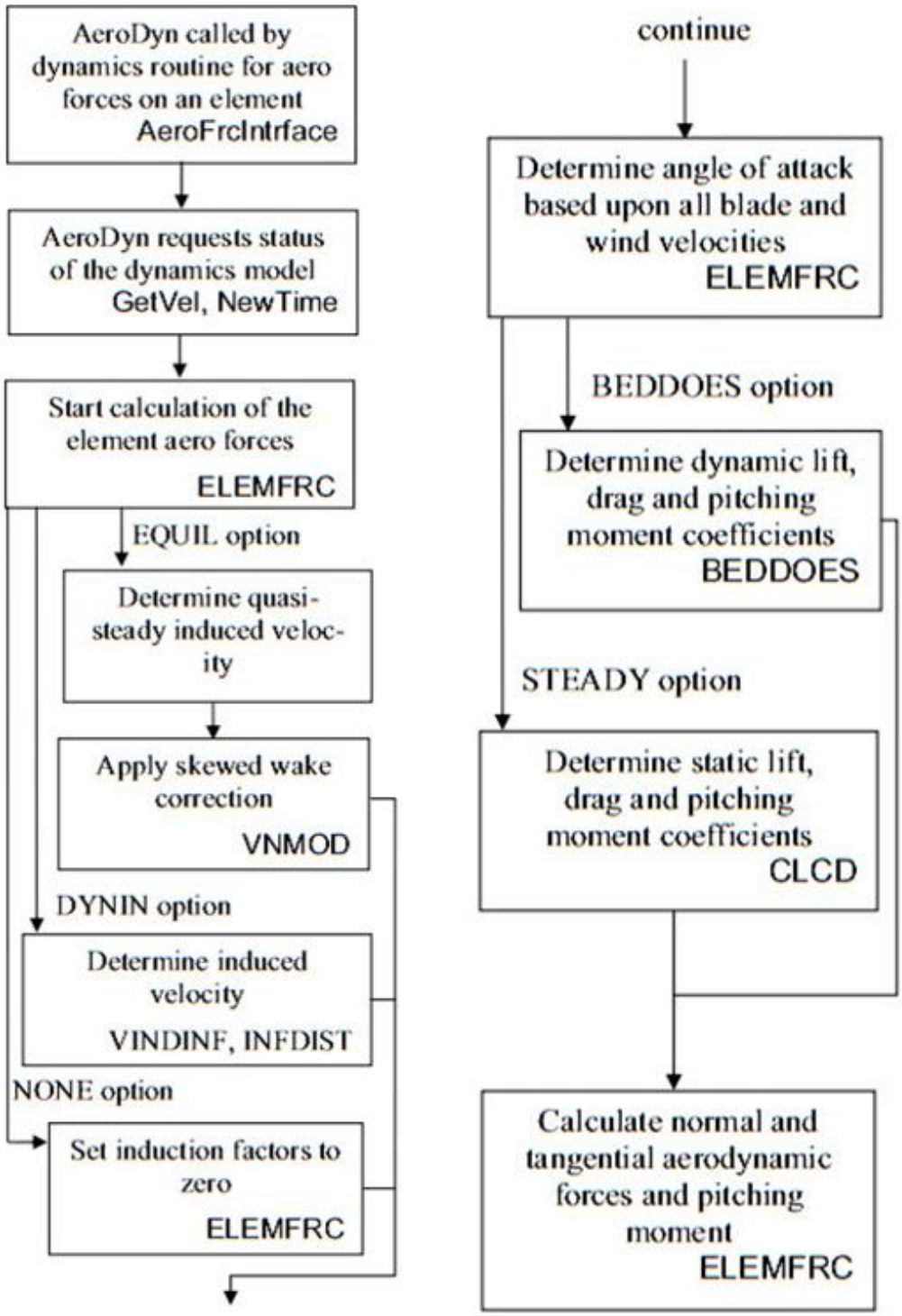

Figure 2.1: Aerodynamic calculation process in AeroDyn.

Blade Element Momentum (BEM) theory is used for calculating induced velocities on wind turbine blades. It assumes that the wake is always in equilibrium with the forces on a blade element. This theory is implemented by breaking the blades of a wind turbine into many elements along the span. The blades trace out annular regions as shown in Figure 2.2, across which the momentum balance takes place. These annular regions are also where the induced velocities from the wake change the local flow velocity at the rotor plane. Prandtl model (Tip-Loss Model) is used to account for the influence of vortices shed from the blade tips into the wake on the induced velocity field. The same method is applied to the Hub-Loss Model which serves to correct the induced velocity resulting from a vortex being shed near the hub of the rotor. Skewed wake correction is based on the method developed by Pitt and Peters (1981). The Beddoes-Leishman dynamic stall model is chosen to calculate the airfoil aerodynamics, which is a semi-empirical model based on airfoil indicial response. Indicial response produces the normal force coefficient and the moment force coefficient as a function of time for a step change in angle of attack. It is derived from the solution of the linearized differential equations for an unsteady, compressible and inviscid fluid. The airfoil attached flow responses because of a certain angle attack history are calculated from the superpositions of individual indicial responses for each step. A modification of the response is necessary based on the position of the effective flow separation point on the low-pressure side of the airfoil. (Patrick J. Moriarty and A. Craig Hansen, 2005)

The wind file data used in this thesis is generated by the PhD candidate Jiang Zhiyu [1] in NTNU and AeroDyn will call these wind data during simulation and calculate forces acting on the blades.

2.2 Introduction to SIMO

SIMO, abbreviation for Simulation of Marine Operations, is a time domain simulation program for study of motions and station-keeping behavior of a complex system of floating vessels and suspended loads. It is featured by (H. Ormberg, H. Lie and F. Meling, 2007)

[1] Link:http://www.cesos.ntnu.no/personnel/phds/13-phds/109-zhiyu

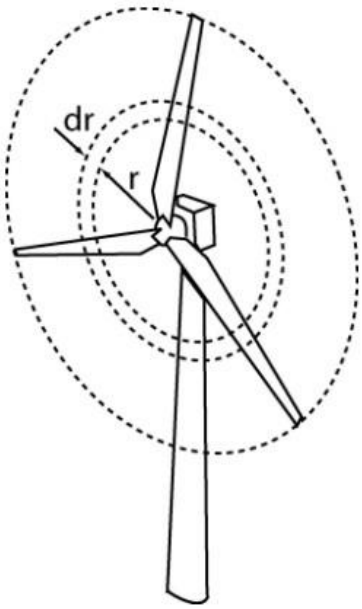

Figure 2.2: Annular plane used in blade element momentum theory.

:

1. Flexible modelling of multibody systems. It applies to surface vessels, such as Tension Leg Platforms(TLP), Semi-submersible; positioning including turret mooring, dynamic positioning; complex marine operations, for instance, offloading, offshore crane operations, installation of TLP.

2. Nonlinear time domain analysis of wave-frequency and even low-frequency forces.

3. External forces due to winds, waves and currents.

4. Control forces (positive and passive).

5. Interactive or batch simulation. Batch simulation is selected in this thesis.

SIMO consists of six modules: INPMOD, STAMOD, DYNMOD,OUTMOD, S2XMOD and PLOMOD. They are communicating by a file system as shown in Table 2.1. INPMOD is for inputting data manipulation.STAMOD defines the initial conditions and static equilibrium and DYNMOD carries out dynamic response calculation.OUTMOD and S2XMOD are used in post-process and they are designed for output and exporting time series to various file formats respectively. The interactive plotting module PLOMOD can give graphic

Table 2.1: File system of SIMO

SIMO Modules		Functions
INPMOD		Read and manipulate system description
STAMOD		Read system description,
	File system	static analyses,define initial condition
DYNMOD	for communication	Dynamic analyse,generation of time series
OUTMOD	between modules	Post-processing of time series
S2XMOD		Export of time series
PLOMOD		Plotting

presentations of simulation results. A complete dynamic analysis have to run the modules INPMOD, STAMOD and DYNMOD. S2XMOD is also executed in order to get the time series of structures' motions in this thesis. Post-processing of simulation results is carried out by Matlab.

A system description file is needed before running the program. It is divided into the following main data groups:

SYSTEM DESCRIPTION SIMO

BODY DATA SPECIFICATION

COUPLING DATA

ENVIRONMENT DATA SPECIFICATION

END

The first one is an identifier of this file type. Body descriptions follow the first one. In our model, there are six bodies in total. They are the Seim-submersible, three WECs, the wind turbine nacelle and hub. Coupling data will be repeated for all couplings. Wind and wave spectrum are defined in 'ENVIRONMENT DATA SPECIFICATION'.

Linear wave potential theory is used and it is also applied in RIFLEX, this will be explained in introduction of RIFLEX. JONSWAP spectrum is used in the simulation. The wave spectrum is given by Equation 2.1,

$$S(\omega) = \frac{\alpha g^2}{\omega^5} \exp\left(-\beta\left(\frac{\omega_p}{\omega}\right)^4\right) \gamma^{\exp\left(-\frac{(\omega/\omega_p - 1)^2}{2\sigma^2}\right)}, \tag{2.1}$$

where

α is spectral parameter,

ω wave frequency,

β form parameter, default value $\beta = 1.25$,

ω_p peak frequency,

γ peakedness parameter,

σ spectral parameter.

Significant wave height, Hs,is often used instead of α to parameterize the spectrum:

$$\alpha = \left(\frac{Hs\omega_p^2}{4g}\right)^2 \frac{1}{0.065\gamma^{0.803} + 0.135}. \tag{2.2}$$

The dynamic motion equation is expressed as:

$$M\ddot{x} + C_M\dot{x} + D_1\dot{x} + D_2 f(\dot{x}) + K(x)\,x = q(t, x, \dot{x}), \tag{2.3}$$

where

M is frequency-dependent mass matrix,

C_M frequency-dependent potential damping matrix,

D_1 linear damping matrix,

D_2 quadratic damping matrix,

f vector function where each elemtnt is given by $f_i = \dot{x}_i|\dot{x}_i|$,

K hydrostatic stiffness matrix,

x position vector,

q exciting force vector.

Exciting force consists of several components:

$$q(t, x, \dot{x}) = q_{WI} + q^{(1)}_{(WA)} + q^{(2)}_{(WA)} + q_{CU} + q_{ext}, \tag{2.4}$$

where

q_{WI} is wind drag force,

$q^{(1)}_{(WA)}$ first-order wave excitation force,

$q^{(2)}_{(WA)}$ second-order wave excitation force,

q_{CU} current drag force,

q_{ext} are any other forces, such as wave drift damping, specified forces, etc.

Wave excitation forces can be split into three contributions: First-order forces that oscillate with wave frequencies; Second-order mean, varying wave drift forces; Higher-order ringing forces.

There are two different ways to run SIMO program, one is interactive mode and the other is batch mode. As the names suggest, commands are executed by selecting commands in prompt window and several interactions between human and SIMO have to be made for a complete simulation progress in the interactive mode as shown in Figure 2.3 (H. Ormberg, H. Lie and F. Meling, 2007). In batch mode, required input files can be prepared in text files and several commands can be given to SIMO in a sequence at one time and all simulation processes will be run continuously in order.

2.3 Introduction to RIFLEX

RIFLEX is an advanced FEM program for static and dynamic analysis of marine slender structures, especially for riser systems. These slender structures are characterized by small bending stiffness, large deflection, large excitation at the upper end, complex cross sections and nonlinear cross section properties. For the analysis of WEC's supporting arms, they can be built as slender structures with a rigid body connected on the upper end, which is the flap and connected with the lower end, which is the PTO mechanism installed on the semisubmersible.

The structures of RIFLEX system is shown in Figure 2.4. It consists of input module, static and dynamic analysis modules, and post processing module which includes output and graphic plotting. In the INPMOD module, most input data is read and prepared for the successive analysis. STAMOD module is designed for static analysis and also initiates configuration for dynamic analysis. DYNMOD module performs dynamic analysis in time domain and it is also very time consuming process. Time series are generated and dynamic responses are obtained and selectively stored. The post processing is performed by

```
************************************************************
*   WELCOME TO                                             *
*                                                          *
*    SSSSSSSSS    III   MMMMM    MMMM     OOOOOOOO      *
*   SSSSSSSSSSS   III   MMMMM   MMMMM    OOOOOOOOOO     *
*   SSS           III   MMMMMM MMMMMM   OOO      OOO    *
*   SSS           III   MMM MMMMM MMM   OOO      OOO    *
*   SSSSSSSSS     III   MMM  MMM  MMM   OOO      OOO    *
*   SSSSSSSSSS    III   MMM   M   MMM   OOO      OOO    *
*           SSS   III   MMM       MMM   OOO      OOO    *
*           SSS   III   MMM       MMM   OOO      OOO    *
*   SSSSSSSSSS    III   MMM       MMM    OOOOOOOOOO     *
*    SSSSSSSS     III   MMM       MMM     OOOOOOOO      *
*                                                          *
*   SIMULATION OF COMPLEX MARINE OPERATIONS                *
************************************************************

Enter system identification > sysa
Enter initial condition identification > inib

I-> SELECTION OF PROGRAM MODULE
I
I      INP  - SIMO INPMOD
I      STA  - SIMO STAMOD
I      DYN  - SIMO DYNMOD
I      OUT  - SIMO OUTMOD
I      PLO  - SIMO/RIFLEX PLOMOD
i      S2X  - SIMO S2XMOD
I
I      PINP - Print postscript inpmod/stamod/outmod file (simo.plt)
I      PPLO - Print postscript plomod file (pscr-meta.dat)
I
I      DEF  - Redefine default files (for default file names)
I      LIS  - List identifiers (for default file name)
I
I      TERM - Terminate
I
Select option >
```

Figure 2.3: Interface of SIMO in interactive mode.

OUTMOD module and interactive plotting can be carried out in PLOMID module. However Matlab is employed for the post processing in this thesis. (Fylling et al., 2008)

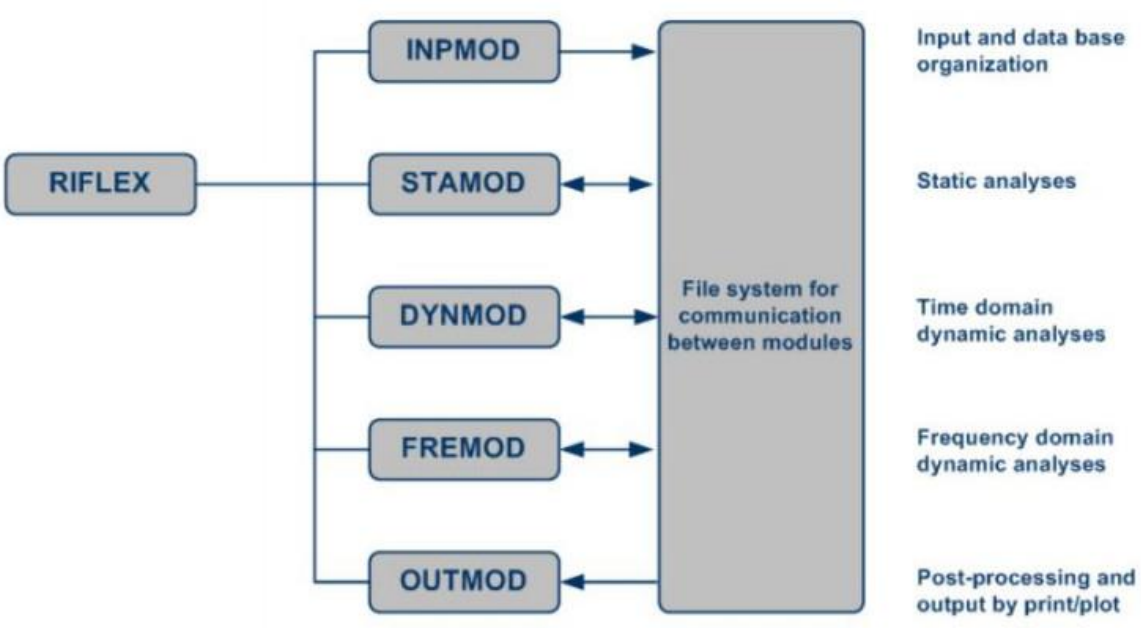

Figure 2.4: Structure of RIFLEX system.

2.3.1 External Loads

For the SFC model, both wind forces and wave loads have to be considered. Wind forces act on the blades of wind turbine, not directly on the WECs. Here wave loads are investigated, which are direct forces affecting the motions and strength of WECs. Current is not included. The coupling effects of winds and waves are simulated simultaneously in the SFC model.

Potential theory is applied to calculate the first order radiation and diffraction forces on the structures. Water is assumed to be continuous and has a uniform density. Cartesian reference frame is used, where Z-axis is pointing upwards and the origin is the crossing point between Z-axis and static water surface. Governing equations, boundary conditions and initial conditions are identified to solve the problem. For the governing equations, conservation of fluid mass and momentum are utilized. The fluid is considered inviscid,

irrotational and incompressible. As a consequence, the only unknown parameter is the velocity potential ϕ. The velocity can be expressed as:

$$V_w = \nabla\phi = \frac{\partial\phi}{\partial x}i + \frac{\partial\phi}{\partial y}j + \frac{\partial\phi}{\partial z}k. \tag{2.5}$$

The pressure can be obtained from the Bernoulli equation,

$$p - p_a = -\rho g z - \rho\frac{\partial\phi}{\partial t} - \frac{1}{2}\left(\nabla\phi\right)^2, \tag{2.6}$$

where

p is water pressure,

p_a atmospheric pressure,

z water depth.

For the governing equation,

$$\nabla^2\phi = 0 \qquad \text{in the controlled domain.} \tag{2.7}$$

For the boundary conditions, usually the impermeability condition,

$$\frac{\partial\phi}{\partial n} = 0 \qquad \text{on the sea bottom,} \tag{2.8}$$

$$\frac{\partial\phi}{\partial n} = V_B \bullet n \qquad \text{on the body surface,} \tag{2.9}$$

are utilized (V_B is the body velocity).

Besides, free surface kinematic condition and dynamic condition have to be considered,

$$\frac{\partial\phi}{\partial z} = \frac{\partial\zeta}{\partial t} + \frac{\partial\phi}{\partial x}\frac{\partial\zeta}{\partial x} + \frac{\partial\phi}{\partial y}\frac{\partial\zeta}{\partial y}, \tag{2.10}$$

and

$$g\zeta + \frac{\partial\phi}{\partial t} + \frac{1}{2}\left[\left(\frac{\partial\phi}{\partial x}\right)^2 + \left(\frac{\partial\phi}{\partial y}\right)^2 + \left(\frac{\partial\phi}{\partial z}\right)^2\right] = 0, \tag{2.11}$$

on free surface,

where

ζ is wave elevation.

Using Taylor expansion of the boundary conditions around the mean boundary configuration (body motions and free surface deformations are expressed as power of a small quantity), the velocity potential and wave elevation can be expresses as:

$$\phi = \tilde{\phi}_1\varepsilon + \tilde{\phi}_2\varepsilon^2 + \tilde{\phi}_3\varepsilon^3 + \ldots, \tag{2.12}$$

$$\zeta = \tilde{\zeta}_1\varepsilon + \tilde{\zeta}_2\varepsilon^2 + \tilde{\zeta}_3\varepsilon^3 + \ldots. \tag{2.13}$$

For linearization, only the first term is considered. As a consequence, the response of the body motion amplitude is proportional to the excitation, the incident wave amplitude. The combined free surface condition is obtained,

$$\frac{\partial^2\phi}{\partial t^2} + g\frac{\partial\phi}{\partial z} = 0 \qquad \text{on } z = 0. \tag{2.14}$$

Considering the steady motions, the solution will have the same frequency as the incoming wave and the fooling equation can be derived from Equation 2.14.

$$-\omega^2\phi + g\frac{\partial\phi}{\partial z} = 0. \tag{2.15}$$

Furthermore, in the linear and steady response condition, velocity potential ϕ can be divided into space dependent part and time dependent part (Equation 2.16). Frequency domain analysis can be employed in this case. But for nonlinear analysis and transient conditions, time domain analysis is required.

$$\phi(x, y, z, t) = R\left[\varphi(x, y, z)e^{i\omega t}\right]. \tag{2.16}$$

For deep water (usually water depth z is greater than half of the wave length λ $(\frac{z}{\lambda} \geq \frac{1}{2})$,

$$\phi = \frac{g\zeta_a}{\omega}e^{kz}cos(\omega t - kx), \tag{2.17}$$

where ζ_a is wave amplitude, k wave number.

As a result, pressure can be got from Equation 2.6, including static pressure and dynamic pressure. If only linear loads are considered, the pressure can be expressed as:

$$p = -\rho \frac{\partial \phi}{\partial t} - \rho g z. \tag{2.18}$$

The first part represents the dynamic pressure which has to be integrated along the mean body wetted surface and the second part stands for the static effect which must be integrated on the instantaneous body surface. Then the external loads are obtained. (Faltinsen, 1993)

When waves come into ocean structures, on one hand, structures are stationary and interacts with waves, which is considered as diffraction problem; on the other hand, the motion of ocean sturctures will affect waves or the static surface if there are no waves, which is defined as radiation problem and the hydrodynamic loads are identified as added-mass, damping and restoring force.

Morison equation is used to calculate wave loads on circular cylindrical structural members when viscous forces matter. It tells that the horizontal force dF on a strip of length dz of a vertical circular cylinder can be written as (Faltinsen, 1993):

$$dF = \rho C_M \frac{\pi D^2}{4} a_1 dz + \frac{\rho}{2} C_D |u| u dz = dF_{Mass} + dF_{Drag}. \tag{2.19}$$

Positive force direction is in the wave propagation direction. D is cylinder diameter, u and a_1 are the horizontal undisturbed fluid velocity and acceleration at the midpoint of the strip. The mass and drag coefficients C_M andC_D have to be empirically determined.The corresponding forces are mass or inertial force and drag force. The drag force is the in-line viscous force. It is connected with the pressure loss due to the boundary layer and the flow separation and with the frictional stresses along the body. The inertial force when the motion of slender structures is excited by waves is considered in the mass term. But Morison equation is a long-wave approximation. To be more specifically, the wave length,λ, has to be five times larger than the typical diamesion of the structure D, $\lambda / D > 5$. As expressed in Figure 2.5, for large structures, diffraction forces are important, they are induced by incident waves and effects on sturctures; for samll-volume structures,

incident waves are not affected by the existance of small structures so much and forces connected with acceleration, which is mass force, and connected with velocity, which is viscous force, are dominant in this case. (Faltinsen, 1993) The implementation is based

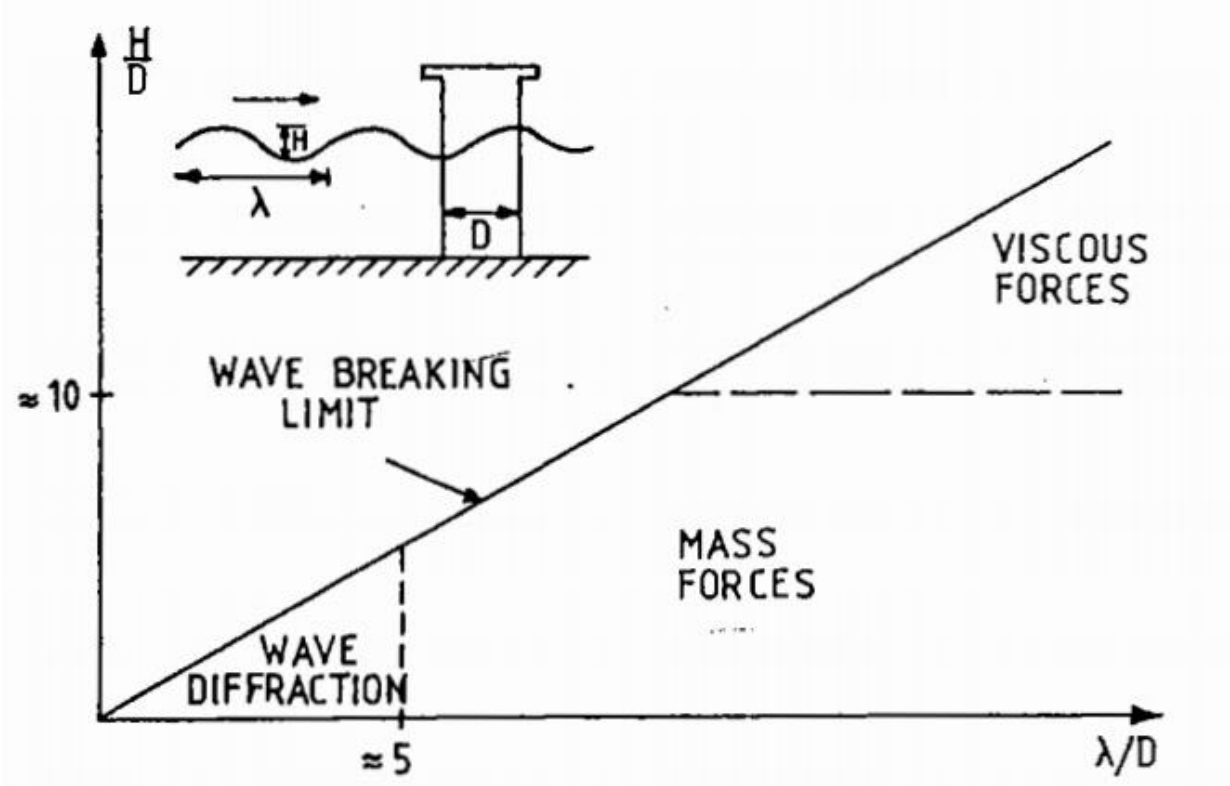

Figure 2.5: Claasification of wave forces. (Faltinsen, 1993)

on Wamit/Wadam [2], which uses a 3D panel method to evaluate velocity potentials and hydrodynamic coefficients. This implementation can be used for infinite and finite water depths, and both single bodies and multiple interacting bodies can be analyzed. Although there are two arms for one flap, the interaction influence between the two arms can be neglected. The flow is ideal and harmonic according to time. The free surface condition is linearized for the first order potential theory while the non-linear free surface condition is imposed for the second order potential theory computation. (Det Norske Veritas, 2010)

[2]Hydrostatic data and transfer functions are generated by Post Doc. Constantine Michailides. Link:http://www.ntnu.edu/employees/constantine.michailides

2.3.2 Dynamic Analysis

For dynamic time domain analysis, the dynamic equilibrium equation of a discretized finite element model can be expressed as:

$$R^I(r,\ddot{r},t) + R^D(r,\dot{r},t) + R^S(r,t) = R^E(r,\dot{r},t), \tag{2.20}$$

where

R^I is inertia force,

R^D damping force,

R^S internal structural reaction force,

R^E external force.

$r,\dot{r},\ddot{r}$ are structural displacement, velocity and acceleration respectively. Displacement depends on inertia and damping forces, and external loads couple with structural displacement and velocity as well. Besides, the relationship between internal forces and displacements is nonlinear. So the dyamic equilibrium is built on a coupled equation. For the discrete finite element model, all force vectors are established by assembling all element froces and specified discrete nodal forces. External forces include: weight and buoyancy, drag and added intertia terms, forced displacements due to support platform motions, and specified nodal forces. The inertia forces consists of structure mass, hydrodynamic mass accounting for the structural acceleration terms in Morison's equation as added mass contributions in local directions, mass because of internal fluid law. The damping force includes internal structural damping force, specified discrete dashpot dampers, and hydrodynamic damping accounting for diffraction effects for floating. They are all displacement dependent.(Fylling et al., 1995)

Dynamic equations are solved in time domain and numerical solutions are stored in output files, including forces acting on supporting arms of WECs, displacements of WECs in six degrees of freedom and motions of Semi-submersible. A relative small and suitable time step should be set in the simulations in order to get convergences at a specified accurary. For the BFWEC, 0.1s is taken as the time step in operational condition and 0.01s in survival condition. For the SFC model, 0.005s will be a good choice in both sea states.

Normally a larger motion requires a smaller time step. But considering all the simulations are carried out in time domain, a bigger time step is always expected. So a suitable time step should be chosen carefully. The output files from RIFLEX are regarded as input for the strength design check and motions for power calculation.

Chapter 3

Model Descriptions and Numerical Modelling

3.1 Descriptions of the Bottom-Fixed Wave Energy Converter

This model is very simple, including three main components: an elliptical cylinder, two supporting arms and a PTO system, as shown in Figure 3.1. The cross section of the elliptical cylinder is defined by Equation 3.1 (Luan et al., 2014b):

$$\left(\frac{Y''}{1.75}\right)^2 + \left(\frac{Z''}{3.5}\right)^2 = 1. \tag{3.1}$$

The coordinate system is shown in Figure 3.2. The major axis of the elliptical cross-section is 7 meters and the minor axis is 3.5 meters. The upper edge of the flap is 2 meters below the sea surface. The arms have circular cross section, whose outer diameter is 1.5 meters and inner diameter 1.4 meters. The information of the arms is listed in Table 3.1 and sketched in Figure 3.3. The distance between the two arms of one WEC is 20 meters, which is also the length of the elliptical cylinder. The flap will rotate rigidly around the Y-axis. For SFC model, three WECs with the same parameters are installed on the Semi-submersible. For a single WEC, dimensions and materials are the same in both models.

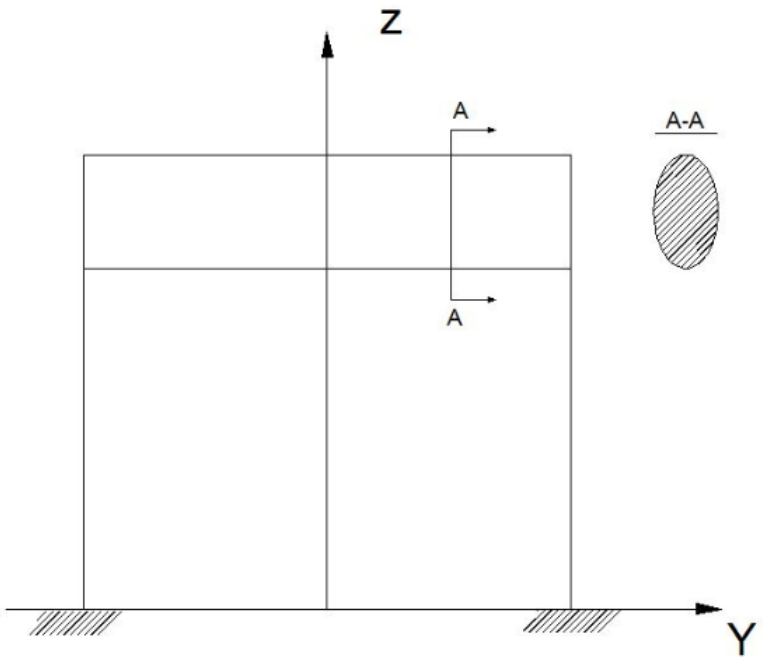

Figure 3.1: Profile view of BFWEC.

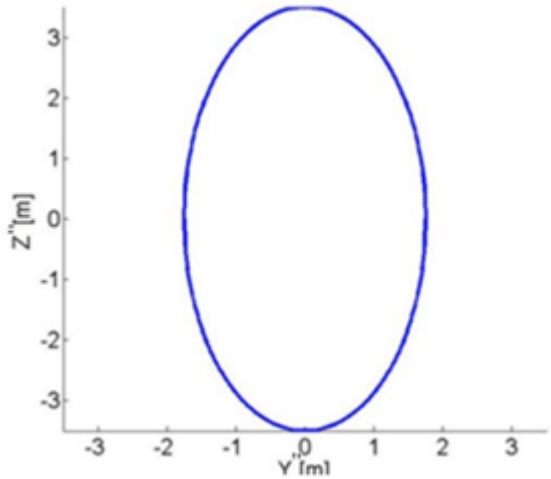

Figure 3.2: Cross section of the elliptical cylinder.

Table 3.1: Parameters of supporting arms of WEC.

Outer Diameter D[m]	Thickness t[m]	Length L[m]	Section Area A[m^2]	D/t	Young's Modulus E[MPa]	Density ρ [kg/m^3]	Yield Stress σ[MPa]	Poisson's Ratio
1.5	0.05	18.5	0.228	30	2.1×10^5	7850	355	0.3

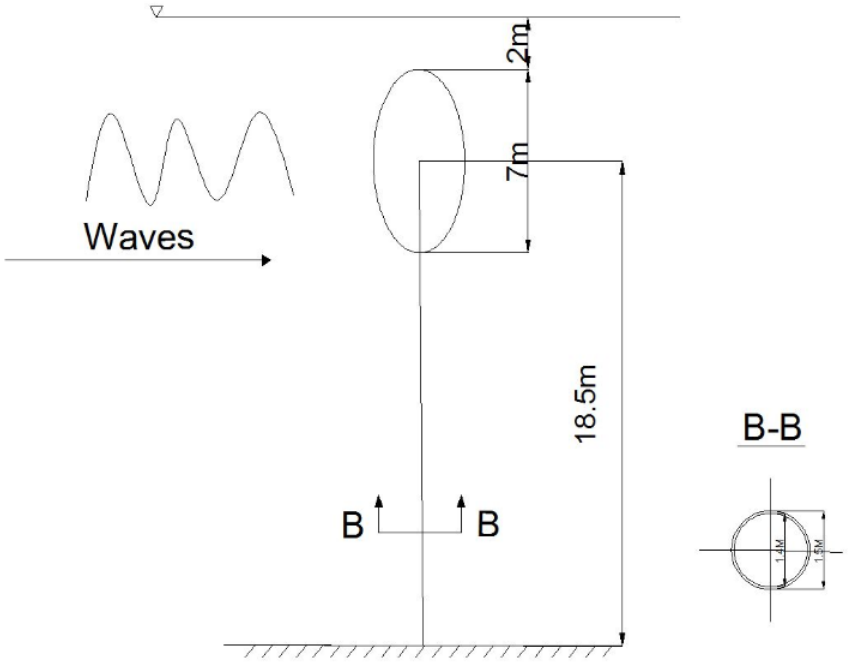

Figure 3.3: Sketches of flap-arm structure.

3.2 Descriptions of the SFC Model

The SFC is a new model developed by Luan et al. (2014b). It combines a 5 MW semi-submersible wind turbine with three flap-type wave energy converters, which may increase the total power production. The flaps are inspired by the optimized bottom-fixed rotating flap-type WEC (Kurniawan,A. and Moan,T., 2013). The SFC model is built in SIMO/RIFLEX/AeroDyn and the BFWEC is built in SIMO/RIFLEX by Post Doc. Constantine Michailides. Small modifications are made according to wind-wave sea states.

The SFC model consists of two parts as shown in Figure 3.4: a 5 MW Semi-submersible wind turbine and three WECs. The first part includes a NREL reference wind turbine (Jonkman et al., 2009), a hull and three catenary mooring lines. A central column is welded on the hull, which is used for supporting the rotor, hub and blades. Three equally distributed side columns are around the central column on the hull. They are designed for providing restoring stiffness to prevent capsizing. Three pontoons connect the central column and three side columns. The distance between the central line of the central column and that of the side column is 41 meters, which is considered to be large. One reason is that sufficient restoring stiffness from the second moment of water line area is needed for

the SFC. Besides, this design provides enough space for the WECs. The second part of the SFC model are the three WECs, whose locations and dimensions are specified in Figure 3.5 and Figure 3.6. (Luan et al., 2014b)

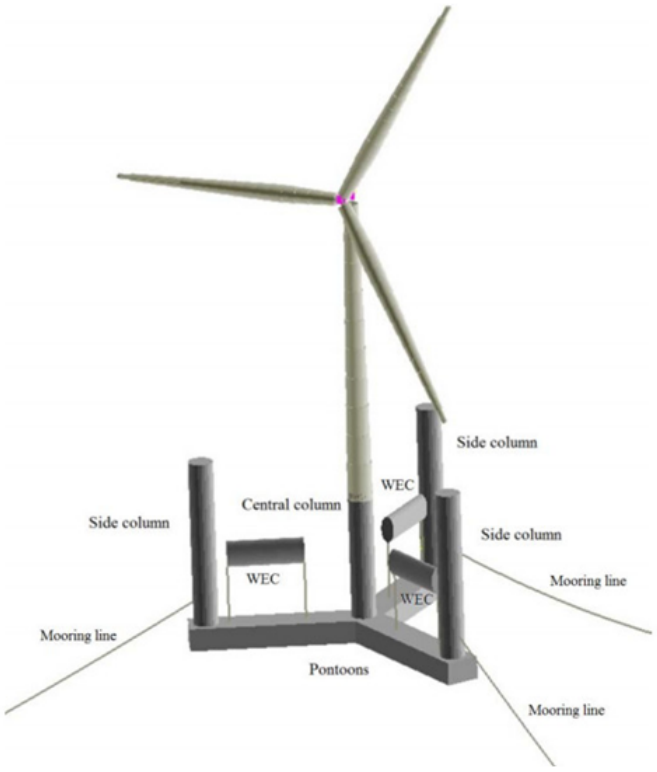

Figure 3.4: The SFC model.

The upper end of the supporting arm is rigidly welded with flap extending to the center of flap cross section and the lower end is connected to surface of the pontoon. The total length of one arm is 18.5 meters. The distance from the central line of the central column to the arm close to the central column is 15 meters. The PTO system is simplified by a constant linear damping coefficient C in the numerical model. The sensitivity study with respect to the effects of the mass of the elliptical cylinders and the damping coefficients on the power production of the WECs is carried out by Michailides et al. (2014), with a conclusion that "a relatively small mass of elliptical cylinders and a relatively small damping coefficient are preferable with respect to increase the mean value of the generated power of the three WECs". Finally the mass of the elliptical cylinder is set to 100 tonnes and the damping coefficient of each flex joint is specified to 650 $kN \cdot m \cdot sec/deg$. WEC will rotate

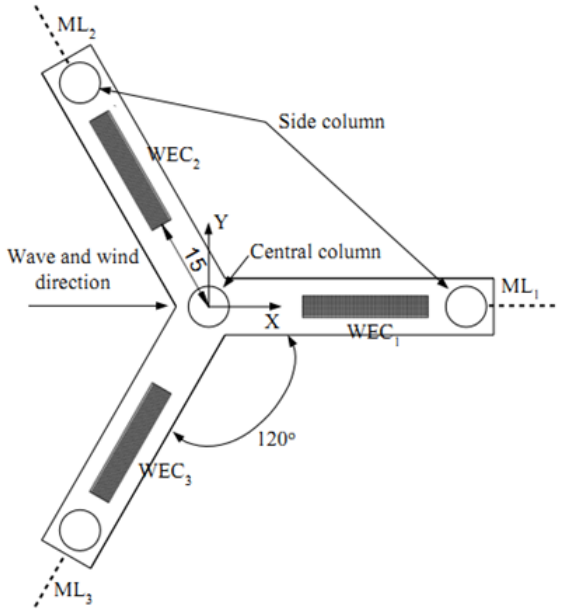

Figure 3.5: The SFC model (plane view).

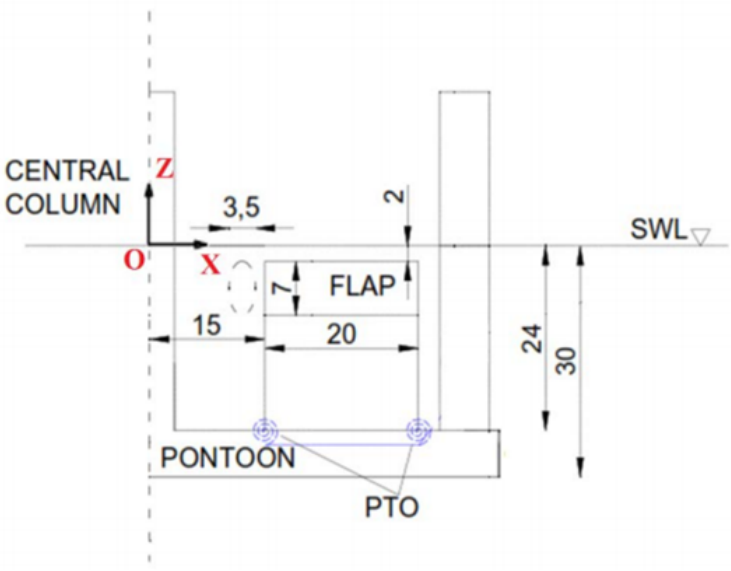

Figure 3.6: Locations and dimensions of WECs (side view).

rigidly around the axis where the PTO system connected to the pontoon. A summary of one WEC is listed in Table 3.2.

Table 3.2: Summary of a WEC.

Parameters	Unit	Magnitude
Major axis length of the flap cross section	[m]	7
Minor axis length of the flap cross section	[m]	3.5
Length of one flap	[m]	20
Mass of one flap	[tonnes]	100
Displacement of one flap	[tonnes]	392.4
Length of one supporting arm	[m]	18.5
Outer diameter of a supporting arm	[m]	1.5
Inner diameter of a supporting arm	[m]	1.4
Mass of two supporting arms	[tonnes]	66.16
Displacement of two supporting arms	[tonnes]	67

3.3 Numerical Modelling

Lines and rigid bodies are used for the arms and flaps respectively in RIFLEX. To establish lines, supernodes have to be defined first. There are three types of supernodes classified according to the boundary conditions: free, fixed and prescribed. Free supernodes don't have any restriction on all degrees of freedoms and therefor the node positions and displacements are to be determined during or after analysis. Fixed supernodes have one or several degrees of freedom are fixed and are used for fixed structures such as the fixed joints between the PTO sytems of WECs and the pontoons of Semi-submersible. If forced dynamic motions are prescribed, then prescribed supernodes are used. For one supporting arm modelling, three supernodes have been defined, points a,b,c in supporting arm 1 and d,e,f in supporing arm 2 as shown in Figure 3.7. A separate supporting arm model is sketched in Figure 3.8. Supernode 1 is fixed for the BFWEC, it is fixed to the seafloor. For the SFC model, it is fixed with the pontoon of Semi-submersible. Supernode 2 is quite close to supernode 1 and it is defined as free. They are connected by line 1. Line 1 is acting as the PTO mechanism with a damping coefficient $C = 650kN \cdot m \cdot sec/deg$. Supernode 3 is the connection point between the arm and flap and it is connected to the flap rigidly. Line 2 is defined by supernode 2 and supernode 3. A line is a linear structural element de-

fined by two supernodes. Properties are defined in line types and a line has to be assigned with a line type. A line type can be defined once and referred several times in the model description, lines with the same properties can have the same line type number. A line is specified in terms of: a) Several segments with homogenous cross sectional properties. Detailed descriptions such as length and number of elements, properties of cross sections are specified for each segment and they will be the input information for finite element discretization. b) Segment intersections can specified in terms of nodal information such as weights, hinges and so on. c) Description of fluid component. An example of line element is shown in Figure 3.9. For line 2 of the supporting arm, it is divided into 4 segments, forces can be got from each of them. The strength design check process will be carried out in these 4 elements. (Fylling et al., 2008)

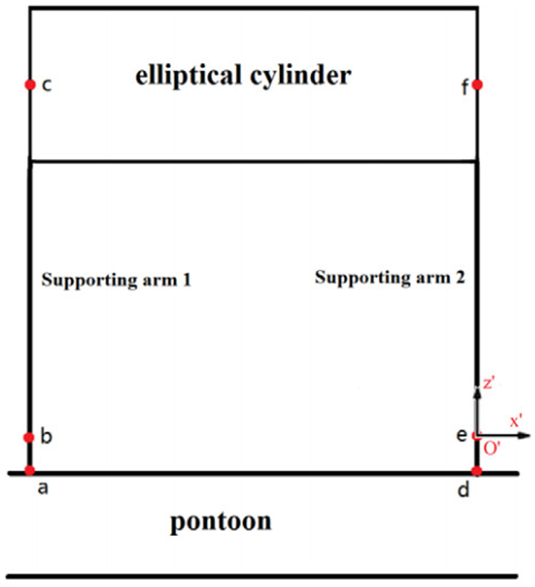

Figure 3.7: Numerical modelling for one of the WECs of the SFC attached to the pontoon.

3.4 Common Features and Differences

For both the BFWEC and WECs installed on Semi-submersible, they share the same flap and supporting arms, dimensions and materials are identical. Each supporting arm is divided into four segments. PTO system is simplified by using a constant damping coef-

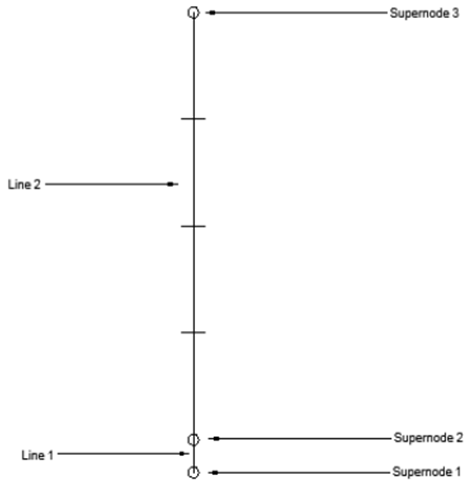

Figure 3.8: Supporting arm model of the WECs.

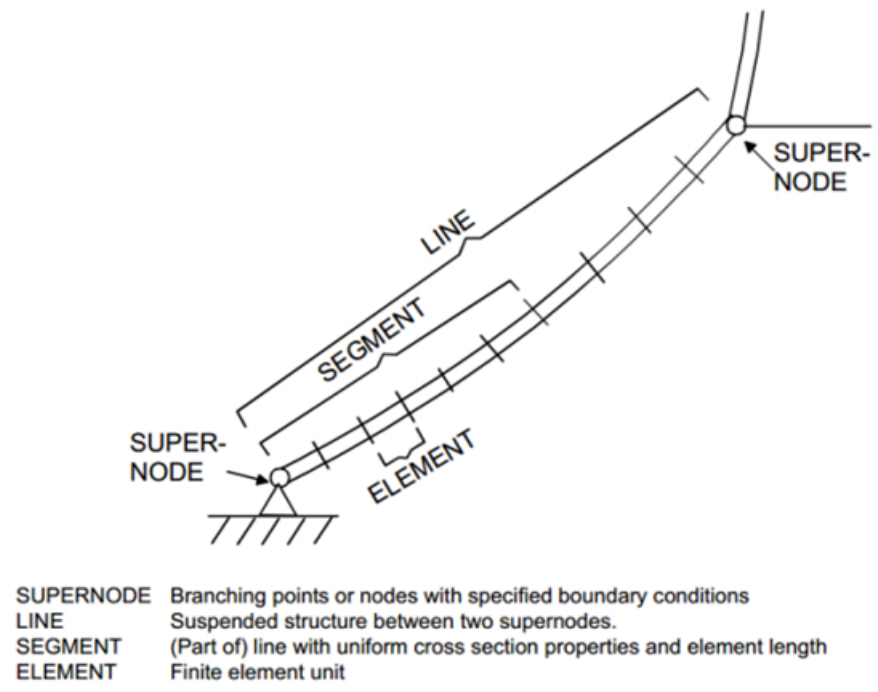

Figure 3.9: Line and segments in RIFLEX.

ficient. Water depth is set to 200 meters. Same wave spectrum (Three-parameter Jonswap Spectrum) is selected and 20 different irregular waves are generated. The cross sectional dimension of the flap is 7 meters, which is less than one third of the water depth, it agrees with the conclusion made by Kurniawan,A. and Moan,T. (2013). In this case, the "water depth" should be regarded as 24 meters.

The biggest difference between these two WECs is that the BFWEC is fixed on the "sea bottom" and the other three WECs are installed on Semi-submersible. The "sea bottom" is quoted because the two supporting arms are fixed at the sea depth of 24 meters instead of 200 meters in order to guarantee that the distance from the lower end of the PTO system to the still sea surface is the same in both models. Another difference is due to the Semi-submersible. It leads to WECs of SFC should be considered in terms of relative motions, which requires more difficult calculation and analysis of produced power and strength check. The last difference is regarding to wind loads. For the BFWEC, there are no wind loads. In the SFC model, three types of wind loads are considered, a more specific illustration will be given in Chapter 4.

Chapter 4

Simulation

This chapter studies the simulation process and results. For the BFWEC model built in SIMO/RIFLEX, only wave loads are considered. WECs of SFC are built with other bodies in SIMO/RIFLEX/AeroDyn and AeroDyn is cited when running SFC simulations in order to include wind loads. So firstly sea states are defined for both models, then simulations are carried out and examples of results are given in the end.

4.1 Wind-Wave Sea States

Comprehensive simulations with varieties of sea states are carried out. The three-parameter Jonswap wave spectrum is chosen with parameters significant wave height Hs, zero crossing wave period Tz and the γ parameter. γ is set to be 3.3 for all wind-sea states. Basically two major working conditions of WECs are investigated, one is the operational condition with significant wave height $Hs = 6m$, zero crossing wave period $Tz = 12.6s$; another one is the survival condition with significant wave height $Hs = 15.6m$, zero crossing wave period $Tz = 14.5s$. Considering symmetry of WECs and SFC, only four wave directions (denoted as θ) are simulated for both operational condition and survival condition, 0^0, 30^0, 45^0, 90^0. For SFC model, three wind loads with different velocities are acting on the wind turbines respectively combined with waves, winds come from the direction of 0^0, which blow to the positive direction of X-axis, as shown in Figure 3.5 with velocities (denoted as V) $8m/s$, $11.4m/s$ and $18m/s$ respectively. So for the BFWEC, there are $2 \times 4 = 8$

sea states in total and for the SFC, there are $2 \times 4 \times 3 = 8$ wind-sea-state combinations. For each sea state, wave spectrum is split into small enough pieces and irregular wave function is generated from it by adding wave expressions with different phase angles, which are described by seed numbers in the simulation tool. With different seed numbers, phase angles generated randomly will give different time series of winds and waves. However, in our case, wind data is provided separately, values of wind loads are stored in four files in the format of HAWC2 [1]: one description file, and three wind velocity files that represent wind speeds in x, y and z directions. So only wave loads are affected by seed numbers and 20 different seed numbers from 300 to 1250 at an interval of 50 are selected to have a more realistic simulation. For produced power by WECs, a mean value can be expected which could be more close to reality with 20 different simulations. For strength check, the maximum forces have to be investigated to ensure designed structure is reliable. Currents are not included in simulations. A summary of all wind-wave sea states is listed in Table 4.1 and Table 4.2.

4.2 Simulation Process

A standard RIFLEX running command is executed in batch mode by giving the following commands to the programme:

riflex inpmod prefix1

riflex stamod prefix1

riflex dynmod prefix1 prefix2

riflex outmod prefix1 prefix2

Prefix1 and prefix2 are identifications for the corresponding modules. 'Irreg' is the identification of BFWEC and 'Analysis' is for SFC. As mentioned in Chapter 2, SIMO could be run in batch mode as well, so commands can be given to the simulation tool at one time as shown below:

For BFWEC,

riflex_ 64bit inpmod Irreg

[1] Wind data is generated by the Affiliated PhD candidate Jiang Zhiyu in NTNU. Link:http://www.cesos.ntnu.no/personnel/phds/13-phds/109-zhiyu

Table 4.1: Simulations of BFWEC.

	$Hs[m]$		$Tz[s]$		$Hs[m]$		$Tz[s]$	
	6		12.6		15.6		14.5	
$\theta[deg]$	0	30	45	90	0	30	45	90
Seed Number	300	300	300	300	300	300	300	300
	350	350	350	350	350	350	350	350
	400	400	400	400	400	400	400	400
	450	450	450	450	450	450	450	450
	500	500	500	500	500	500	500	500
	550	550	550	550	550	550	550	550
	600	600	600	600	600	600	600	600
	650	650	650	650	650	650	650	650
	700	700	700	700	700	700	700	700
	750	750	750	750	750	750	750	750
	800	800	800	800	800	800	800	800
	850	850	850	850	850	850	850	850
	900	900	900	900	900	900	900	900
	950	950	950	950	950	950	950	950
	1000	1000	1000	1000	1000	1000	1000	1000
	1050	1050	1050	1050	1050	1050	1050	1050
	1100	1100	1100	1100	1100	1100	1100	1100
	1150	1150	1150	1150	1150	1150	1150	1150
	1200	1200	1200	1200	1200	1200	1200	1200
	1250	1250	1250	1250	1250	1250	1250	1250

Table 4.2: Simulations of SFC.

	$Hs[m]$			$Tz[s]$	$Hs[m]$			$Tz[s]$
	6			12.6	15.6			14.5
$\theta[deg]$	0	30	45	90	0	30	45	90
$V[m/s]$	8/11.4/18				8/11.4/18			
Seed Number	300	300	300	300	300	300	300	300
	350	350	350	350	350	350	350	350
	400	400	400	400	400	400	400	400
	450	450	450	450	450	450	450	450
	500	500	500	500	500	500	500	500
	550	550	550	550	550	550	550	550
	600	600	600	600	600	600	600	600
	650	650	650	650	650	650	650	650
	700	700	700	700	700	700	700	700
	750	750	750	750	750	750	750	750
	800	800	800	800	800	800	800	800
	850	850	850	850	850	850	850	850
	900	900	900	900	900	900	900	900
	950	950	950	950	950	950	950	950
	1000	1000	1000	1000	1000	1000	1000	1000
	1050	1050	1050	1050	1050	1050	1050	1050
	1100	1100	1100	1100	1100	1100	1100	1100
	1150	1150	1150	1150	1150	1150	1150	1150
	1200	1200	1200	1200	1200	1200	1200	1200
	1250	1250	1250	1250	1250	1250	1250	1250

simo_ 64bit Irreg dummy stamod batch sta-Irreg

riflex_ 64bit stamod Irreg

simo_ 64bit Irreg dummy dynmod batch dyn-Irreg

riflex_ 64bit dynmod Irreg

simo_ 64bit Irreg dummy s2xmod batch s2x-Irreg

For SFC,

riflex_ 64bit inpmod Analysis

simo_ 64bit Analysis dummy stamod batch sta-Analysis

riflex_ 64bit stamod Analysis

simo_ 64bit Analysis dummy dynmod batch dyn-Analysis

riflex_ 64bit dynmod Analysis

simo_ 64bit Analysis dummy s2xmod batch s2x-Analysis

It begins with "INPMOD" in RIFLEX which gives descriptions of models, hydro data from

Wamit or Wadam and wind-wave sea state. Then a result file and an internal communication file will be generated for later modules and be called by another programme, that's SIMO in this case. These result files and internal communication files will be generated by other internal modules as well. Then "STAMOD" of SIMO is executed on the basis of results from 'INPMOD' in RIFLEX, following by static analysis of RIFLEX, which is the 'STAMOD'. Then dynamic analysis is carried out in both SIMO and RIFLEX, called 'DYNMOD'. The final executing command is called 'S2XMOD', which is used for exporting time series to ASCII files and Matlab '.mat' files. In this thesis, six-degree motions of Semi-submersible and three WECs of SFC are written into ASCII files. They will be useful for motion analysis, especially for relative motions between WECs and the Semi-submersible. For the BFWEC, it is not necessary to do so.

Simulation time step is a very key factor that has to been dealt with. It affects convergence in the simulation tool for both SIMO and RIFLEX. Besides, a smaller time step means longer simulation time. For a complex ocean structure model, a good choice of time step will save much time and energy. Time steps are listed in Table 4.3 used in the BFWEC and SFC. It can be seen that a smaller time step is required in survival condition than in operational condition. This is because much larger motions are expected in survival condition. Due to complexity of SFC, some bodies defined in SFC are requiring smaller time step than a single BFWEC. A relative good time step can be found by keeping changing time step from a big value to a smaller value until it converges. For the BFWEC, only a few minutes are consumed for one simulation, but it takes several hours for one SFC simulation. Simulation time is set to be 3 hours. But in total 4100 seconds are set in simulation tool in order to get steady responses. The first 500 seconds will be deleted when post-process is carried on.

Table 4.3: Time steps used for simulations.

	BFWEC		SFC	
	Operational	Survival	Operational	Survival
Sea State	$Hs = 6m$ $Tz = 12.6s$	$Hs = 15.6m$ $Tz = 14.5s$	$Hs = 6m$ $Tz = 12.6s$	$Hs = 15.6m$ $Tz = 14.5s$
Time Step	0.1s	0.01s	0.005s	0.005s

4.3 Simulation Results

Results are output according to the output data defined in "dynmod.inp" file, both displacements and forces can be stored according to time series at an interval of certain time steps. Displacements include motions in X,Y and Z directions and forces include axial forces, torsional moments, moments about local Y-axis and Z-axis, shear forces in local Y-direction and Z-direction. They are stored in '.ASC' format which can be loaded by Matlab directly. The '.ASC' file varies from dozens of Megabytes to hundreds of Megabytes depending how much data is output. It will take a long time to load the '.ASC' file if it is too large. So it has to been considered carefully which displacements and forces should be used in the post-process. One suggestion is that as much as data should be output from SIMO/RIFLEX/AeroDyn for later study, so different researchers don't need to run the model again. In this thesis, WECs are mainly concerned, so most of output data is related to them, including forces acting on the four segments of each supporting arm of WECs, displacements of PTO, supporting arms, flaps, and Semi-submersible. Plots of motions and forces according to time series are shown from Figure 4.1 to Figure 4.8. Figure 4.1 and Figure 4.2 show the rotation motions of WECs. For each segment, there are six displacement related motion in degrees of freedom, including three translations along X-axis, Y-axis and Z-axis; three rotations around X-axis, Y-axis and Z-axis. These motions can be directly got from result files. But the rotation motions of flaps are the ones to be cared. They will be used to calculate produced power by WECs. Time series of different forces acting on one segment of supporting arms are plotted from Figure 4.3 to Figure 4.8, including axial tension (N_{Sd}), bending moments about local Y-axis and Z-axis (M_{Sd}), shear forces in local Y-direction and Z-direction (V_{Sd}), and torsional moments ($M_{T,Sd}$) (Local coordinate system refers to Figure 3.7). Forces will be loaded into Matlab codes which are an implementation of the "NORSOK Standard N004" to perform ULS check.

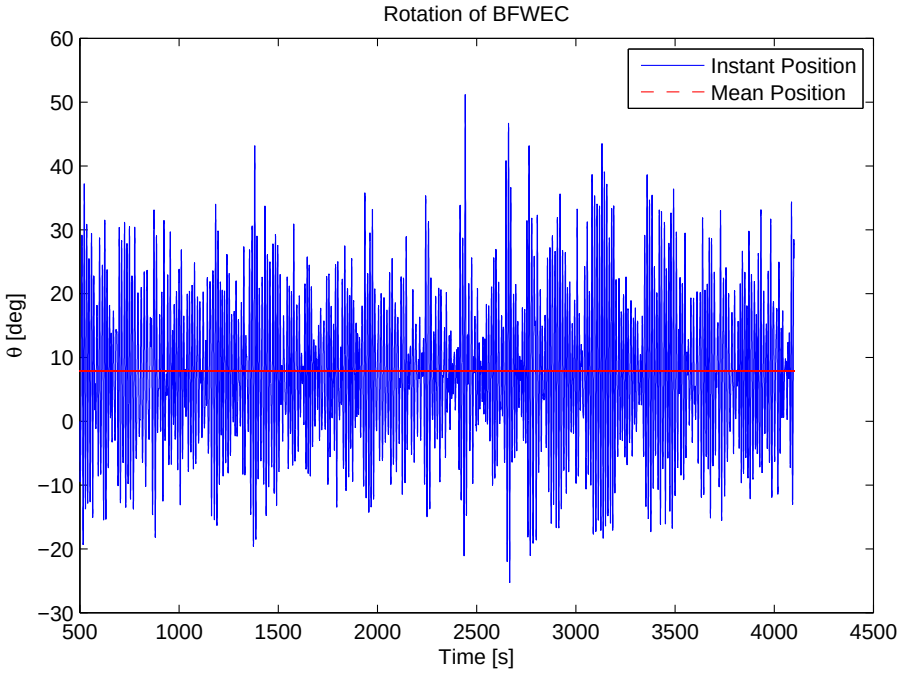

Figure 4.1: An example of time series for rotations of BFWEC.

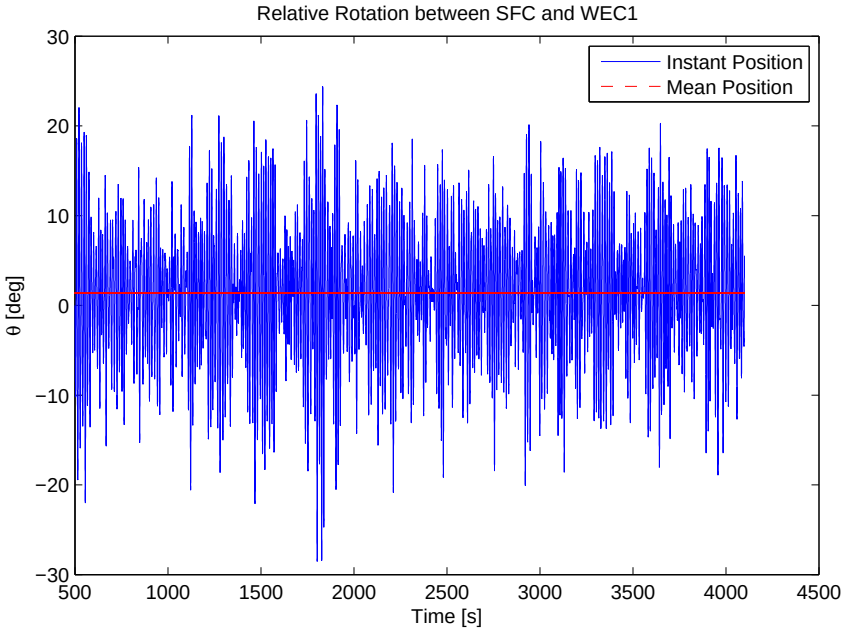

Figure 4.2: An example of time series for relative rotations between WEC and Semi-submersible.

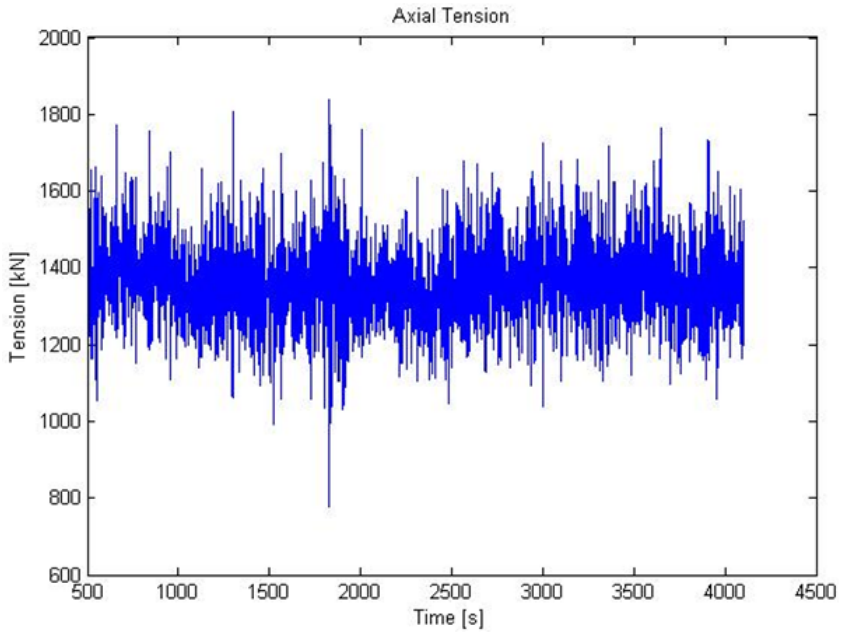

Figure 4.3: An example of time series for tensions acting on one segment of supporting arm of WEC.

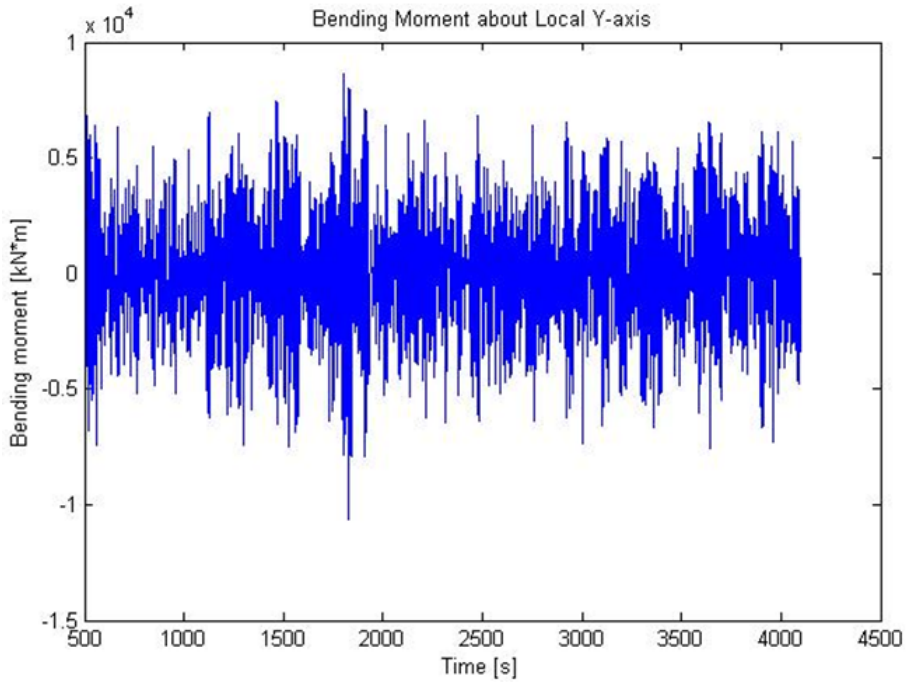

Figure 4.4: An example of time series for bending moments about Local Y-axis acting on one segment of supporting arm of WEC.

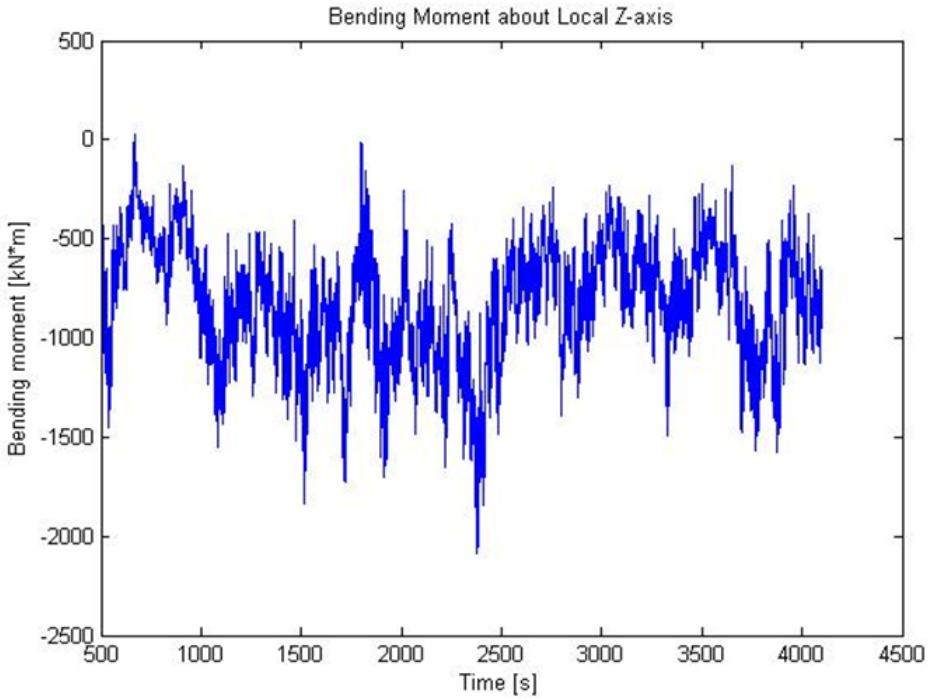

Figure 4.5: An example of time series for bending moments about Local Z-axis acting on one segment of supporting arm of WEC.

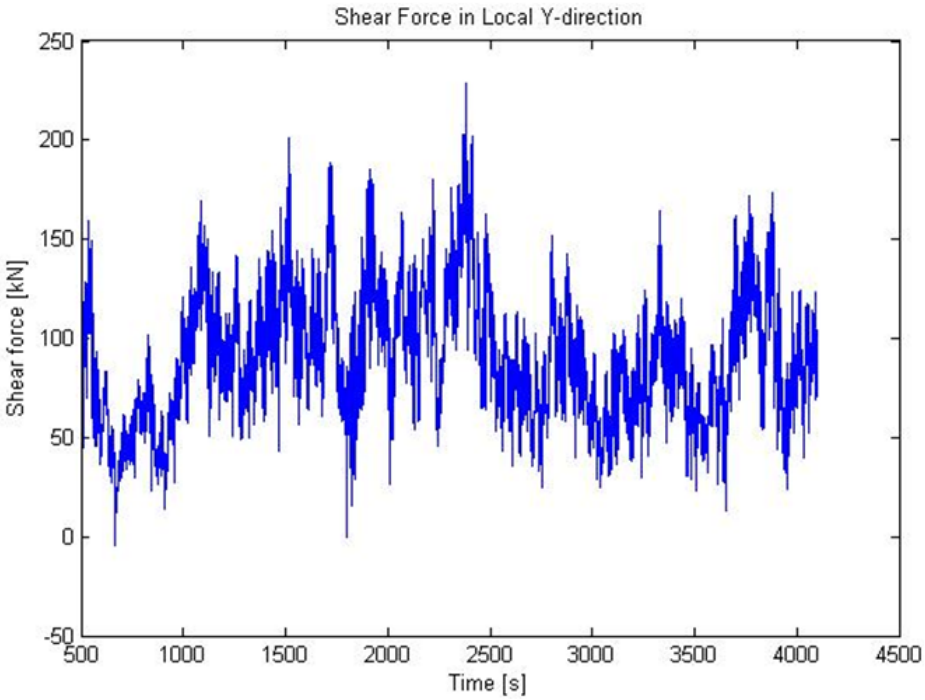

Figure 4.6: An example of time series for shear forces in local Y-axis acting on one segment of supporting arm of WEC.

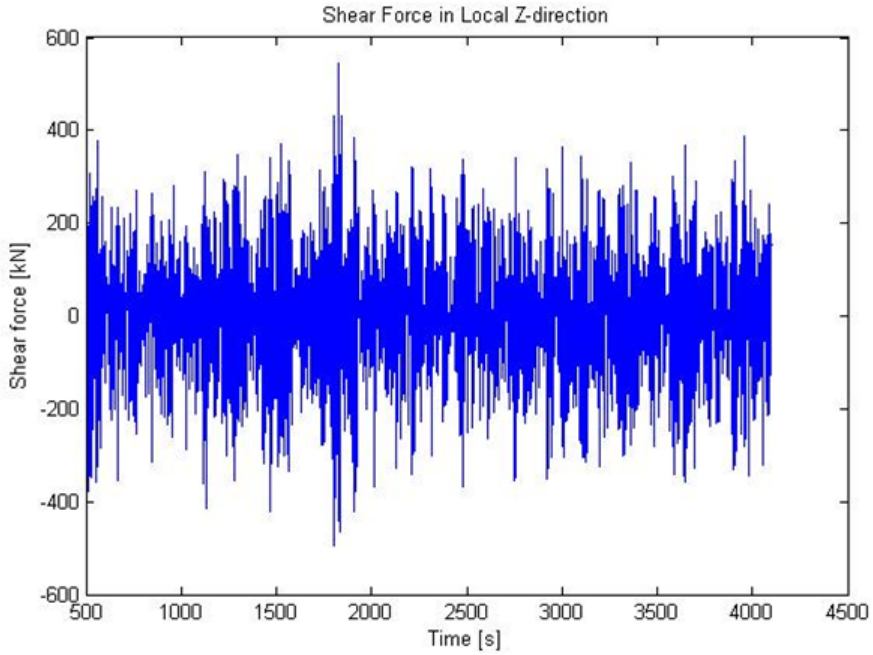

Figure 4.7: An example of time series for shear forces in local Z-axis acting on one segment of supporting arm of WEC.

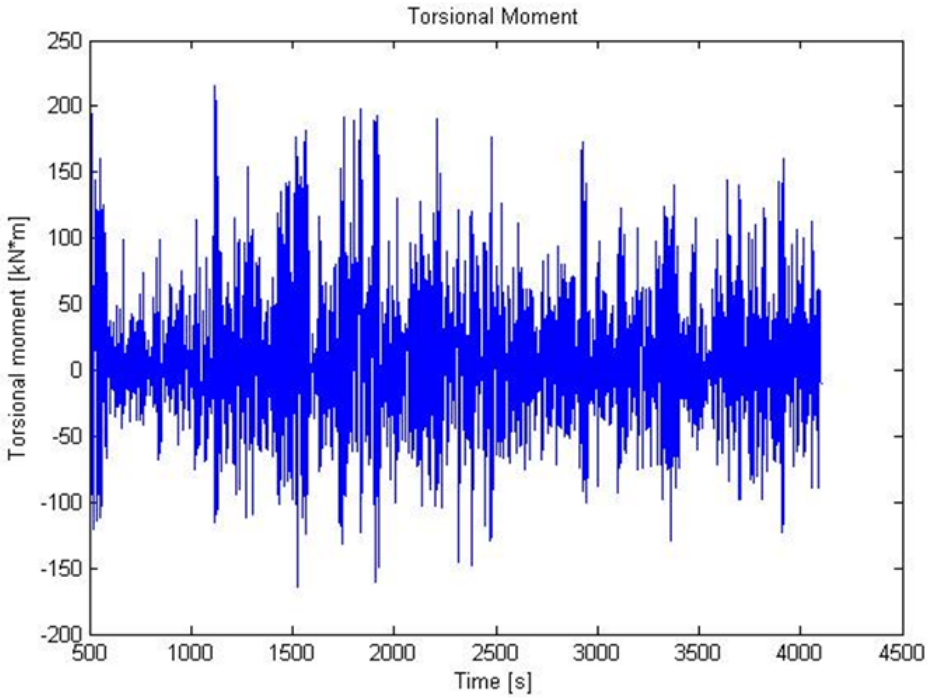

Figure 4.8: An example of time series for torsional moments acting on one segment of supporting arm of WEC.

Chapter 5

Natural Period of Bottom-Fixed Wave Energy Converter

Natural period of BFWEC in pitching motion is presented in this chapter. The coordinate is shown in Figure 3.1. It is evaluated analytically in Excel, denoted as T_n^E and numerically by simulation in SIMO/RIFLEX, denoted as T_n^S. A very basic conclusion derived from the comparison between T_n^E and T_n^S is that there is quite good agreement between them.

5.1 Analytic evaluation by Excel

Parameters of WEC and evaluation process is presented in Table 5.1. Two supporting arms and a flap are considered for the BFWEC. A detailed descriptions of WEC can be found in Chapter 3. In general, the natural frequency of a structure is given by (Clough and Penzien, 1993)

$$\omega_n = \sqrt{\frac{k}{m}}, \tag{5.1}$$

the natural period T_n^E is calculated by

$$T_n^E = \frac{2\pi}{\omega_n}, \tag{5.2}$$

where

k is the stiffness. Here it stands for the total stiffness of the BFWEC, which is provided by restoring moment. It comes from the difference between the gravity and buoyancy of BFWEC; m is the mass. In evaluation process, total inertia moment of BFWEC has to be calculated according to the mass. Total inertia moment consists of two parts, the inertia moment and added inertia moment. The former one is provided by the mass of BFWEC, the later one comes from added masses in surging and pitching motions.

BFWEC will rotate around Y-axis and added inertia mass in surging is denoted as A_{11}, added inertia moment in pitching is denoted as A_{55} in Table 5.1. A_{11} and A_{55} are calculated based on potential theory from simulation results in SIMO by Post Doc. Constantine Michailides. Both the restoring moments and inertia moments have to be calculated based on Y-axis. According to Table 5.1, the natural period T_n^E equals $14.3s$. Special attentions have to be paid to the choice of the added inertia moments in terms of the flap's motion and reasonable simulation results from SIMO.

5.2 Simulation of Decay Test in SIMO/RIFLEX

The model has been developed in SIMO/RIFLEX. Similar characteristics as presented in the analytic evaluation in Table 5.1 are used for the development of the numerical model. The basic principle for this decay test is that the flap will rotate around the Y-axis with smaller and smaller amplitudes when an external force is removed after acting on the flap for a certain period of time. Before starting the simulation, the sea surface has to be absolute calm. But if the wave height is set to be zero, it will result in the simulation problem in SIMO/RIFLEX. So a very small wave height of 0.001 m was defined in the three-parameter Jonswap wave spectrum. At the beginning, an external force F with magnitude $1500kN$ is acting on the centre of the flap, it lasts from t=0s to t=500s. During this period, the flap won't rotate but tilt at a certain angle, around 47^0 in Figure 5.1. When the external force is released, the flap will roatate around Y-axis. The rotation motion of flap is limited by the PTO system, which is simplified as a damping coefficient $C = 100kN * m * sec/deg$. So the flap will rotate with a smaller and smaller amplitude. The calculated decay curve

is plotted in Figure 5.1, where the horizontal axis is the time and the vertical axis is the rotation angle. From appropriate calculations using the decay curve, the natural period of the flap, T_n^S, is calculated to be around $15s$.

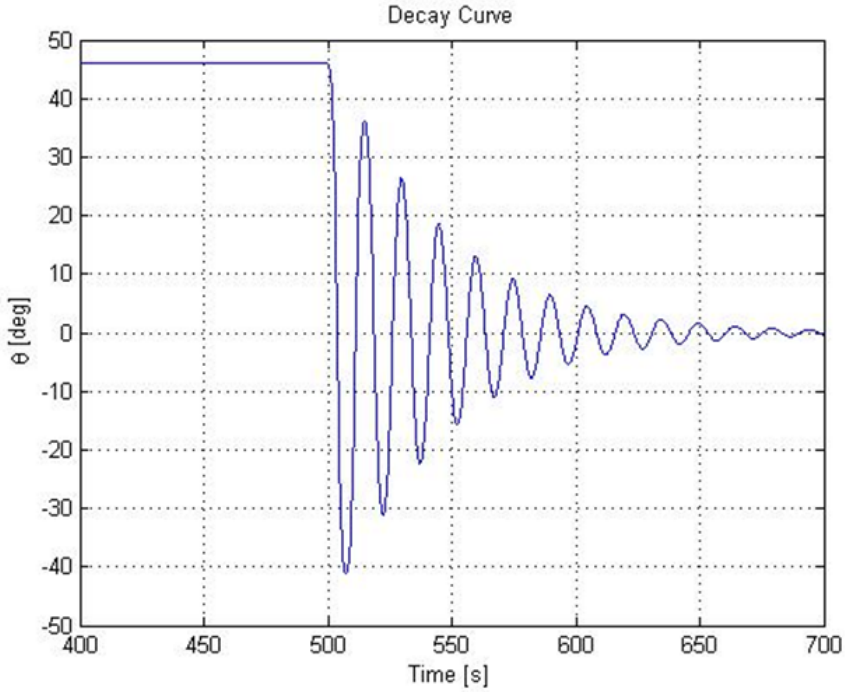

Figure 5.1: Decay curve of the BFWEC for pitching when $C = 100kN * m * sec/deg$.

Damping ratio of the system is donated as ζ, the damped natural frequency ω_d and undamped natural frequency ω_n. Then ω_n can be calculated as below(Clough and Penzien, 1993):

$$\omega_d = \frac{2\pi}{T_d}, \tag{5.3}$$

$$\omega_n = \frac{\omega_d}{\sqrt{1-\zeta^2}}, \tag{5.4}$$

where T is the period of the waveform, it is read from the time difference between two successive amplitudes in the decay curve. The average period is used in this case because there are several successive amplitudes as shown in Figure 5.1. The logarithmic decrement is defined as

$$\delta = \frac{1}{n} \cdot ln\left(\frac{x_0}{x_n}\right), \tag{5.5}$$

where $x_i (i = 0, 1, 2, \ldots, n)$ is the amplitude of the peak. The damping ratio is calculated by

$$\zeta = \frac{1}{\sqrt{1 + \left(\frac{2\pi}{\delta}\right)^2}} \tag{5.6}$$

Finally the natural period is calculated by

$$T_n = \frac{2\pi}{\omega_n}. \tag{5.7}$$

It is 14.9s.

The damping coefficient $C = 650kN * m * sec/deg$ is used in this thesis, another decay test is performed by setting damping coefficient $C = 650kN * m * sec/deg$. Since the damping coefficient is relatively large, the flap rotation will die out soon after releasing the external force as shown in Figure 5.2. Based on the decay curve, the same natural period $T_n = 14.9s$ is got.

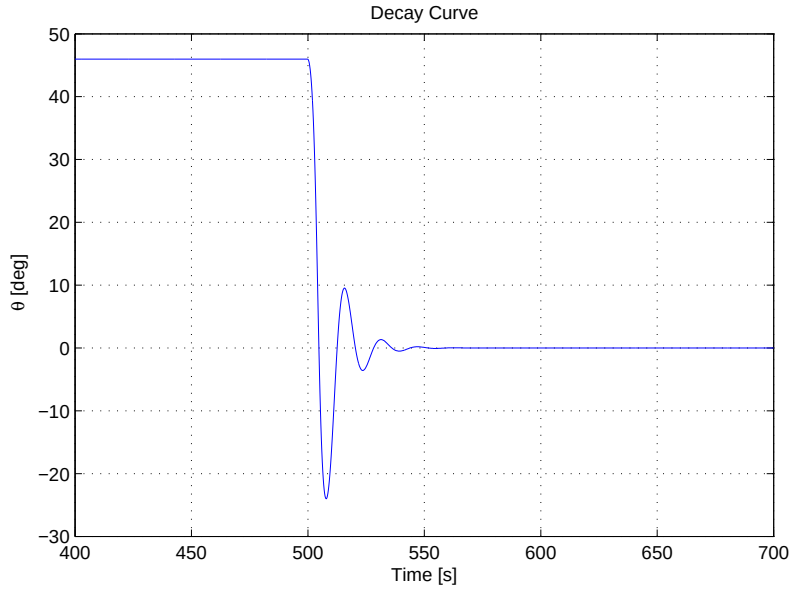

Figure 5.2: Decay curve of the BFWEC for pitching when $C = 650kN * m * sec/deg$.

5.3 Discussion on the Two Methods

The difference between these two natural periods is 0.6s, which is 4%. The result is acceptable. For the calculation of the natural period in the numerical modeling, sea surface is not absolutely calm which may result in minor difference. Also since the added inertia moments are got from SIMO, they will have influence on the final result. One suggestion to get a more accurate natural period is to do the modeling test in basin tank.

Table 5.1: Analytic evaluation of pitching natural period of BFWEC.

Structure	Parameter	Symbol	Unit	Magnitude
Arm	Sea Water Density	ρ_w	kg/m^3	1025
	Outer Diameter	D	m	1.5
	Thickness	t	m	0.05
	Length	L_A	m	18.5
	Section Area	A	m^2	0.228
	D/t			30
	Young's Modulus	E	MPa	2.1×10^5
	Density	ρ	kg/m^3	7850
	Volume	V	m^3	4.214
	Mass	M_A	$tonnes$	33.077
	2× Mass	$2M_A$	$tonnes$	66.154
	Displacement	∇_A	$tonnes$	33.510
	2× Displacement	$2\nabla_A$	$tonnes$	67.019
	Centre of Gravity	$C.O.G$	m	9.25
	Centre of Buoyancy	$C.O.B$	m	9.25
	Inertia Moment	I_{11}	$tonnes$	33.077
		I_{55}	$ton \cdot m^2$	943.39
		$I_{11} \cdot C.O.G^2 + I_{55}$	$ton \cdot m^2$	7547.123
	Added Inertia Moment	A_{A11}	$tonnes$	28.740
		A_{A55}	$ton \cdot m^2$	1848
		$A_{A11} \cdot C.O.G^2 + A_{A55}$	$ton \cdot m^2$	8614.133
Flap	Mass	M_F	$tonnes$	100
	Length	L_F	m	20
	Length of Major Axis	L_{ma}	m	7
	Length of Minor Axis	L_{mi}	m	3.5
	Displacement	∇_F	$tonnes$	394.466
	Centre of Gravity	$C.O.G$	m	18.5
	Centre of Buoyancy	$C.O.B$	m	18.5
	Inertia Moment	I_{F11}	$tonnes$	100
		I_{F55}	$ton \cdot m^2$	654.87
		$I_{F11} \cdot C.O.G^2 + I_{F55}$	$ton \cdot m^2$	34879.87
	Added Inertia Moment	A_{F11}	$tonnes$	602.9
		A_{F55}	$ton \cdot m^2$	19140
		$A_{F11} \cdot C.O.G^2 + A_{F55}$	$ton \cdot m^2$	225482.525
WEC	Centre of Gravity	$C.O.G$	m	14.817
	Centre of Buoyancy	$C.O.B$	m	17.157
	Total Mass	M	$tonnes$	166.154
	Total Displacement	∇	$tonnes$	461.485
	Restoring Moment	k	$ton \cdot m$	53519.653
	Added Inertia Moment	m_{ai}	$ton \cdot m^2$	234096.658
	Inertia Moment	m_i	$ton \cdot m^2$	42426.993
	Total Inertia Moment	m	$ton \cdot m^2$	276523.650
	Natural Frequency	ω_n	rad/s	0.440
	Natural Period	T_n^E	s	14.3

Chapter 6

Design Check for Ultimate Limit States

External forces acting on WECs are exported from simulations as explained in Chapter 4. Strength check of Ultimate Limit States(ULS) is made based on the NORSOK Standard N004 (Standards Norway, 2004). For the supporting arms of WECs, corresponding stresses have to meet the requirements of tubular members given by the standard.

6.1 Strength Requirements

In NORSOK Standard N004, each force has to be calculated directly or indirectly and a result will be got from that, which should be smaller than a ULS value. Utility factor(UF) is used to have more intuitive and consistent results through different forces and their combinations. It is defined as calculated result of external force divided by suggested value or limited strength made by the standard. They will be defined separately in the following.

The arm subjected to the axial tensile loads should be designed to satisfy the following condition:

$$N_{Sd} \leq N_{t,Rd} = \frac{A f_y}{\gamma_M}$$

On the left side of the inequity sign, N_{Sd} is the axial force acting on WECs, which is defined as external force. On the right side, $N_{t,Rd}$ is limited axial strength calculated according to

the suggested formula. N_{Sd} should be smaller than $N_{t,Rd}$ in the design. Utility Factor(UF) is defined as

$$UF = \frac{N_{Sd}}{N_{t,Rd}}$$

If UF is smaller than one, then the structural design in terms of tension is safe. A smaller UF means more strength reserve. But designed structure is not fully made use of. Comparison between UF and One is used for all forces instead of comparison between two forces. A more detailed explanation about formula and letters can be found in the NORSOK Standard N004.

Not only a single force is checked, combinations of different forces are more critical. An example is the combination of shear force and bending moment. The structure should satisfy the following condition:

$$\frac{M_{Sd}}{M_{Rd}} \leq \sqrt{1.4 - \frac{V_{Sd}}{V_{Rd}}} \qquad \text{for} \qquad \frac{V_{Sd}}{V_{Rd}} \geq 0.4$$

$$\frac{M_{Sd}}{M_{Rd}} \leq 1.0 \qquad \text{for} \qquad \frac{V_{Sd}}{V_{Rd}} < 0.4$$

In this case, Utility Factor is defined as

$$UF = \frac{\frac{M_{Sd}}{M_{Rd}}}{\sqrt{1.4 - \frac{V_{Sd}}{V_{Rd}}}} \qquad \text{for} \qquad \frac{V_{Sd}}{V_{Rd}} \geq 0.4$$

$$UF = \frac{M_{Sd}}{M_{Rd}} \qquad \text{for} \qquad \frac{V_{Sd}}{V_{Rd}} < 0.4$$

In summary, the following forces and combinations are checked: axial tension, bending moment, shear stress, combination of axial tension and bending moment without hydrostatic pressure, interaction between shear and bending moment and interaction between shear, bending moment, and torsional moment. The utility factors are defined in Table 6.1.

Table 6.1: Utility Factors for different forces.

Forces	UF
Axial tension	$\frac{N_{Sd}}{N_{t,Rd}}$
Bending moment	$\frac{M_{Sd}}{M_{Rd}}$
Shear force	$\frac{V_{Sd}}{V_{Rd}}$
Torsion moment	$\frac{M_{T,Sd}}{M_{T,Rd}}$
Combination: Tension and Bending	$\left(\frac{N_{Sd}}{N_{t,Rd}}\right)^{1.75} + \frac{\sqrt{M_{y,Sd}^2 + M_{z,Sd}^2}}{M_{Rd}} \leq 1.0$
Combination: Shear and Bending	$\frac{\frac{M_{Sd}}{M_{Rd}}}{\sqrt{1.4 - \frac{V_{Sd}}{V_{Rd}}}}$ for $\frac{V_{Sd}}{V_{Rd}} \geq 0.4$
	$\frac{M_{Sd}}{M_{Rd}} \leq 1.0$ for $\frac{V_{Sd}}{V_{Rd}} < 0.4$
Combination: Shear, Bending and Torsion	$\frac{\frac{M_{Sd}}{M_{Red,Rd}}}{\sqrt{1.4 - \frac{V_{Sd}}{V_{Rd}}}}$ for $\frac{V_{Sd}}{V_{Rd}} \geq 0.4$
	$\frac{M_{Sd}}{M_{Red,Rd}}$ for $\frac{V_{Sd}}{V_{Rd}} < 0.4$

6.2 Strength Check

Since external forces are generated according to time history series, strength check is also carried out in this manner, thus time history series of UFs are got for different forces. The NORSOK Standard N004 is coded in Matlab (Appendix A), external forces got from RIFLEX are loaded and can be checked according to the standard continuously in Matlab. If all UFs are smaller than one in all series, then the design can be regarded as safe and reliable. There are some differences in the UFs between operational sea state ($Hs = 6m$, $Tz = 12.6s$) and survival sea state($Hs = 15.6m$, $Tz = 14.5s$), they will be discussed separately.

6.2.1 Strength Check in Operational Sea Sate

For the model of SFC, a maximum utility factor of 0.509 is observed in all simulations of operational sea state, when $Hs = 6m$, $Tz = 12.6s$, wind velocity $V = 18m/s$, wave direction $\theta = 30^0$ and seed number is set to 300. It happens to the left supporting arm of WEC2. So strength check in this case (called the Critical Case) will be explained and discussed in detail as an example. Another maximum utility factor of 0.509 is observed when $Hs = 6m$, $Tz = 12.6s$, wind velocity $V = 11.4m/s$, wave direction $\theta = 30^0$ and seed number is set to 300. But the former one will be discussed in detail as an example.

Firstly, all the external forces acting on WECs are output by simulations. More specifically, there are four segments for each supporting arm, which means forces are stored for each segment separately. Time histories of forces for each segment are much like the ones shown from Figure 4.3 to Figure 4.8 , the only difference for different segments and various sea states is the force magnitude. There are six forces in total and for strength check their combinations have to been considered as well. Secondly, UFs are calculated as defined before by Matlab, time histories of UFs for segment one in the Critical Case are plotted from Figure 6.1 to Figure 6.7. Since there are two bending moments and two shear forces, a lot of force combinations should be checked. But in reality, only the bigger force is concerned and one bending moment and one shear force are checked as a result. So there are seven UFs in total for one segment in one sea state. As mentioned, what is

concerned is the biggest value, the maximum utility factor. As the third step, a maximum utility factor is picked out from the seven time histories of utility factors for each segment. For one supporting arm, there are four maximum utility factors and their corresponding forces or force combinations. The results are shown in Table 6.2 for the Critical Case. The biggest one of the four maximum utility factors is selected out as the Maximum Utility Factor (MUF) of one supporting arm for a given sea state with a specified seed number. It can be told from Table 6.2 and Figure 6.8 that segment one is the most critical one with the maximum forces and maximum utility factors as expected. Because segment one can be simply understood as a fixed end (fixed to the PTO system) and segment four is a free end connected to the flap that can rotate without any restrictions. As a result, maximum bending moments and shear forces are experienced by segment one. Besides, MUFs always come from combination forces. Fourthly, twenty seed numbers are chosen for each sea state, which means twenty different realizations of simulation. Thus there will be twenty maximum utility factors in total for one sea state. They are expressed in the form as shown in Figure 6.9. From that, the Final Maximum Utility Factor (FMUF) can be recognized and it is 0.509 when seed number is 300 for the Critical Case. These steps are implemented for all the sea states. The maximum utility factor figures for all sea states are put in Appendix B.

Utility factors of WECs for all sea states are summarized in Table 6.3 and from Figure 6.10 to Figure 6.13. From Figure B.4, Figure B.5 and Figure B.6 in Appendix B and Figure 6.10, it can be told that UFs for WEC2 and WEC3 are almost the same when wave direction is set to be 0^0 . Because the SFC model is symmetric about X-axis in the coordinate (Figure 3.5), although the Semi-submersible will move in six degrees of freedom induced by waves and winds, it doesn't have much influence on the external loads experienced by WEC2 and WEC3. WEC1 has the maximum utility factor when wave direction is 90^0, and WEC2 has the maximum utility factor when wave direction is 30^0 , in both cases waves propagate perpendicularly to the flap.

For the BFWEC, the same steps are carried out in previous project thesis. The MUF figures for all operational sea states are put in Appendix B. They are also summarized in

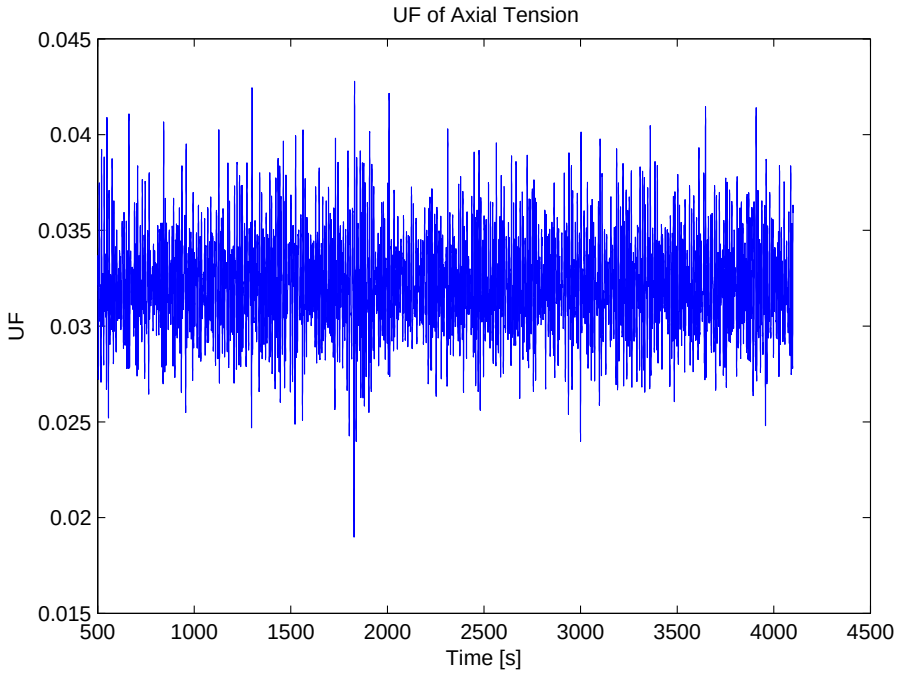

Figure 6.1: UFs' time history of axial tensions when $Hs = 6m, Tz = 12.6s, V = 18m/s, \theta = 30^0, WEC2$.

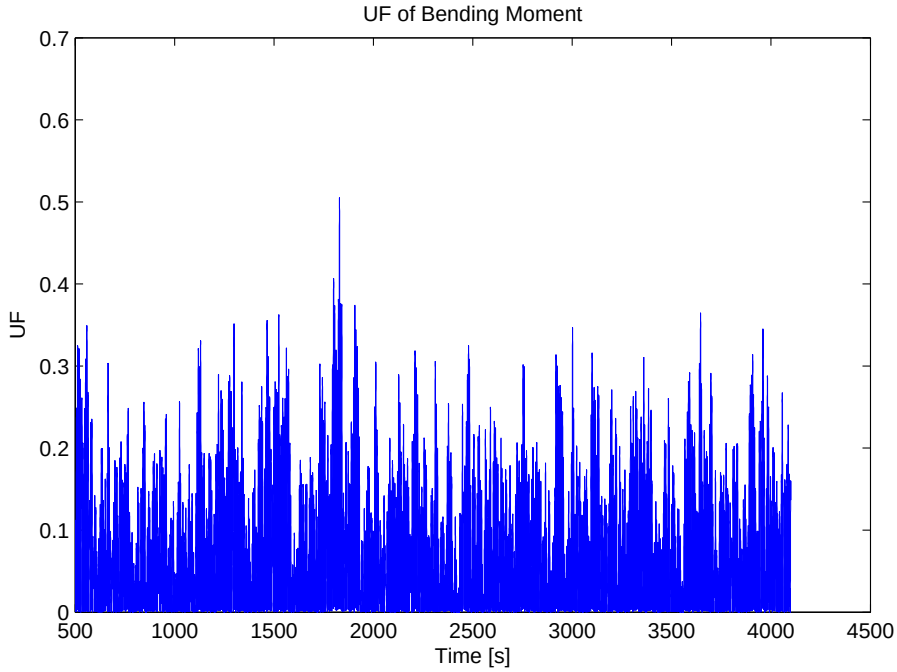

Figure 6.2: UFs' time history of bending moments when $Hs = 6m, Tz = 12.6s, V = 18m/s, \theta = 30^0, WEC2$.

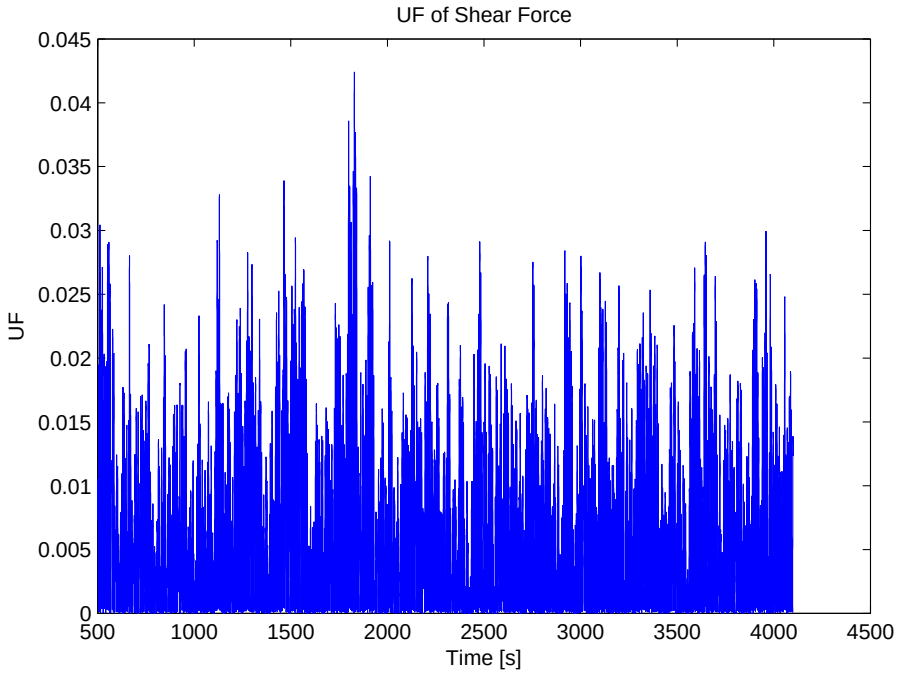

Figure 6.3: UFs' time history of shear forces when $Hs = 6m, Tz = 12.6s, V = 18m/s, \theta = 30^0, WEC2$.

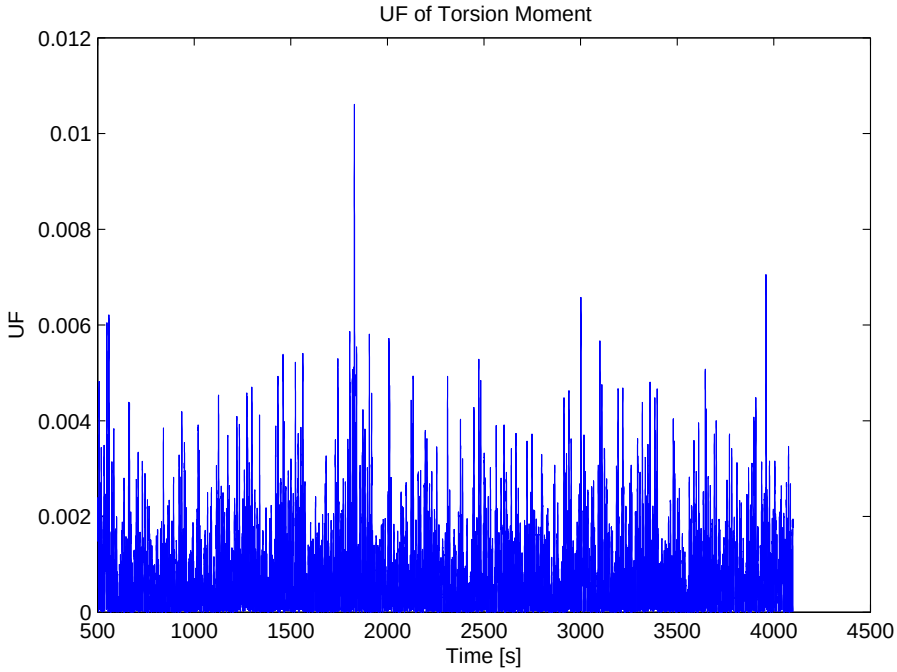

Figure 6.4: UFs' time history of torsion moments when $Hs = 6m, Tz = 12.6s, V = 18m/s, \theta = 30^0, WEC2$.

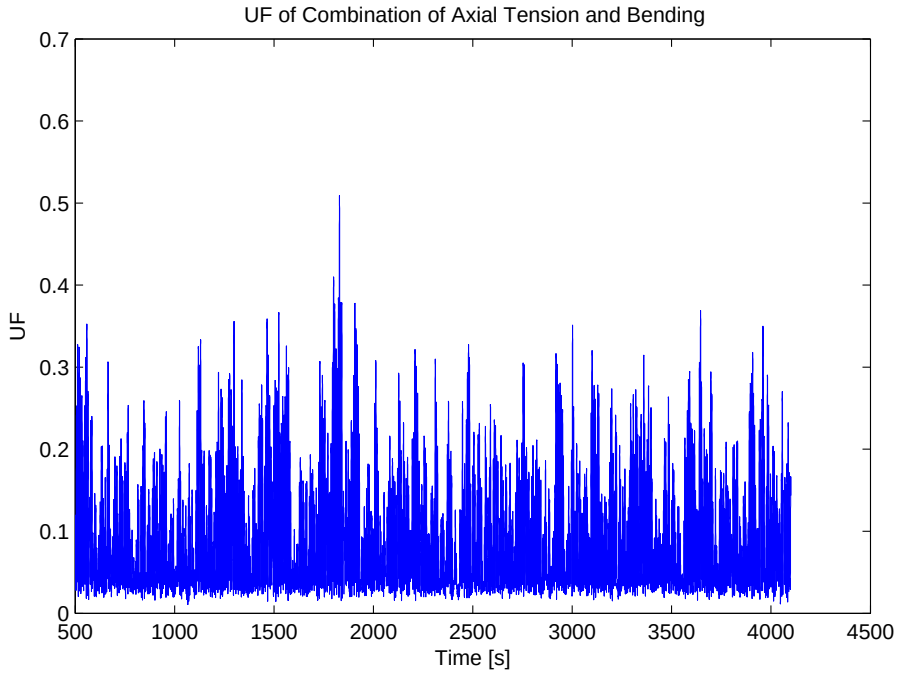

Figure 6.5: UFs' time history of combinations of axial tension and bending when $Hs = 6m, Tz = 12.6s, V = 18m/s, \theta = 30^0, WEC2$.

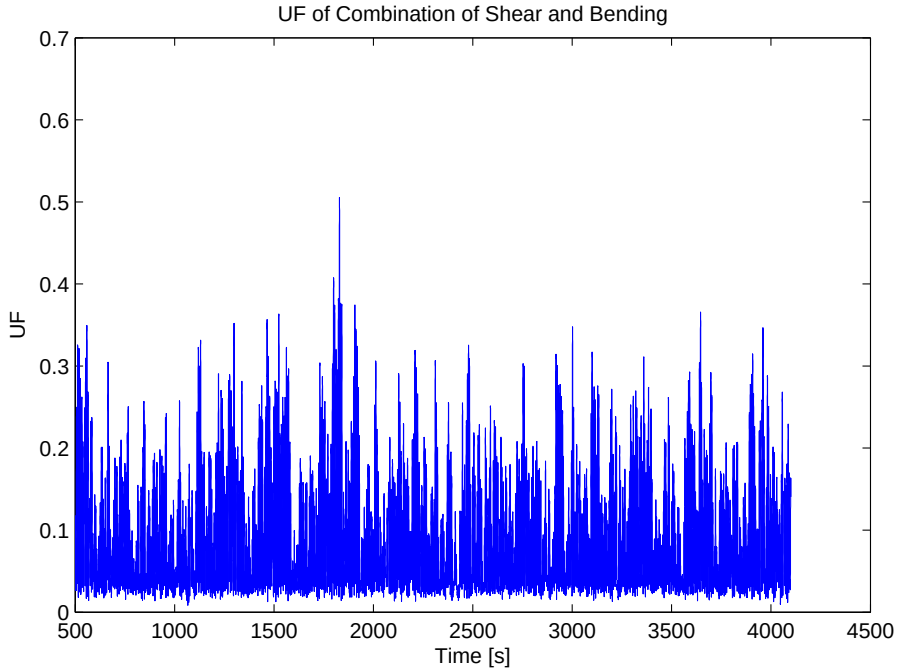

Figure 6.6: UFs' time history of combinations of shear and bending when $Hs = 6m, Tz = 12.6s, V = 18m/s, \theta = 30^0, WEC2$.

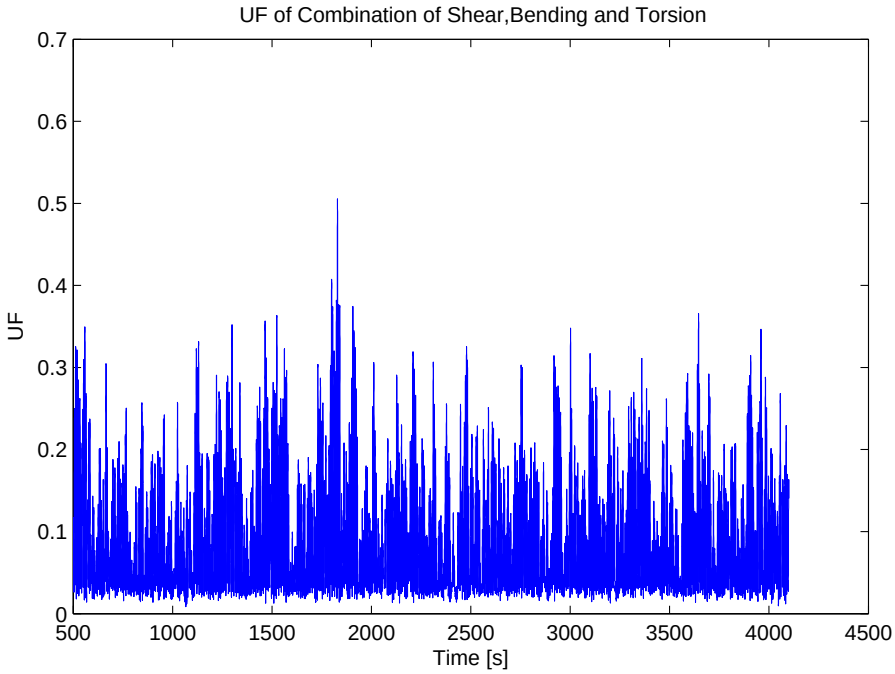

Figure 6.7: UFs' time history of combinations of shear, bending and torsion when $Hs = 6m, Tz = 12.6s, V = 18m/s, \theta = 30^0, WEC2$.

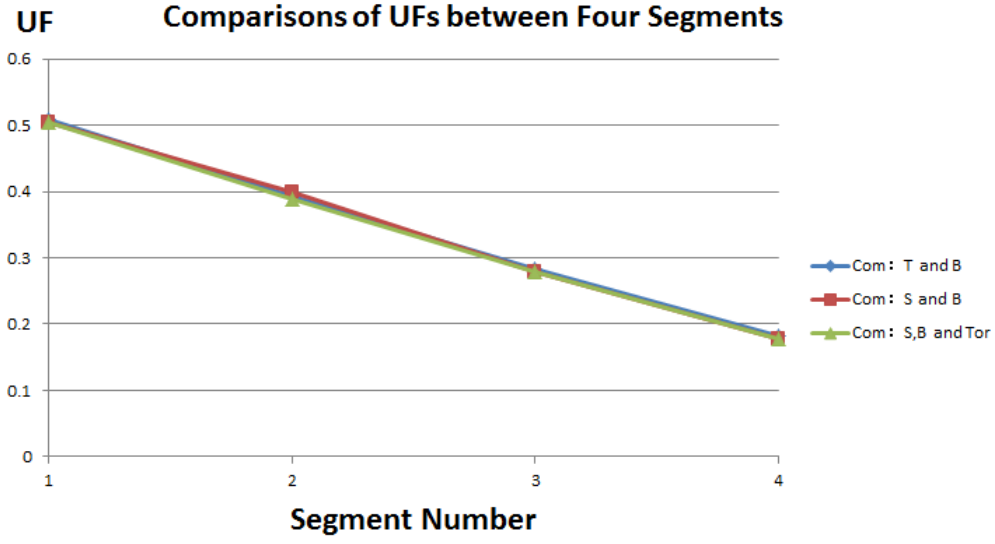

Figure 6.8: Comparisons of UFs between Four Segments for left supporting arm of WEC2 when $Hs = 6m, Tz = 12.6s, V = 18m/s$, seed number= 300.

Table 6.2: Maximum forces and UFs of four segments for left supporting arm of WEC2 when $Hs = 6m, Tz = 12.6s, V = 18m/s$, seed number= 300.

Element		$N[N]$	$My[N*m]$	$Mz[N*m]$	$Vy[N]$	$Vz[N]$	$M_T[N*m]$	Com:N and M	Com:V and M	Com:V, M and M_T
1	Value	1991233	10848795	950156	104143	569545	200064			
	UF	0.043	0.505	0.044	0.008	0.042	0	0.509	0.505	0.505
2	Value	1986018	8364291	471061	103472	571579	200049			
	UF	0.043	0.389	0.022	0.008	0.043	0	0.393	0.398	0.389
3	Value	1976579	6001521	9763	102789	592805	200035			
	UF	0.042	0.279	0.000	0.008	0.044	0	0.283	0.279	0.279
4	Value	1962824	3788390	477811	102055	645108	200019			
	UF	0.042	0.176	0.022	0.008	0.048	0	0.181	0.177	0.177
Max	Value	1991233	10848795	950156	104143	569545	200064			
	UF	0.043	0.505	0.044	0.008	0.042	0	0.509	0.505	0.505

Symbols:N is axial tension, My is bending moment about local Y-axis, Mz is bending moment about local Z-axis, Vy is shear force in local Y-direction, Vz is shear force in local Z-direction, M_T is torsional moment, Com is abbreviation for force combination. Coordinate system refers to Figure 3.7

Table 6.3: Maximum Utility Factors of WECs of SFC operational sea state.

(a) Maximum Utility Factors of WECs of SFC in operational sea state when $V = 8m/s$.

Sea state		$Hs[m]$	6		$Tz[s]$	12.6		$V[m/s]$	8	
θ^0	0			30			45			90	
WECs	WEC1	WEC2	WEC3	WEC1	WEC2	WEC3	WEC1	WEC2	WEC3	WEC1	WEC2	WEC3
Seed number	300	450	450	300	300	300	300	300	450	300	300	450
MUF	0.252	0.470	0.465	0.350	0.506	0.336	0.422	0.506	0.263	0.500	0.343	0.345

(b) Maximum Utility Factors of WECs of SFC in operational sea state when $V = 11.4m/s$.

Sea state		$Hs[m]$	6		$Tz[s]$	12.6		$V[m/s]$	11.4	
θ^0	0			30			45			90	
WECs	WEC1	WEC2	WEC3	WEC1	WEC2	WEC3	WEC1	WEC2	WEC3	WEC1	WEC2	WEC3
Seed number	300	450	450	300	300	300	300	300	300	300	300	450
MUF	0.276	0.465	0.463	0.363	0.509	0.342	0.425	0.507	0.267	0.493	0.339	0.347

(c) Maximum Utility Factors of WECs of SFC in operational sea state when $V = 18m/s$.

Sea state		$Hs[m]$	6		$Tz[s]$	12.6		$V[m/s]$	18	
θ^0	0			30			45			90	
WECs	WEC1	WEC2	WEC3	WEC1	WEC2	WEC3	WEC1	WEC2	WEC3	WEC1	WEC2	WEC3
Seed number	300	450	450	300	300	450	300	300	650	300	300	450
MUF	0.252	0.470	0.468	0.352	0.509	0.340	0.422	0.506	0.262	0.497	0.340	0.339

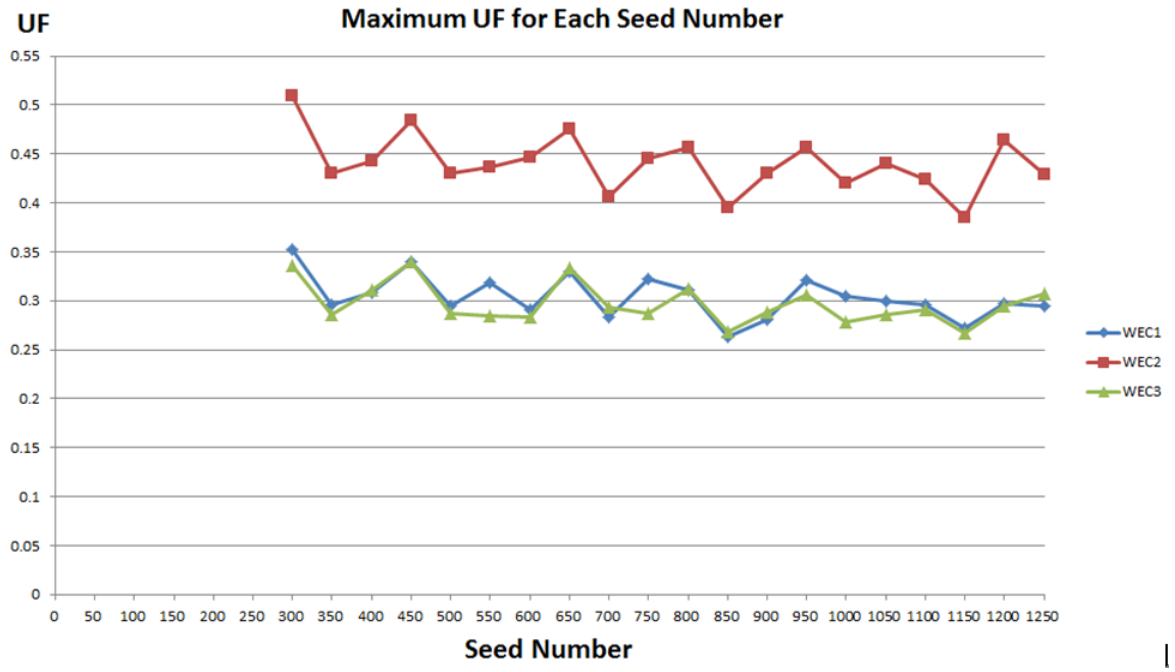

Figure 6.9: Maximum utility factor for each seed number when $Hs = 6m, Tz = 12.6s, V = 18m/s, \theta = 30^0$.

Table 6.4. The MUF happens to segment one as well. The FMUF is 0.654 when wave direction is 0^0, this also happens to segment one of the supporting arm. The FMUF is bigger than that of WECs in the SFC model, which is 0.509.

Table 6.4: MUFs of BFWEC in operational sea state.

Sea state	$Hs = 6m$		$Tz = 12.6s$	
θ^0	0	30	45	90
Seed number	650	300	300	300
MUF	0.654	0.587	0.501	0.249

When making comparisons between the BFWEC and WECs of SFC, wave directions have to be considered because of locations of WECs in their own coordinate systems. In other words, if two WECs are put together to make comparisons, their wave directions have to be the same. For example, the BFWEC with wave direction 0^0 can be compared with WEC1 of SFC when wave direction is 90^0, and WEC2 of SFC when wave direction is

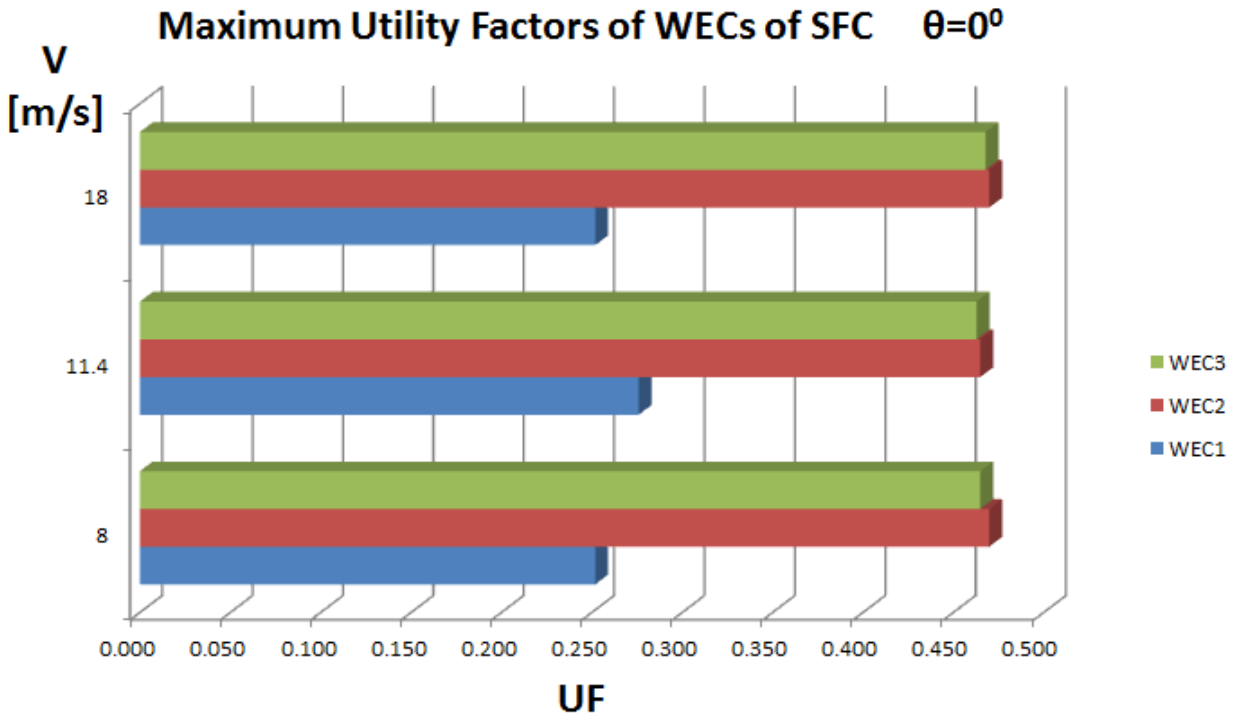

Figure 6.10: MUFs of WECs of SFC when $\theta = 0^0$ in operational sea state.

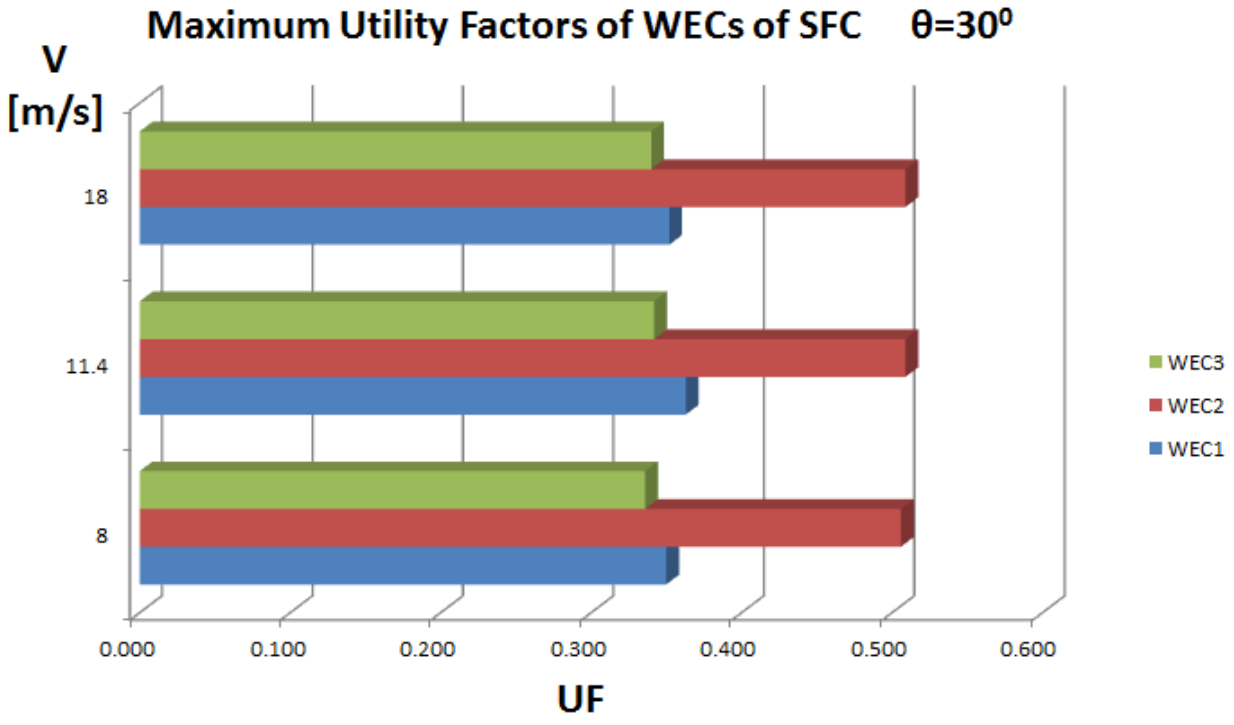

Figure 6.11: MUFs of WECs of SFC when $\theta = 30^0$ in operational sea state.

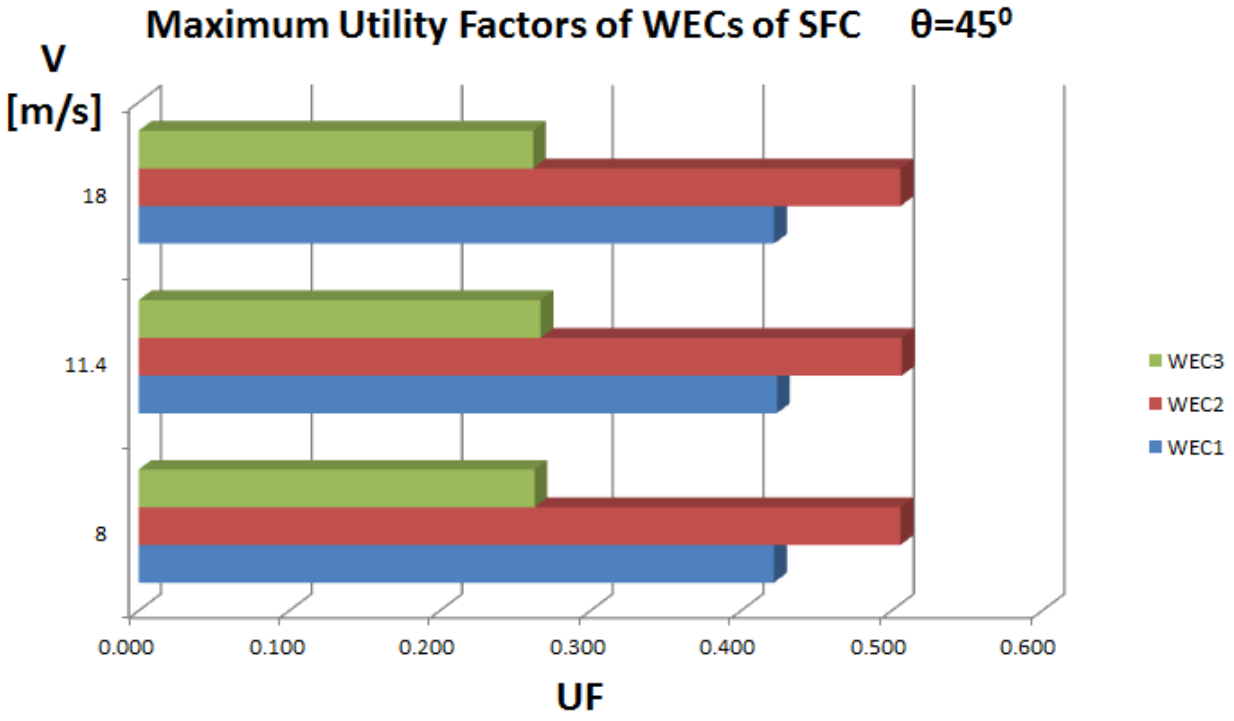

Figure 6.12: MUFs of WECs of SFC when $\theta = 45^0$ in operational sea state.

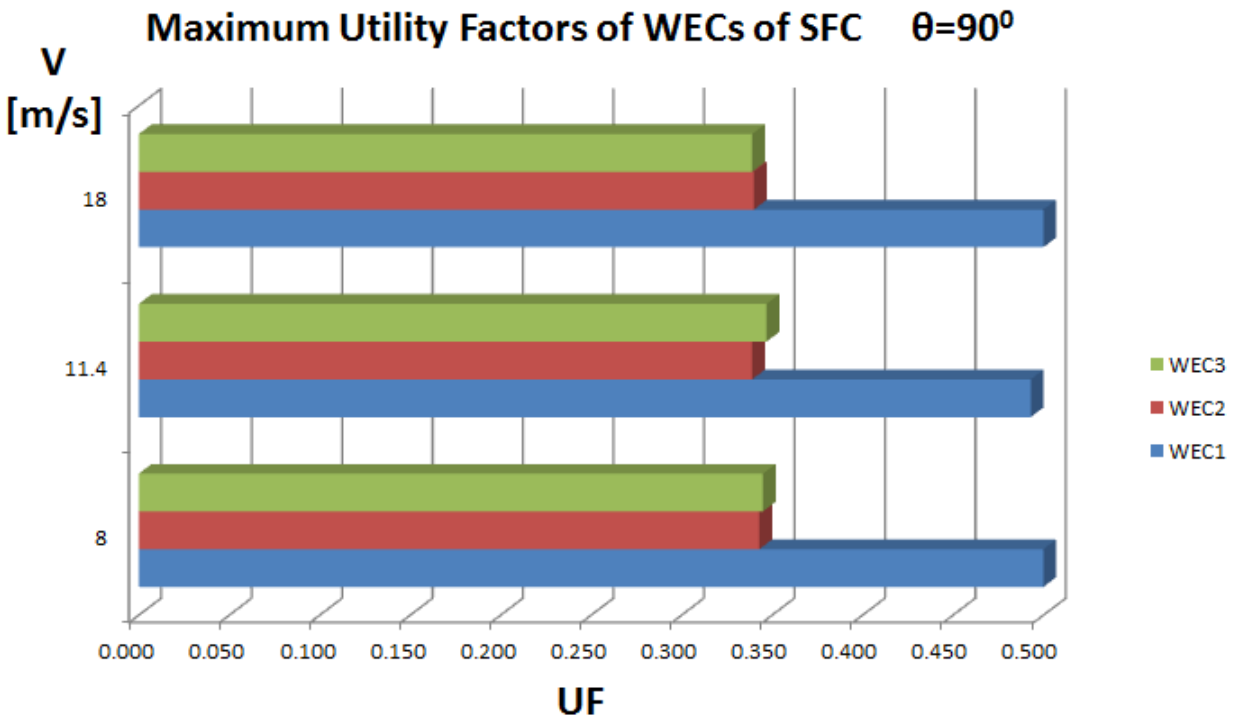

Figure 6.13: MUFs of WECs of SFC when $\theta = 90^0$ in operational sea state.

30^0. For clarity, WECs with the same wave direction are listed in Table 6.5. The comparisons of MUFs are plotted in Figure 6.14. In Figure 6.14, the wave direction is regarding to the coordinate system of BFWEC, the corresponding MUFs of WECs of SFC are plotted together with BFWEC. Generally UFs of WECs of SFC are smaller than those of BFWEC. Wind-wave-induced motions of SFC will have relative motions between WECs and the hull, which reduces external loads acting on the supporting arms. It is a good point that external loads are reduced and even not, the FMUF is still much smaller than one, that means this design is safe for the operational sea state, or maybe a little bit conservative. As to the wind-wave-induced motions of SFC, they also have influences on produced power, which should catch more attention. So wind-wave-induced motions of SFC and relative motions between WECs and Semi-submersible will be discussed in next chapter. Besides, for both BFWEC and WECs of SFC, the maximum MUFs happen when wave direction is 0^0 and the minimum ones happen when wave direction is 90^0.

Table 6.5: WECs with the same wave direction.

BFWEC	WECs of SFC			
	0^0	30^0	45^0	90^0
0^0		WEC2		WEC1
30^0	WEC2, WEC3			
45^0			WEC1	
90^0	WEC1			

6.2.2 Strength Check in Survival Sea State

The same steps apply to the strength check in survival sea state. The time histories of utility factors can be got in the same way as illustrated in operational sea state.

For WECs of SFC, the MUFs are listed in Table 6.6 and also plotted from Figure 6.15 to Figure 6.18. The FMUF is 0.826 when wind velocity is $11.4 m/s$ and wave direction is 30^0 (called the Critical Case). It happens to the left supporting of WEC2 when seed number is set to 650. The FMUF is very close to one and in this case the structure has been fully made use of with some strength reserve. In this sea state, the maximum forces and utility factors of four segments for left supporting arm of WEC2 are listed in Table 6.7 and a comparion between the four segments is plotted in Figure 6.19. It can tell that segments one is no

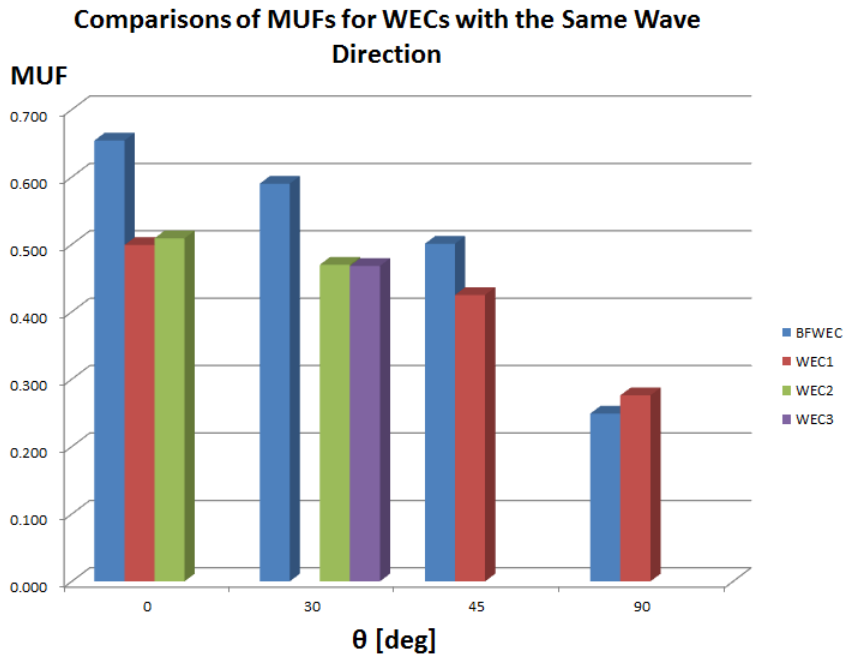

Figure 6.14: Comparisons of MUFs between BFWEC and WECs of SFC with the same wave direction.

longer the most critical segment that experiences the maximum utiity factor, instead segment four does. This is the effect of damping coefficient when it is set to zero. In this case, the lower end of supporting arm connected to the PTO system can be regarded as simply surpported. The upper end connected to the flap will be restricted by the flap motions. This is a major difference between the opearational sea state and survival sea state. WEC2 and WEC3 still have very close MUFs when wave direction is zero.

For the BFWEC, the MUFs for each wave direction are listed in Table 6.8. The FMUF is 0.566 when wave directions are 30^0 and 90^0, seed numbers are 300 and 800 respectively. The maximum UF of the four MUFs happens when wave directions are 30^0 and 90^0, not 0^0 any more. It is very surpsising that the FMUF happens when waves propagate parrallel to the flap, not perpendicular to the flap. From Table 6.9, it indicates that the FMUF happens to segment four when wave direction is 30^0 and segment one when wave direction is 90^0. Besides, the FMUF of BFWEC is quite small compared to the FMUF of WECs of SFC in survival condition, which is 0.826. The FMUF of BFWEC in survival condition is even smaller than the FMUF of BFWEC in operational condition, which is 0.654. The comparisons of BFWEC between these two conditions are plotted in Figure 6.20. It indicates the

Table 6.6: Maximum Utility Factors of WECs of SFC survival sea state.

(a) Maximum Utility Factors of WECs of SFC survival sea state when $V = 8m/s$.

Sea state		$Hs[m]$	15.6		$Tz[s]$	14.5		$V[m/s]$	8	
$\theta[^0]$	0			30			45			90	
WECs	WEC1	WEC2	WEC3	WEC1	WEC2	WEC3	WEC1	WEC2	WEC3	WEC1	WEC2	WEC3
Seed number	800	650	600	950	650	650	800	650	650	800	800	850
MUF	0.497	0.420	0.400	0.436	0.793	0.483	0.424	0.660	0.534	0.468	0.408	0.492

(b) Maximum Utility Factors of WECs of SFC survival sea state when $V = 11.4m/s$.

Sea state		$Hs[m]$	15.6		$Tz[s]$	14.5		$V[m/s]$	11.4	
$\theta[^0]$	0			30			45			90	
WECs	WEC1	WEC2	WEC3	WEC1	WEC2	WEC3	WEC1	WEC2	WEC3	WEC1	WEC2	WEC3
Seed number	800	950	650	800	650	800	800	650	800	600	1000	800
MUF	0.534	0.461	0.442	0.471	0.826	0.492	0.397	0.684	0.540	0.446	0.401	0.494

(c) Maximum Utility Factors of WECs of SFC survival sea state when $V = 18m/s$.

Sea state		$Hs[m]$	15.6		$Tz[s]$	14.5		$V[m/s]$	18	
θ^0	0			30			45			90	
WECs	WEC1	WEC2	WEC3	WEC1	WEC2	WEC3	WEC1	WEC2	WEC3	WEC1	WEC2	WEC3
Seed number	800	600	600	800	650	800	800	650	650	600	1000	800
MUF	0.514	0.408	0.398	0.446	0.733	0.478	0.412	0.611	0.531	0.458	0.403	0.481

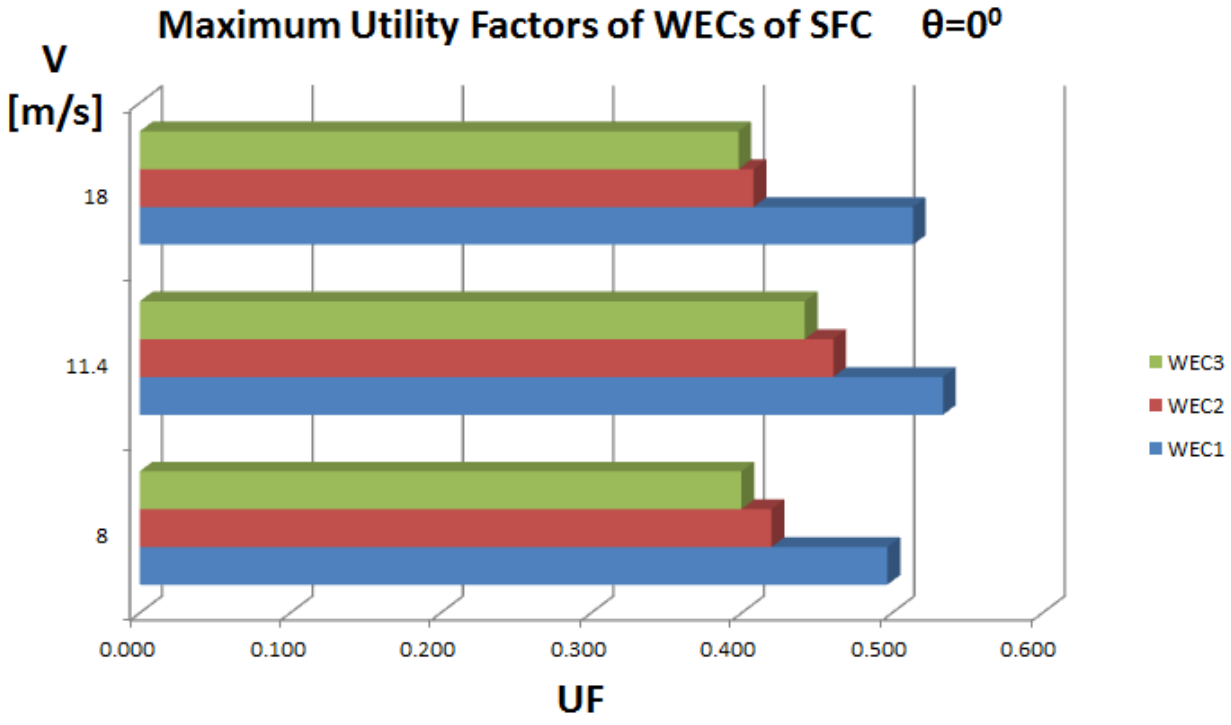

Figure 6.15: MUFs of WECs of SFC when $\theta = 0^0$ in survival sea state.

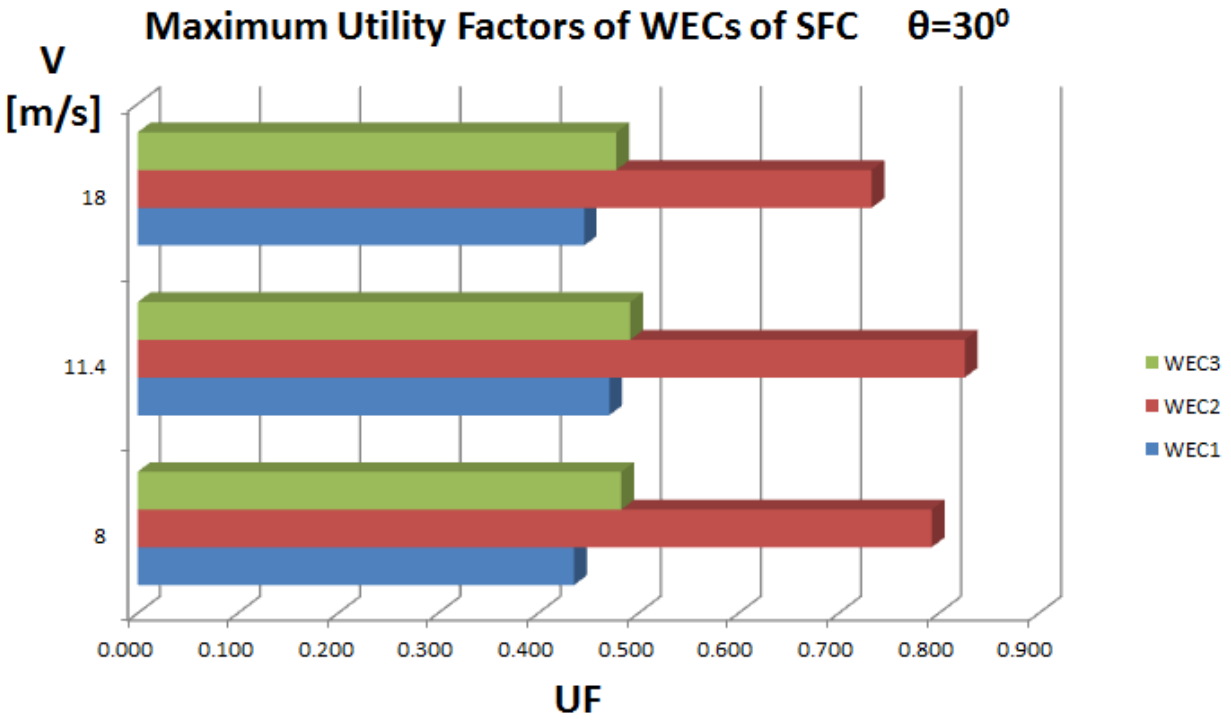

Figure 6.16: MUFs of WECs of SFC when $\theta = 30^0$ in survival sea state.

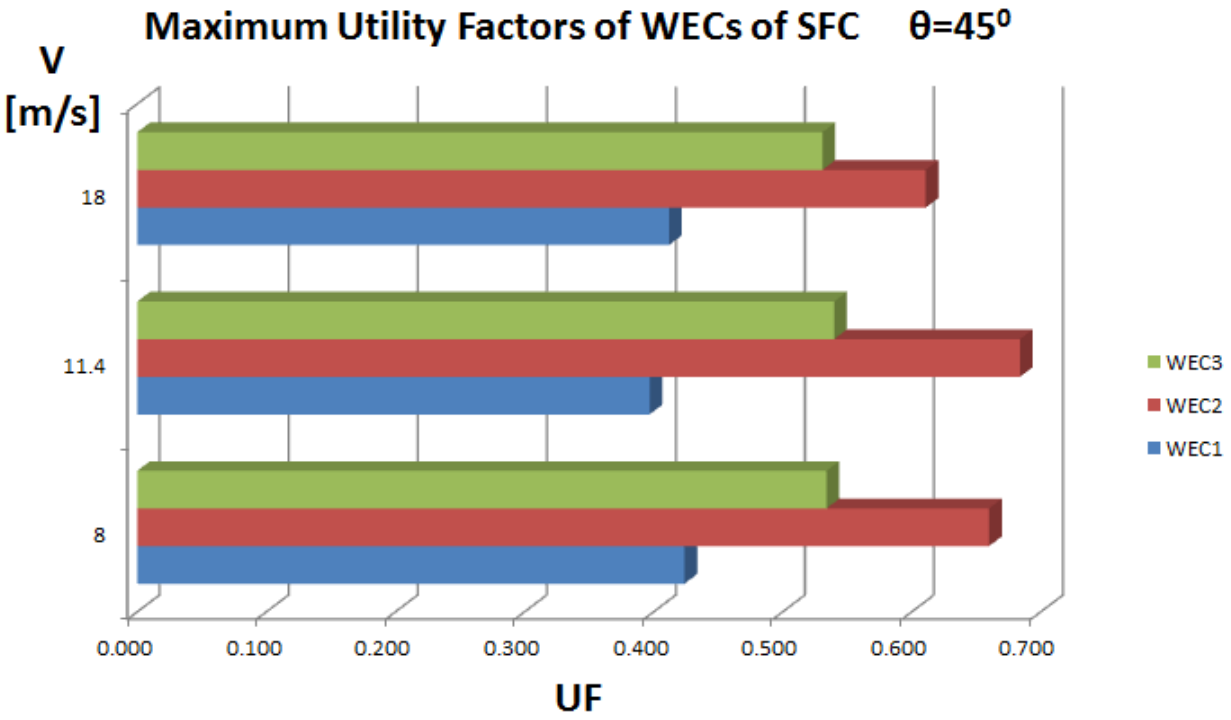

Figure 6.17: MUFs of WECs of SFC when $\theta = 45^0$ in survival sea state.

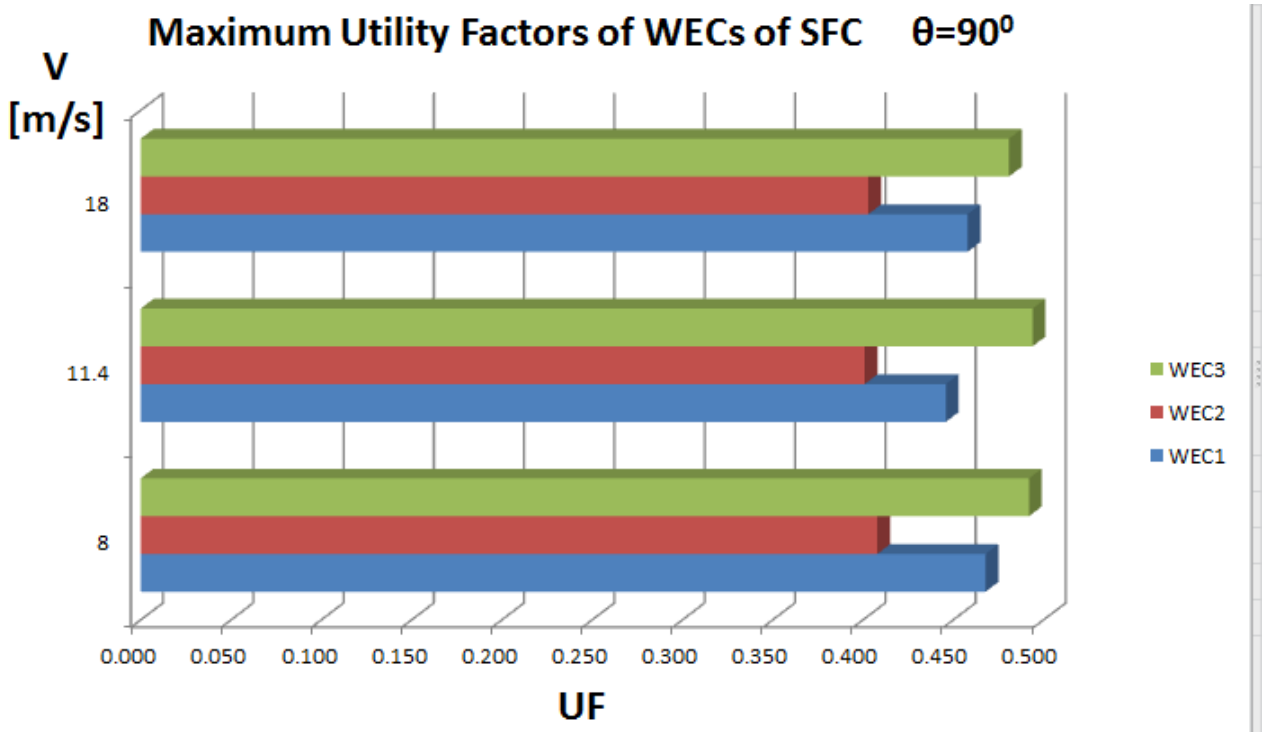

Figure 6.18: MUFs of WECs of SFC when $\theta = 90^0$ in survival sea state.

Table 6.7: Maximum forces and utility factors of four segments for left supporting arm of WEC2 when $Hs = 15.6m$, $Tz = 14.5s$, $V = 11.4m/s$, seed number= 650.

Element		$N[N]$	$My[N*m]$	$Mz[N*m]$	$Vy[N]$	$Vz[N]$	$M_T[N*m]$	Com:N and M	Com:V and M	Com:V, M and M_T
1	Value	2835225	21789	4820203	537572	1320490	3383961			
	UF	0.061	0.001	0.224	0.040	0.098	0.179	0.229	0.224	0.225
2	Value	2825976	6064020	2343920	528783	1295000	3383693			
	UF	0.061	0.282	0.109	0.039	0.096	0.179	0.287	0.282	0.284
3	Value	2809960	12015287	96039	509526	1226920	3382980			
	UF	0.060	0.559	0.004	0.038	0.091	0.179	0.564	0.559	0.562
4	Value	2787307	17650365	2440313	479981	1144583	3381684			
	UF	0.060	0.821	0.114	0.036	0.085	0.179	0.826	0.821	0.826
Max	Value	2835225	17650365	4820203	537572	1320490	3383961			
	UF	0.061	0.821	0.224	0.040	0.098	0.179	0.826	0.821	0.826

Symbols:N is axial tension, My is bending moment about local Y-axis, Mz is bending moment about local Z-axis, Vy is shear force in local Y-direction, Vz is shear force in local Z-direction, M_T is torsional moment, Com is abbreviation for force combination. Coordinate system refers to Figure 3.7.

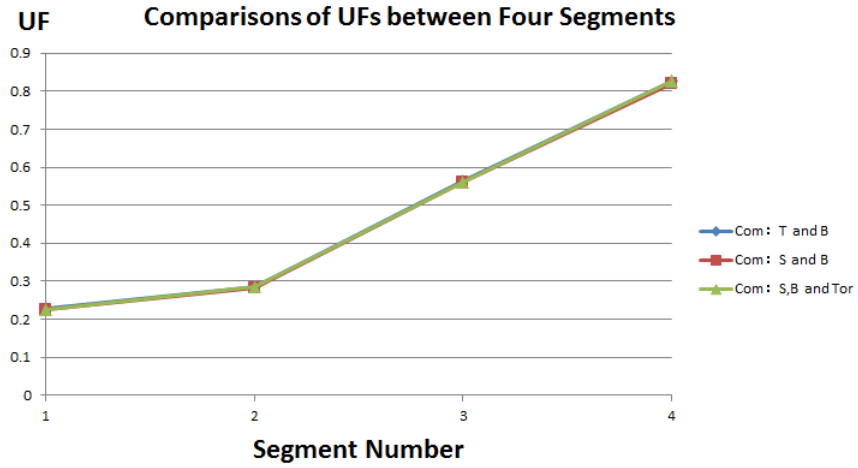

Figure 6.19: Comparisons of UFs between Four Segments for left supporting arm of WEC2 when $Hs = 15.6m$, $Tz = 14.5s$, $V = 11.4m/s$, seed number= 650.

MUFs in survival condition are smaller than MUFs in operational condition in the four wave directions. It has quite different results for the BFWEC compared to WECs of SFC.

Table 6.8: MUFs of BFWEC in survival sea state.

Sea state	$Hs = 15.6m$		$Tz = 14.5s$	
θ^0	0	30	45	90
Seed number	800	300	300	800
MUF	0.548	0.566	0.458	0.566

Table 6.9: Maximum forces and UFss of four segments for left supporting arm of BFWEC when $Hs = 15.6m$, $Tz = 14.5s$.

(a) Maximum forces and UFss of four segments for BFWEC when $\theta = 30^0$, seed number= 300.

Element		$N[N]$	$My[N*m]$	$Mz[N*m]$	$Vy[N]$	$Vz[N]$	$M_T[N*m]$	Com:N and M	Com:V and M	Com:V, M and M_T
1	Value	3001393	53960	6212609	696283	827982	4329257			
	UF	0.064	0.003	0.289	0.052	0.062	0.230	0.295	0.289	0.290
2	Value	2992444	4150959	3000445	695423	819231	4329197			
	UF	0.064	0.193	0.140	0.052	0.061	0.230	0.210	0.206	0.207
3	Value	2959025	8123245	163318	816922	794744	4329023			
	UF	0.064	0.378	0.008	0.061	0.059	0.230	0.382	0.378	0.379
4	Value	2957955	11972183	3105903	1108964	759834	4328732			
	UF	0.064	0.557	0.145	0.083	0.057	0.230	0.566	0.562	0.564
Max	Value	3001393	11972183	6212609	1108964	827982	4329257			
	UF	0.064	0.557	0.289	0.083	0.062	0.230	0.566	0.562	0.564

(b) Maximum forces and UFss of four segments for BFWEC when $\theta = 90^0$, seed number= 800.

Element		$N[N]$	$My[N*m]$	$Mz[N*m]$	$Vy[N]$	$Vz[N]$	$M_T[N*m]$	Com:N and M	Com:V and M	Com:V, M and M_T
1	Value	3061594	0	12030214	1356197	0	0			
	UF	0.066	0.000	0.560	0.101	0.000	0.000	0.566	0.560	0.560
2	Value	3062704	0	5814733	1339448	0	0			
	UF	0.066	0.000	0.271	0.100	0.000	0.000	0.277	0.271	0.271
3	Value	3061341	0	255448	1284528	0	0			
	UF	0.066	0.000	0.012	0.096	0.000	0.000	0.017	0.012	0.012
4	Value	3062216	0	5994865	1216129	0	0			
	UF	0.066	0.000	0.279	0.091	0.000	0.000	0.285	0.279	0.279
Max	Value	3062704	0	12030214	1356197	0	0			
	UF	0.066	0.00	0.560	0.101	0.000	0.000	0.566	0.560	0.560

Symbols:N is axial tension, My is bending moment about local Y-axis, Mz is bending moment about local Z-axis, Vy is shear force in local Y-direction, Vz is shear force in local Z-direction, M_T is torsional moment, Com is abbreviation for force combination. Coordinate system refers to Figure 3.7.

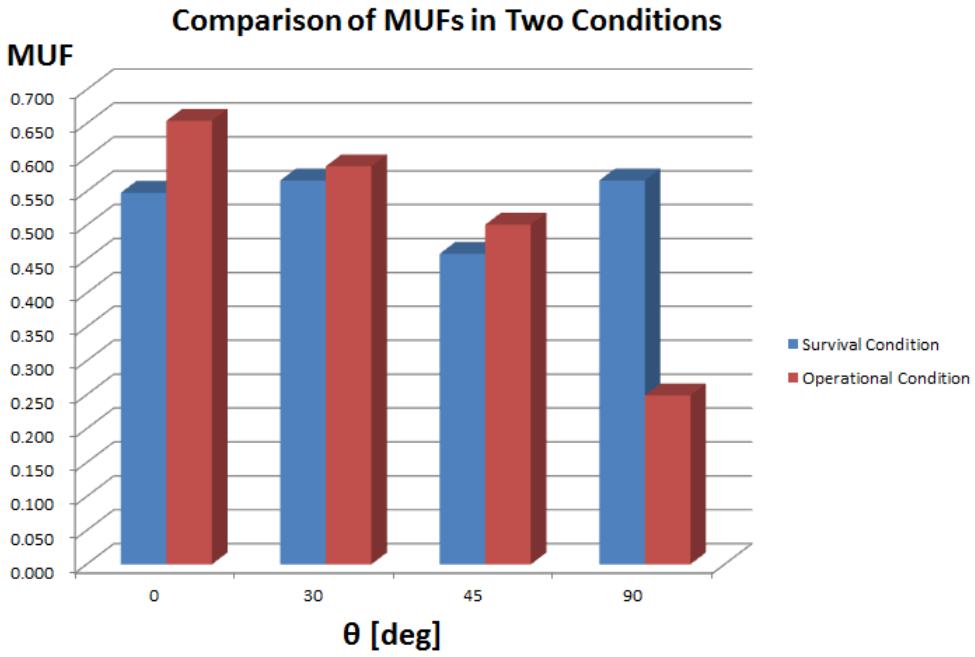

Figure 6.20: MUF comparison of BFWEC in operational condition and survival condition.

Chapter 7

Produced Power

WECs will rotate around an axis under the effects of wave motions. The reciprocal rotations can be made use of to generate electricity power. In this chapter, the power produced by the WECs' rotataional motions will be estimated. The corresponding converted electricity power from wave energy will be less than the estimated value because of conversion efficiency.

Produced power is estimated by Matlab code given in Appendix A. If rotational velocity is denoted as ω_R, damping coefficient is denoted as C, then the produced power is expressed as:

$$P = 2 \cdot C \cdot \omega_R \cdot \omega_R \tag{7.1}$$

Because there are two PTO sytems for one WEC, so the power should be multiplied by two at the beginning. And in survival condition there will be no power produced by WECs because the damping coefficient will be set to zero at that case. The power discussed in the following is all in operational sea state.

7.1 Power Produced by WECs of SFC

An example of relative rotation between WEC and Semi-submersible is shown in Figure 4.2. Special attention has to be paid to the rotation of WECs, because not only Semi-submersible will move in six degrees of freedom under the actions of wind and wave loads, but WECs have their own motions. So their relative motions have to be calculated and then

the relative rotations can be got.

Since there are twenty cases with different seed nubmers for each sea state, an example of produced power for the three WECs is plotted in Figure 7.1 when $Hs = 6m, Tz = 12.6s, V = 8m/s, \theta = 0^0$. The power produced by WEC1 is too small, because waves propagate parallel to the flap. Power produced by WEC2 and WEC3 is almost the same. The maximum power produced by a single WEC is 419 kW, which is produced by WEC2 when wind velocity is $11.4m/s$ and wave direction is 30^0.

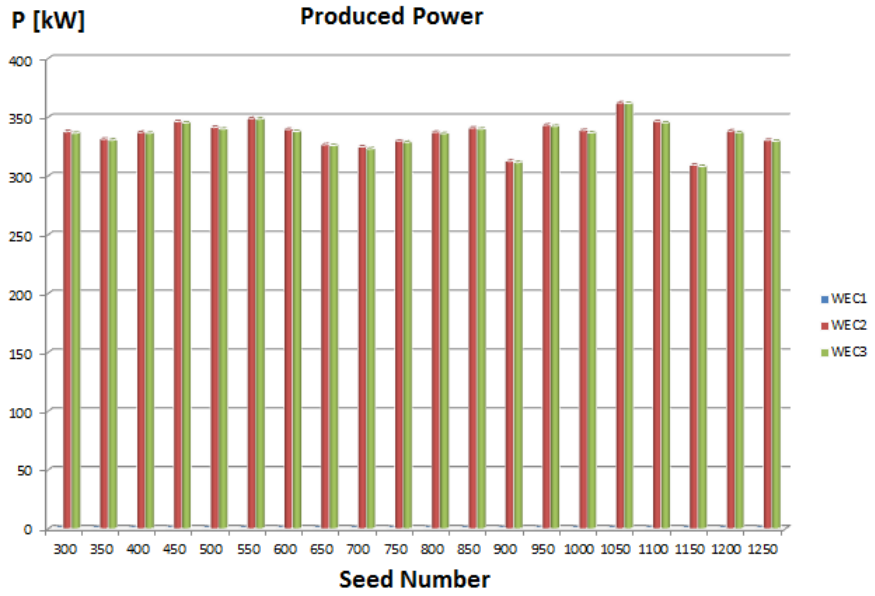

Figure 7.1: Produced Power by WECs when $Hs = 6m, Tz = 12.6s, V = 18m/s, \theta = 0^0$.

If all the power produced by the three WECs is summed up for each wave direction at a given wind velocity, the total power produced by WECs of SFC can be got. Here the average values of the twenty cases are plotted from Figure 7.2 to Figure 7.4. It tells that the total power is almost the same for a given wave direction and wind velocity, between $600kW$ and $700kW$.

7.2 Power Produced by BFWEC

The produced power by the BFWEC in four wave directions is plotted in Figure 7.5. Power produced when wave direction is 0^0 has the maximum value compared those of the other three wave directions. The maximum value reaches 867 kW. It indicates that when

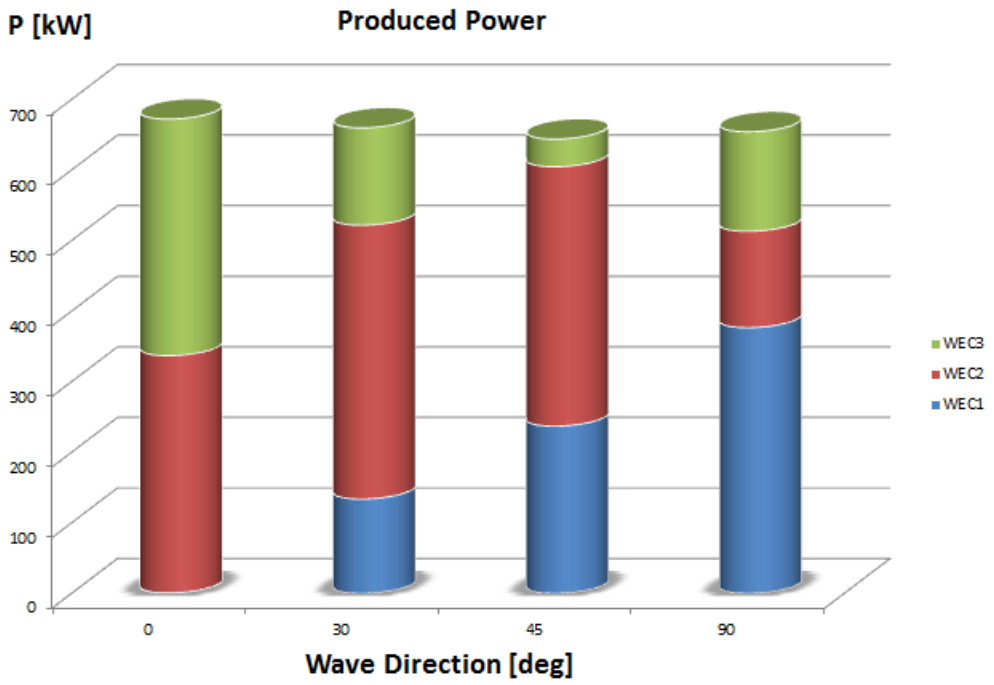

Figure 7.2: Total Produced Power by WECs when $Hs = 6m, Tz = 12.6s, V = 8m/s$.

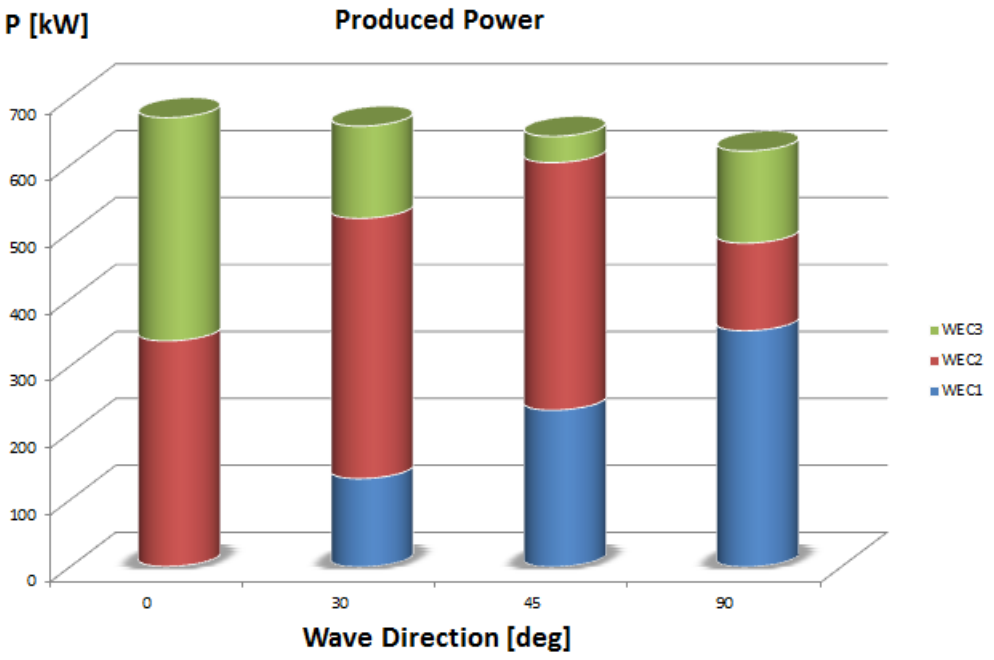

Figure 7.3: Total Produced Power by WECs when $Hs = 6m, Tz = 12.6s, V = 11.4m/s$.

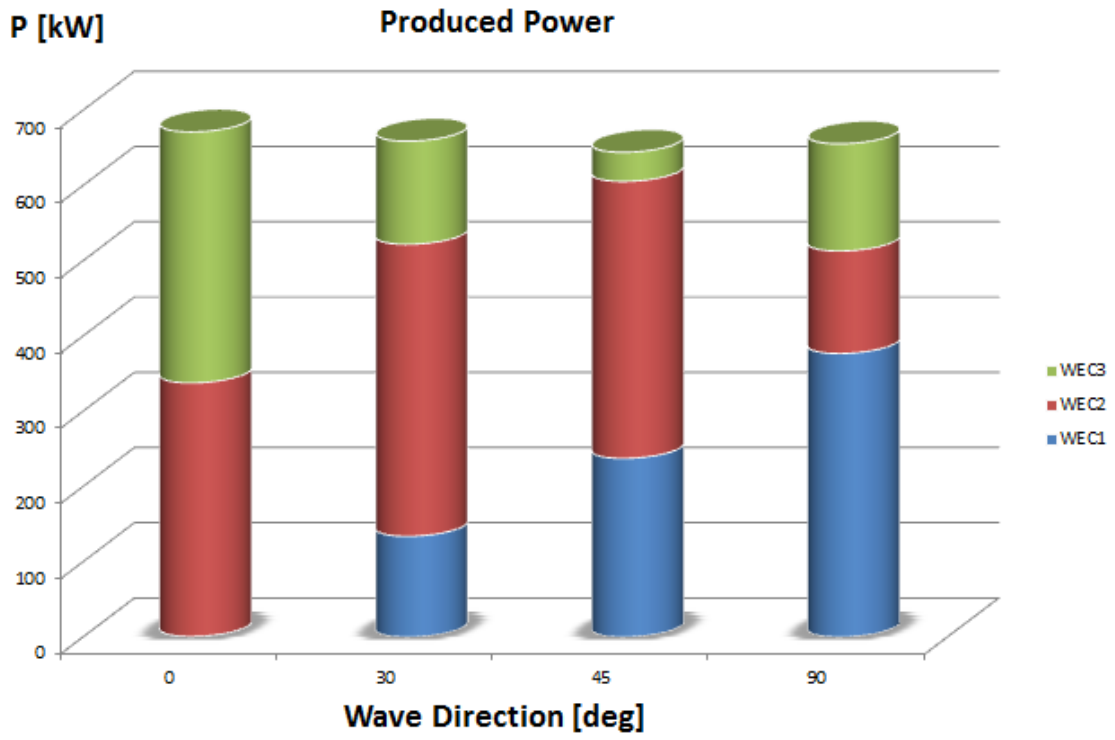

Figure 7.4: Total Produced Power by WECs when $Hs = 6m, Tz = 12.6s, V = 18m/s$.

waves propagate perpendicularly to the flap, a larger rotation motion happens and more power is produced.

7.3 Comparison

In terms of produced power by a single WEC, the BFWEC produces much more power compared to the WECs of SFC as shown in Figure 7.6. This is mainly due to the motion of Semi-submersible which reduces the relatvie motion bwtween WECs and the hull. For convenience, the motions of SFC are investigated when wind velocity is $11.4m/s$ and wave direction is 90^0. In this case, waves propagate perpendicularl to the flap of WEC1. Relative yaw motion between WEC1 and Semisubmersible is plotted in Figure 7.7. While there is no yaw motion for the BFWEC. Relative roll motion between WEC1 and Semisubmersible is plotted in Figure 7.8 and the corresponding motion of BFWEC is pitching plotted in Figure 7.9. It tells that the BFWEC has larger rotation angles than WEC1 in generally, and the mean rotation position for WEC1 is around -20^0 because of the motions of SFC while the

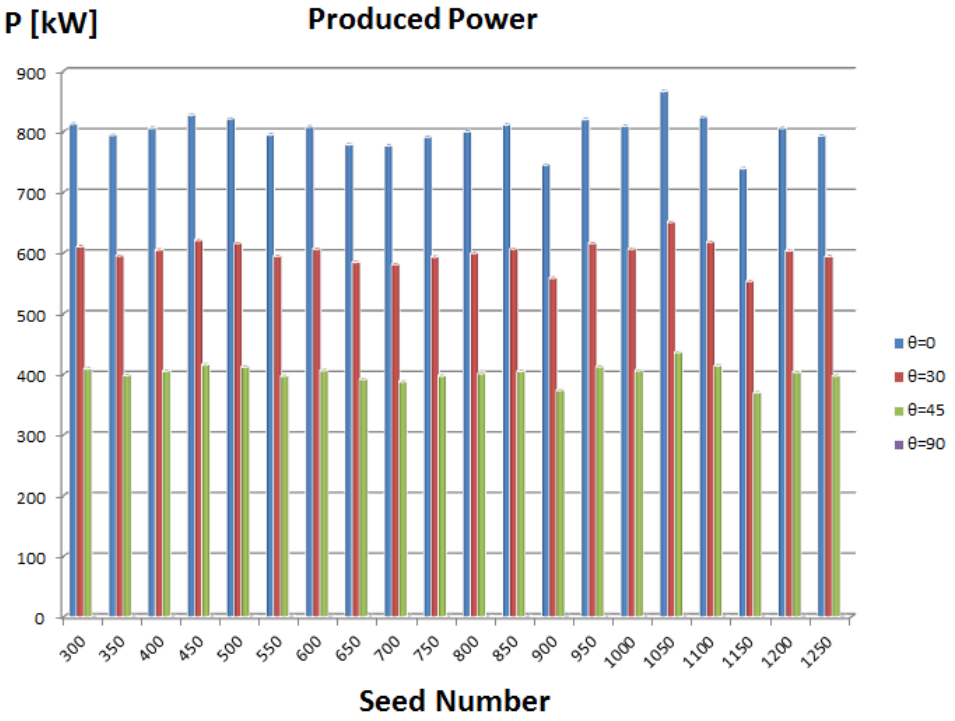

Figure 7.5: Total Produced Power by BFWEC when $Hs = 6m, Tz = 12.6s$.

mean position for BFWEC is around 0^0 as expected. Since the time step for storing rotation positions is the same for both BFWEC and WEC1, a bigger rotation angle means a faster roational velocity which results in more produced power. When considering a single WEC, it is better to arrange the flap of WEC perpendicularly to the wave propagating direction. If several WECs are installed on a floating hull, like the SFC, it is better to consider the positions of WECs. If for a given ocean site, waves are propagating in almost the same direction in most time, then more WECs can be considered to be installed in the direction perpendicular to that of waves.

Although for a single WEC, BFWEC will produce more power, WECs of SFC can generate almost 650 kW in the four wave directions. More steady power can be expected for WECs of SFC. It brings a new challenge to increase relative rotation motion between WECs and Semi-submersible.

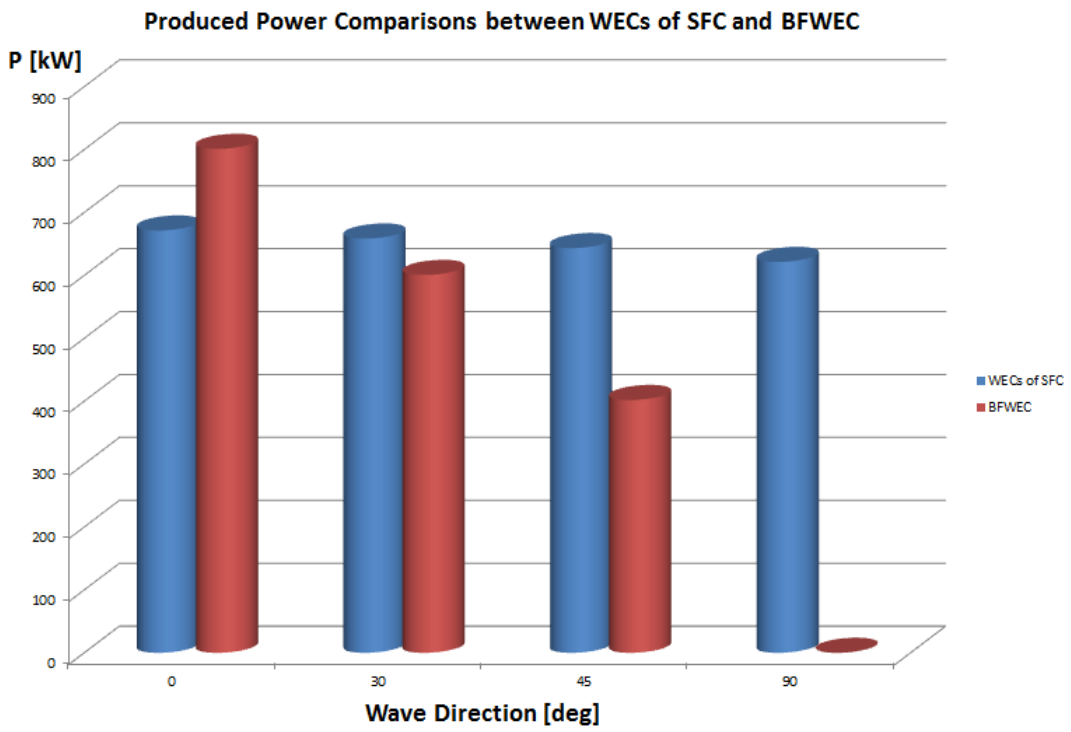

Figure 7.6: Produced power comparisons between WECs of SFC when wind velocity is $11.4 m/s$ and BFWEC.

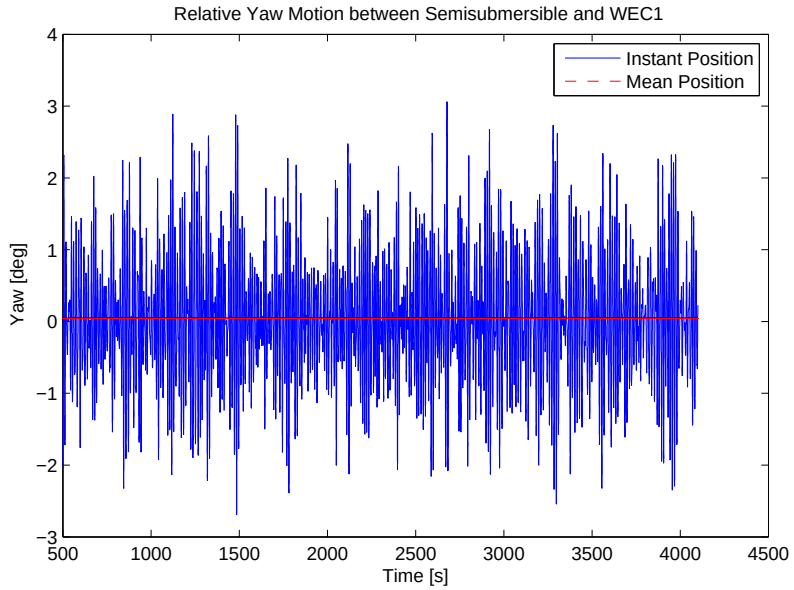

Figure 7.7: Relative yaw motion between Semisubmersible and WEC1 when wind velocity is $11.4 m/s$ and wave direction is 90^0.

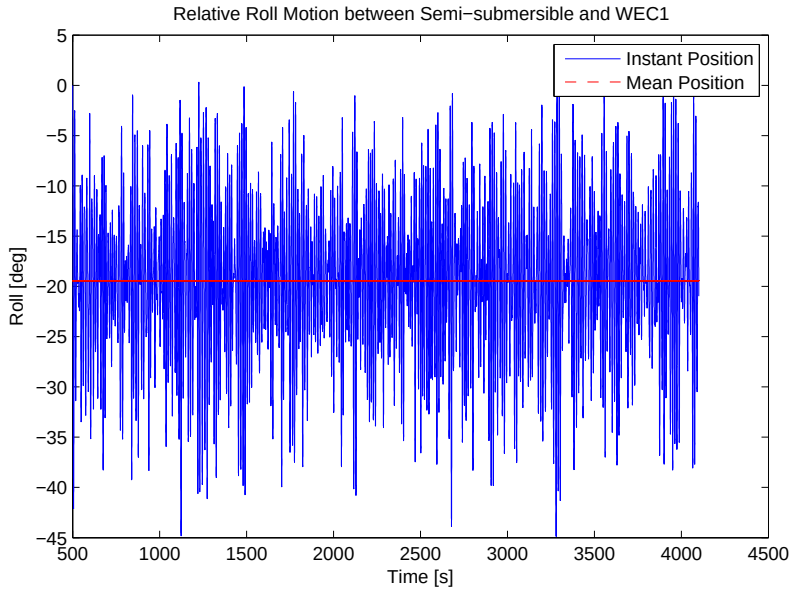

Figure 7.8: Relative roll motion between Semisubmersible and WEC1 when wind velocity is $11.4 m/s$ and wave direction is 90^0.

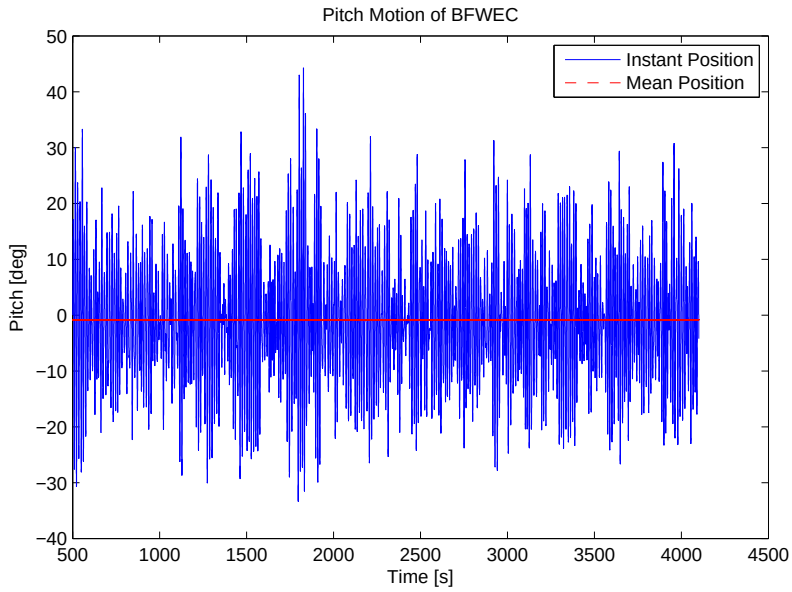

Figure 7.9: Pitch motion of BFWEC when wave direction is 0^0.

Chapter 8

Conclusions and Further Work

8.1 Conclusions

This thesis mainly studies the ULS strength check of supporting arms of WECs and produced power calculation of WECs. All the simulations are carried out in SIMO/RIFLEX/AeroDyn or without AeroDyn. The natural pitching period of BFWEC is investigated by both evaluation in Excel and simulation decay test in SIMO/RIFLEX. A natural period of 14.3s is got from the former method and 14.9s from simulation decay test. In terms of ULS strength check, the NORSOK Standard N004 is used as the criterion. In order to have more intuitive and consistent results through different forces and their combinations, UF is introduced, defined as calculated result of external force divided by suggesting value or limited strength made by the standard. The following conclusions are got in strength check:

1. For the model of SFC, a FMUF of 0.509 is observed in WEC2 for all simulations of operational sea state, when $Hs = 6m, Tz = 12.6s$, wind velocity $V = 18m/s$, wave direction $\theta = 30^0$ and seed number is set to 300.

2. For BFWEC, a FMUF of 0.654 is observed in all simulations of operational sea state, when $Hs = 6m, Tz = 12.6s$, wave direction $\theta = 0^0$ and seed number is set to 650.

3. Generally UFs of BFWEC are bigger than those of WECs of SFC in operational condition. For both models, there is much strength reservation.

4. For the model of SFC, a FMUF of 0.826 is observed in WEC2 for all simulations of survival sea state, when $Hs = 15.6m, Tz = 14.5s$, wind velocity $V = 11.4m/s$, wave direction $\theta = 30^0$ and seed number is set to 650.

5. For BFWEC, a FMUF of 0.566 is observed for all simulations of survival sea state, when $Hs = 15.6m, Tz = 14.5s$, wave direction $\theta = 30^0$ and $\theta = 90^0$, seed number is set to 300 and 800 respectively. The FMUF of BFWEC in survival condition is even smaller than the FMUF in operational condition.

6. MUFs of BFWEC are smaller than those of WECs of SFC in survival condition.

In the end, produced power by WECs is estimated. There will be no produced power in survival condition, only operational condition is considered. The conclusions are summarized as following:

1. Maximum power is produced when waves propagate perpendicular to flap.

2. For WECs of SFC, total power produced by WECs is almost the same in the four wave directions: $\theta = 0^0, 30^0, 45^0, 90^0$, between $600kW$ and $700kW$.

3. For BFWEC, maximum produced power reaches $870kW$ when wave direction $\theta = 0^0$.

4. For a single WEC, BFWEC produces more power than WECs of SFC; more steady power can be expected for WECs of SFC.

8.2 Recommendations for Future Work

The combination concept of wind turbine and WECs is a new challenge. There are a lot of designing and testing problems to be solved.

Firstly, only the pitching natural period of BFWEC is invesitgated in this thesis. Futher work can be carried out to evaluate the period of WECs of SFC and the whole SFC's period to avoid resonance with waves and winds.

Secondly, the design of WECs is safe and reliable enough in operational condition. More dimensions of supporting arms and flaps can be tested to reduce weight and materials in order to be more cost effective.

Thirdy, the supporting arms are connected to the flap rigidly in this thesis. More connection ways should be tested and compared. These connections can be discussed futher in terms of welding and connection strength.

Fourthly, the PTO system is simplified just as a constant damping coefficient. Until now, there are many PTO systems to choose. In terms of simulation in programme, a linear or even nonlinear damping can be further simulated; in terms of model testing, a proper PTO system has to be chosen considering functions, convertion efficiency, construction and cost. In the end, locations of WECs on the Semi-submersible maybe changed according to wave states. As stated before, maximum produced power is expected when waves propagate perpendicular to flap. So if waves usually come from amolst one direction, then more WECs may be located perpendicualr to that direction. In that case, the SFC will not be symmetric any more and a complete new design should be considered.

Appendix A

Matlab Code

There are mainly two Matlab files used in this thesis. The first one is coded according to the NORSOK Standard N004 (Standards Norway, 2004), used for the strength check of WECs. Another one is used to calculate produced power by WECs. For the BFWEC, a little change of the force numbers and displacement numbers in the code according to the force result files and displacement result files respectively is needed.

A.1 Matlab Code for Strength Check

```
clear all;
clc;
%%=====================================================================
%input parameters
D=1.5;        % Outer diameter.
t=0.05;       % wall thickness
fy=235*1e6;   % Pa  Characteristic yield strength
E=2.1*1e11;   % MPa, young's modulus of elasticity.
L=15;         % m  length of tubular between stiffening rings,
              %diaphragms, or end connections.
Q=5*1e5;      % N shear force
p_sd=0;       %  design hydrostatic pressure
%%=====tubular members=================================================
```

```
%--check if D and t meet the tubular assumptions.
if t<0.006 || D/t>=120
    error('Chang D and t');
end
A=D^2*pi/4-(D-2*t)^2*pi/4;  %Crossing sectional area.
                            %D-outer diameter, t-thickness.
gama_M_A=1.15;              % gama_M in axial tension
Ntrd=A*fy/gama_M_A;
W=pi*(D^4-(D-2*t)^4)/32/D;  % elastic section modulus;
Z=(D^3-(D-2*t)^3)/6;        % plastic section modulus;
%%=====================================================================
%---------------------------------------------------------------------
    % Choose  gama_M_B
    % fcl  ----characteristic elastic local buckling strength.
    fcle=2*0.3*E*t/D;
    if fy/fcle<=0.170
        fcl=fy;
    elseif fy/fcle>0.170 && fy/fcle<= 1.911
        fcl=(1.047-0.274*fy/fcle)*fy;
    else
        fcl=fcle;
    end
    % fh  ----characteristic hoop buckling strength.
    mu=L/D*sqrt(2*D/t);   % geometric parameter
    % L-length of tubular between stiffening rings,diaphragms,
    %or end connections.
    if mu>=1.6*D/t
        Ch=0.44*t/D;
    elseif mu>=0.825*t/D  && mu<1.6*D/t
        Ch=0.44*t/D+0.21*(D/t)^3/(mu^4);
    elseif mu>=1.5 && mu<0.825*D/t
        Ch=0.737/(mu-0.579);
    elseif mu<1.5
        Ch=0.80;
    end

```

```
50      fhe=2*Ch*E*t/D;
51
52      if fhe>2.44*fy
53          fh=fy;
54      elseif fhe<=2.44*fy && fhe>0.55*fy
55          fh=0.7*fy*(fhe/fy)^0.4;
56      elseif fhe<=0.55*fy
57          fh=fhe;
58      end
59
60      lambda_c=sqrt(fy/fcle);
61      lambda_h=sqrt(fy/fhe);
62      sigma_psd=p_sd*D/2/t;
63      %-----------------------------------------------------------------
64      %choose fm
65      p=fy*D/(E*t);
66      if p>0 && p<0.0517;
67          fm=Z/W*fy;
68      elseif p>0.0517 && p<=0.1034;
69          fm=(1.13-2.58*(fy*D/E/t))*(Z/W)*fy;
70      elseif p>0.1034 && p<=120*fy/E;
71          fm=(0.94-0.76*(fy*D/E/t))*(Z/W)*fy;
72      else
73          error('fm not found');
74      end
75  %%=================================================================
76  % READ RIFLEX FORCE RESULTS
77   data = load('Analysis_elmfor.asc'); save('data.mat','data');
78  % load data;
79  time = data(10001:82000,1);
80  %=================================================================
81  % WEC1 L  Line4
82  N_1 = data(10001:82000,2);
83  Tor_1=data(10001:82000,3);
84  My1_1=data(10001:82000,4);
85  Mz1_1 = data(10001:82000,6);
```

```
Qy1_1 = data(10001:82000,8);
Qz1_1 = data(10001:82000,10);

N_2 = data(10001:82000,12);
Tor_2=data(10001:82000,13);
My1_2=data(10001:82000,14);
Mz1_2 = data(10001:82000,16);
Qy1_2 = data(10001:82000,18);
Qz1_2 = data(10001:82000,20);

N_3 = data(10001:82000,22);
Tor_3=data(10001:82000,23);
My1_3=data(10001:82000,24);
Mz1_3 = data(10001:82000,26);
Qy1_3 = data(10001:82000,28);
Qz1_3 = data(10001:82000,30);

N_4 = data(10001:82000,32);
Tor_4=data(10001:82000,33);
My1_4=data(10001:82000,34);
Mz1_4 = data(10001:82000,36);
Qy1_4 = data(10001:82000,38);
Qz1_4 = data(10001:82000,40);
%%=====================================================================
%maximum forces
max1=zeros(8,9);
max1(1,1)=max(abs(N_1));
max1(1,2)=max(abs(My1_1));
if max1(1,2)<0.1;
    max1(1,2)=0;
end
max1(1,3)=max(abs(Mz1_1));
if max1(1,3)<0.1;
    max1(1,3)=0;
end
max1(1,4)=max(abs(Qy1_1));
```

```
122 if max1(1,4)<0.1;
123     max1(1,4)=0.00000;
124 end
125 max1(1,5)=max(abs(Qz1_1));
126 if max1(1,5)<0.1;
127     max1(1,5)=0.00000;
128 end
129 max1(1,6)=max(abs(Tor_1));
130 if max1(1,6)<0.1;
131     max1(1,6)=0.00000;
132 end
133
134 max1(3,1)=max(abs(N_2));
135 max1(3,2)=max(abs(My1_2));
136 if max1(3,2)<0.1;
137     max1(3,2)=0;
138 end
139 max1(3,3)=max(abs(Mz1_2));
140 if max1(3,3)<0.1;
141     max1(3,3)=0;
142 end
143 max1(3,4)=max(abs(Qy1_2));
144 if max1(3,4)<0.1;
145     max1(3,4)=0.00000;
146 end
147 max1(3,5)=max(abs(Qz1_2));
148 if max1(3,5)<0.1;
149     max1(3,5)=0.00000;
150 end
151 max1(3,6)=max(abs(Tor_2));
152 if max1(3,6)<0.1;
153     max1(3,6)=0.00000;
154 end
155
156 max1(5,1)=max(abs(N_3));
157 max1(5,2)=max(abs(My1_3));
```

```
158 if max1(5,2)<0.1;
159     max1(5,2)=0;
160 end
161 max1(5,3)=max(abs(Mz1_3));
162 if max1(5,3)<0.1;
163     max1(5,3)=0;
164 end
165 max1(5,4)=max(abs(Qy1_3));
166 if max1(5,4)<0.1;
167     max1(5,4)=0.00000;
168 end
169
170 max1(5,5)=max(abs(Qz1_3));
171 if max1(5,5)<0.1;
172     max1(5,5)=0.00000;
173 end
174 max1(5,6)=max(abs(Tor_3));
175 if max1(5,6)<0.1;
176     max1(5,6)=0.00000;
177 end
178
179 max1(7,1)=max(abs(N_4));
180 max1(7,2)=max(abs(My1_4));
181 if max1(7,2)<0.1;
182     max1(7,2)=0;
183 end
184 max1(7,3)=max(abs(Mz1_4));
185 if max1(7,3)<0.1;
186     max1(7,3)=0;
187 end
188 max1(7,4)=max(abs(Qy1_4));
189 if max1(7,4)<0.1;
190     max1(7,4)=0.00000;
191 end
192
193 max1(7,5)=max(abs(Qz1_4));
```

```
194 if max1(7,5)<0.1;
195     max1(7,5)=0.00000;
196 end
197 max1(7,6)=max(abs(Tor_4));
198 if max1(7,6)<0.1;
199     max1(7,6)=0.00000;
200 end
201 max1=1000*max1;
202 %%=====================================================================
203 % element 1
204 N =N_1;
205 Tor=Tor_1;
206 My1 = My1_1; % My end 1       KN*m
207 Mz1 = Mz1_1; % Mz end 1       KN*m
208 Qy1 = Qy1_1; % Qy end 1       KN
209 Qz1 = Qz1_1; % Qz end 1       KN
210 ii=size(N);
211 for j=1:1:ii
212     Nsd=abs(N(j)*1000);
213     Mysd=abs(My1(j)*1000);
214     Mzsd=abs(Mz1(j)*1000);
215     Q=abs(Qz1(j)*1000);
216     Q2=abs(Qy1(j)*1000);
217     Mtsd=abs(Tor(j)*1000);
218     sigma_csd=Nsd/A+sqrt(Mysd^2+Mzsd^2)/W;
219     lambda_s=abs(sigma_csd)/fcl*lambda_c+(sigma_psd/fh)^2*lambda_h;
220     if lambda_s<0.5
221         gama_M=1.15;
222     elseif lambda_s>=0.5 && lambda_s<=1.0
223         gama_M=0.85+0.60*lambda_s;
224     elseif lambda_s>1.0
225         gama_M=1.45;
226     end
227     gama_M_B=gama_M;
228     Mrd=fm*W/gama_M_B;                %gama_M in bending
229     %-------------------------------------------------------------------
```

```
230     Vrd=A*fy/(2*sqrt(3))/gama_M_A; %shear force
231     %=====================================================================
232     % axial tension   R11 R12
233     R11(j)=abs(Nsd/Ntrd);
234     %=====================================================================
235     % bending    R21  R22
236     R21(j)=abs(Mysd/Mrd);
237     R22(j)=abs(Mzsd/Mrd);
238     %=====================================================================
239     % shear without torsion    R31  R32
240     % The shear force in y direction is so small that is neglected.
241     R31(j)=abs(Q/Vrd);
242     R32(j)=abs(Q2/Vrd);
243     %=====================================================================
244     % Shear from torsional moment  R81
245     Ip=pi/32*(D^4-(D-2*t)^4);
246     M_TRd=2*Ip*fy/(D*sqrt(3)*gama_M);
247     R81(j)=Mtsd/M_TRd;
248     %=====================================================================
249     % hoop buckling  R41 R42
250     R41(j)=abs(sigma_psd/(fh/gama_M));
251     %=====================================================================
252     % axial tension and bending without hydrostatic pressure  R51  R52
253     R51(j)=abs((Nsd/Ntrd)^1.75+sqrt(Mysd^2+Mzsd^2)/Mrd);
254     %=====================================================================
255     % shear and bending   R61 R62
256     Vrd=A*fy/(2*sqrt(3))/gama_M_A;
257     if Q/Vrd>=0.4
258         R61(j)=abs(sqrt(Mysd^2+Mzsd^2)/Mrd/(sqrt(1.4-Q/Vrd)));
259     elseif Q/Vrd<0.4
260         R61(j)=abs(sqrt(Mysd^2+Mzsd^2)/Mrd);
261     end
262     %=====================================================================
263     % Interaction shear, bending, moment and torsional moment   R71 R72
264     fd=fy/gama_M;
265     tau_TSd=Mtsd/(2*pi*(D/2)^2*t);
```

```
266      f_mred=fm*sqrt(1-3*(tau_TSd/fd)^2);
267      M_redrd=W*f_mred/gama_M;
268      if Q/Vrd<0.4
269          R71(j)=sqrt(Mysd^2+Mzsd^2)/M_redrd;
270      else
271          R71(j)=sqrt(Mysd^2+Mzsd^2)/(M_redrd*sqrt(1.4-Q/Vrd));
272      end
273  end
274  max1(2,1)=max(abs(R11));
275  max1(2,2)=max(abs(R21));
276  if max1(2,2)<0.001;
277      max1(2,2)=0;
278  end
279  max1(2,3)=max(abs(R22));
280  if max1(2,3)<0.001;
281      max1(2,3)=0;
282  end
283  max1(2,4)=max(abs(R32));
284  if max1(2,4)<0.001;
285      max1(2,4)=0;
286  end
287  max1(2,5)=max(abs(R31));
288  if max1(2,5)<0.001;
289      max1(2,5)=0;
290  end
291  max1(2,6)=max(R81);
292  if max1(2,6)<0.001;
293      max1(2,6)=0;
294  end
295  max1(2,7)=max(abs(R51));
296  max1(2,8)=max(abs(R61));
297  max1(2,9)=max(abs(R71));
298  %%=====================================================================
299  % element 2
300  N =N_2;
301  Tor=Tor_2;
```

```
My1 = My1_2; % My end 1       KN*m
Mz1 = Mz1_2; % Mz end 1       KN*m
Qy1 = Qy1_2; % Qy end 1       KN
Qz1 = Qz1_2; % Qz end 1       KN
ii=size(N);
for j=1:1:ii
    Nsd=abs(N(j)*1000);
    Mysd=abs(My1(j)*1000);
    Mzsd=abs(Mz1(j)*1000);
    Q=abs(Qz1(j)*1000);
    Q2=abs(Qy1(j)*1000);
    Mtsd=abs(Tor(j)*1000);
    sigma_csd=Nsd/A+sqrt(Mysd^2+Mzsd^2)/W;
    lambda_s=abs(sigma_csd)/fcl*lambda_c+(sigma_psd/fh)^2*lambda_h;
    if lambda_s<0.5
        gama_M=1.15;
    elseif lambda_s>=0.5 && lambda_s<=1.0
        gama_M=0.85+0.60*lambda_s;
    elseif lambda_s>1.0
        gama_M=1.45;
    end
    gama_M_B=gama_M;
    Mrd=fm*W/gama_M_B;                %gama_M in bending
    %-------------------------------------------------------------------
    Vrd=A*fy/(2*sqrt(3))/gama_M_A; %shear force
    %===================================================================
    % axial tension   R11 R12
    R11(j)=abs(Nsd/Ntrd);
    %===================================================================
    % bending    R21  R22
    R21(j)=abs(Mysd/Mrd);
    R22(j)=abs(Mzsd/Mrd);
    %===================================================================
    % shear without torsion    R31  R32
    % The shear force in y direction is so small that is neglected.
    R31(j)=abs(Q/Vrd);
```

```
338     R32(j)=abs(Q2/Vrd);
339     %=====================================================================
340     % Shear from torsional moment  R81
341     Ip=pi/32*(D^4-(D-2*t)^4);
342     M_TRd=2*Ip*fy/(D*sqrt(3)*gama_M);
343     R81(j)=Mtsd/M_TRd;
344     %=====================================================================
345     % axial tension and bending without hydrostatic pressure  R51  R52
346     R51(j)=abs((Nsd/Ntrd)^1.75+sqrt(Mysd^2+Mzsd^2)/Mrd);
347     %=====================================================================
348     % shear and bending   R61 R62
349     Vrd=A*fy/(2*sqrt(3))/gama_M_A;
350     if Q/Vrd>=0.4
351         R61(j)=abs(sqrt(Mysd^2+Mzsd^2)/Mrd/(sqrt(1.4-Q/Vrd)));
352
353     elseif Q/Vrd<0.4
354         R61(j)=abs(sqrt(Mysd^2+Mzsd^2)/Mrd);
355     end
356     %=====================================================================
357     % Interaction shear, bending, moment and torsional moment   R71 R72
358     fd=fy/gama_M;
359     tau_TSd=Mtsd/(2*pi*(D/2)^2*t);
360     f_mred=fm*sqrt(1-3*(tau_TSd/fd)^2);
361     M_redrd=W*f_mred/gama_M;
362     if Q/Vrd<0.4
363         R71(j)=sqrt(Mysd^2+Mzsd^2)/M_redrd;
364     else
365         R71(j)=sqrt(Mysd^2+Mzsd^2)/(M_redrd*sqrt(1.4-Q/Vrd));
366     end
367 end
368 max1(4,1)=max(abs(R11));
369 max1(4,2)=max(abs(R21));
370 if max1(4,2)<0.001;
371     max1(4,2)=0;
372 end
373 max1(4,3)=max(abs(R22));
```

```
374 if max1(4,3)<0.001;
375     max1(4,3)=0;
376 end
377 max1(4,4)=max(abs(R32));
378 if max1(4,4)<0.001;
379     max1(4,4)=0;
380 end
381 max1(4,5)=max(abs(R31));
382 if max1(4,5)<0.001;
383     max1(4,5)=0;
384 end
385 max1(4,6)=max(R81);
386 if max1(4,6)<0.001;
387     max1(4,6)=0;
388 end
389 max1(4,7)=max(abs(R51));
390 max1(4,8)=max(abs(R61));
391 max1(4,9)=max(abs(R71));
392 %%=====================================================================
393 % element 3
394 N =N_3;
395 Tor=Tor_3;
396 My1 = My1_3; % My end 1       KN*m
397 Mz1 = Mz1_3; % Mz end 1       KN*m
398 Qy1 = Qy1_3; % Qy end 1       KN
399 Qz1 = Qz1_3; % Qz end 1       KN
400 ii=size(N);
401 for j=1:1:ii
402     Nsd=abs(N(j)*1000);
403     Mysd=abs(My1(j)*1000);
404     Mzsd=abs(Mz1(j)*1000);
405     Q=abs(Qz1(j)*1000);
406     Q2=abs(Qy1(j)*1000);
407     Mtsd=abs(Tor(j)*1000);
408     sigma_csd=Nsd/A+sqrt(Mysd^2+Mzsd^2)/W;
409     lambda_s=abs(sigma_csd)/fcl*lambda_c+(sigma_psd/fh)^2*lambda_h;
```

```
410     if lambda_s<0.5
411         gama_M=1.15;
412     elseif lambda_s>=0.5 && lambda_s<=1.0
413         gama_M=0.85+0.60*lambda_s;
414     elseif lambda_s>1.0
415         gama_M=1.45;
416     end
417     gama_M_B=gama_M;
418     Mrd=fm*W/gama_M_B;                  %gama_M in bending
419     %-------------------------------------------------------------------
420     Vrd=A*fy/(2*sqrt(3))/gama_M_A; %shear force
421     %===================================================================
422     % axial tension   R11 R12
423     R11(j)=abs(Nsd/Ntrd);
424     %===================================================================
425     % bending    R21  R22
426     R21(j)=abs(Mysd/Mrd);
427     R22(j)=abs(Mzsd/Mrd);
428     %===================================================================
429     % shear without torsion    R31  R32
430     % The shear force in y direction is so small that is neglected.
431     R31(j)=abs(Q/Vrd);
432     R32(j)=abs(Q2/Vrd);
433     %===================================================================
434     % Shear from torsional moment  R81
435     Ip=pi/32*(D^4-(D-2*t)^4);
436     M_TRd=2*Ip*fy/(D*sqrt(3)*gama_M);
437     R81(j)=Mtsd/M_TRd;
438     %===================================================================
439     % axial tension and bending without hydrostatic pressure  R51  R52
440     R51(j)=abs((Nsd/Ntrd)^1.75+sqrt(Mysd^2+Mzsd^2)/Mrd);
441     %===================================================================
442     % shear and bending   R61 R62
443     Vrd=A*fy/(2*sqrt(3))/gama_M_A;
444     if Q/Vrd>=0.4
445         R61(j)=abs(sqrt(Mysd^2+Mzsd^2)/Mrd/(sqrt(1.4-Q/Vrd)));
```

```
446
447     elseif Q/Vrd<0.4
448         R61(j)=abs(sqrt(Mysd^2+Mzsd^2)/Mrd);
449     end
450     %=====================================================================
451     % Interaction shear, bending, moment and torsional moment   R71 R72
452     fd=fy/gama_M;
453     tau_TSd=Mtsd/(2*pi*(D/2)^2*t);
454     f_mred=fm*sqrt(1-3*(tau_TSd/fd)^2);
455     M_redrd=W*f_mred/gama_M;
456     if Q/Vrd<0.4
457         R71(j)=sqrt(Mysd^2+Mzsd^2)/M_redrd;
458     else
459         R71(j)=sqrt(Mysd^2+Mzsd^2)/(M_redrd*sqrt(1.4-Q/Vrd));
460     end
461 end
462
463 max1(6,1)=max(abs(R11));
464 max1(6,2)=max(abs(R21));
465 if max1(6,2)<0.001;
466     max1(6,2)=0;
467 end
468 max1(6,3)=max(abs(R22));
469 if max1(6,3)<0.001;
470     max1(6,3)=0;
471 end
472 max1(6,4)=max(abs(R32));
473 if max1(6,4)<0.001;
474     max1(6,4)=0;
475 end
476 max1(6,5)=max(abs(R31));
477 if max1(6,5)<0.001;
478     max1(6,5)=0;
479 end
480 max1(6,6)=max(R81);
481 if max1(6,6)<0.001;
```

```
482     max1(6,6)=0;
483 end
484 max1(6,7)=max(abs(R51));
485 max1(6,8)=max(abs(R61));
486 max1(6,9)=max(abs(R71));
487 %%=====================================================================
488 % element 4
489 N =N_4;
490 Tor=Tor_4;
491 My1 = My1_4; % My end 1       KN*m
492 Mz1 = Mz1_4; % Mz end 1       KN*m
493 Qy1 = Qy1_4; % Qy end 1       KN
494 Qz1 = Qz1_4; % Qz end 1       KN
495 ii=size(N);
496 for j=1:1:ii
497     Nsd=abs(N(j)*1000);
498     Mysd=abs(My1(j)*1000);
499     Mzsd=abs(Mz1(j)*1000);
500     Q=abs(Qz1(j)*1000);
501     Q2=abs(Qy1(j)*1000);
502     Mtsd=abs(Tor(j)*1000);
503     sigma_csd=Nsd/A+sqrt(Mysd^2+Mzsd^2)/W;
504     lambda_s=abs(sigma_csd)/fcl*lambda_c+(sigma_psd/fh)^2*lambda_h;
505     if lambda_s<0.5
506         gama_M=1.15;
507     elseif lambda_s>=0.5 && lambda_s<=1.0
508         gama_M=0.85+0.60*lambda_s;
509     elseif lambda_s>1.0
510         gama_M=1.45;
511     end
512     gama_M_B=gama_M;
513     Mrd=fm*W/gama_M_B;                %gama_M in bending
514     %---------------------------------------------------------------
515     Vrd=A*fy/(2*sqrt(3))/gama_M_A; %shear force
516     %=====================================================================
517     % axial tension   R11 R12
```

```
518     R11(j)=abs(Nsd/Ntrd);
519     %=====================================================================
520     % bending    R21  R22
521     R21(j)=abs(Mysd/Mrd);
522     R22(j)=abs(Mzsd/Mrd);
523     %=====================================================================
524     % shear without torsion    R31  R32
525     % The shear force in y direction is so small that is neglected.
526     %=====================================================================
527     % shear without torsion    R31  R32
528     % The shear force in y direction is so small that is neglected.
529     R31(j)=abs(Q/Vrd);
530     R32(j)=abs(Q2/Vrd);
531     %=====================================================================
532     % Shear from torsional moment  R81
533     Ip=pi/32*(D^4-(D-2*t)^4);
534     M_TRd=2*Ip*fy/(D*sqrt(3)*gama_M);
535     R81(j)=Mtsd/M_TRd;
536     %=====================================================================
537     % axial tension and bending without hydrostatic pressure  R51  R52
538     R51(j)=abs((Nsd/Ntrd)^1.75+sqrt(Mysd^2+Mzsd^2)/Mrd);
539     %=====================================================================
540     % shear and bending   R61 R62
541     Vrd=A*fy/(2*sqrt(3))/gama_M_A;
542     if Q/Vrd>=0.4
543         R61(j)=abs(sqrt(Mysd^2+Mzsd^2)/Mrd/(sqrt(1.4-Q/Vrd)));
544     elseif Q/Vrd<0.4
545         R61(j)=abs(sqrt(Mysd^2+Mzsd^2)/Mrd);
546     end
547     %=====================================================================
548     % Interaction shear, bending, moment and torsional moment   R71 R72
549     fd=fy/gama_M;
550     tau_TSd=Mtsd/(2*pi*(D/2)^2*t);
551     f_mred=fm*sqrt(1-3*(tau_TSd/fd)^2);
552     M_redrd=W*f_mred/gama_M;
553     if Q/Vrd<0.4
```

```
554         R71(j)=sqrt(Mysd^2+Mzsd^2)/M_redrd;
555     else
556         R71(j)=sqrt(Mysd^2+Mzsd^2)/(M_redrd*sqrt(1.4-Q/Vrd));
557     end
558 end
559 max1(8,1)=max(abs(R11));
560 max1(8,2)=max(abs(R21));
561 if max1(8,2)<0.001;
562     max1(8,2)=0;
563 end
564 max1(8,3)=max(abs(R22));
565 if max1(8,3)<0.001;
566     max1(8,3)=0;
567 end
568 max1(8,4)=max(abs(R32));
569 if max1(8,4)<0.001;
570     max1(8,4)=0;
571 end
572 max1(8,5)=max(abs(R31));
573 if max1(8,5)<0.001;
574     max1(8,5)=0;
575 end
576 max1(8,6)=max(R81);
577 if max1(8,6)<0.001;
578     max1(8,6)=0;
579 end
580 max1(8,7)=max(abs(R51));
581 max1(8,8)=max(abs(R61));
582 max1(8,9)=max(abs(R71));
```

A.2 Matlab Code for Power Calculation

```
1 clear all;
2 clc;
```

```
3  BPTO = 650;
4  dataall = load('Analysis_noddis.asc');
5  data = dataall (10001:1:end,:);
6  save('data.mat','data');
7  time = data(:,1);
8
9  WEC1pos = data(:,5:7);
10
11 anch11 = data(:,17:19);
12 anch12 = data(:,23:25);
13 anch1t   = (anch11+anch12)/2;
14 anch1y    = anch12 - anch11;
15
16 joint11 = data(:,14:16);
17 joint21 = data(:,20:22);
18
19 vec21 = (WEC1pos-anch1t);
20
21 ang1 = zeros(length(vec21),1);
22 angle1=zeros(length(vec21),1);
23 for ii = 1:length(vec21)-1
24     v11 = vec21(ii,:)/norm(vec21(ii,:));
25     v12 = vec21(ii+1,:)/norm(vec21(ii+1,:));
26     vn1 = anch1y(ii,:)/norm(anch1y(ii,:));
27     xx1 = dot(vn1,cross(v11,v12));
28     ang1(ii) = acos(dot(v11,v12))*sign(xx1);
29     angle1(ii+1)=ang1(ii)+angle1(ii);
30
31 end
32
33 dtheta1 = ang1./0.05;
34 Force1 = dtheta1*180/pi*BPTO;
35 Power1 = 2*Force1.*dtheta1;
36
37 figure(1)
38 plot(time-500,Power1)
```

```
39 title('Produced Power of WEC1 of SFC');
40 xlabel('Time [s]')
41 ylabel('Produced Power WEC1 [kW]')
42 hold on
43 plot([time(1)-500 time(end)-500],[mean(Power1) mean(Power1)],'r--')
44 legend('Instant Power','Mean Value')
45
46 WECpos2 = data(:,8:10);
47
48 anch21 = data(:,29:31);
49 anch22 = data(:,35:37);
50 anch2t   = (anch21+anch22)/2;
51 anch2y    = anch22 - anch21;
52
53 joint21 = data(:,26:28);
54 joint22 = data(:,32:34);
55
56 vec22 = (WECpos2-anch2t);
57
58 ang2 = zeros(length(vec22),1);
59 angle2=zeros(length(vec22),1);
60 for ii = 1:length(vec22)-1
61     v21 = vec22(ii,:)/norm(vec22(ii,:));
62     v22 = vec22(ii+1,:)/norm(vec22(ii+1,:));
63     vn2 = anch2y(ii,:)/norm(anch2y(ii,:));
64     xx2 = dot(vn2,cross(v21,v22));
65     ang2(ii) = acos(dot(v21,v22))*sign(xx2);
66     angle2(ii+1)=ang2(ii)+angle2(ii);
67 end
68
69 dtheta2 = ang2./0.05;
70 Force2 = dtheta2*180/pi*BPTO;
71 Power2 = 2*Force2.*dtheta2;
72
73 figure(2)
74 plot(time-500,Power2)
```

```
title('Produced Power of WEC2 of SFC');
xlabel('Time [s]')
ylabel('Produced Power WEC2 [kW]')
hold on
plot([time(1)-500 time(end)-500],[mean(Power2) mean(Power2)],'r--')
legend('Instant Power','Mean Value')
saveas(figure(2),'Power WEC2','fig')

vec22 = (WECpos2-anch2t);

WECpos3 = data(:,11:13);

anch31 = data(:,47:49);
anch32 = data(:,41:43);
anch3t   = (anch31+anch32)/2;
anch3y    = anch32 - anch31;

joint31 = data(:,38:40);
joint32 = data(:,44:46);

vec32 = (WECpos3-anch3t);

ang3 = zeros(length(vec32),1);
angle3=zeros(length(vec32),1);
for ii = 1:length(vec32)-1
    v31 = vec32(ii,:)/norm(vec32(ii,:));
    v32 = vec32(ii+1,:)/norm(vec32(ii+1,:));
    vn3 = anch3y(ii,:)/norm(anch3y(ii,:));
    xx3 = dot(vn3,cross(v31,v32));
    ang3(ii) = acos(dot(v31,v32))*sign(xx3);
    angle3(ii+1)=ang3(ii)+angle3(ii);
end

dtheta3 = ang3./0.05;
Force3 = dtheta3*180/pi*BPTO;
Power3 = 2*Force3.*dtheta3;
```

```
111
112 figure(3)
113 plot(time-500,Power3)
114 title('Produced Power of WEC3 of SFC');
115 xlabel('Time [s]')
116 ylabel('Produced Power, WEC3 [kW]')
117 hold on
118 plot([time(1)-500 time(end)-500],[mean(Power3) mean(Power3)],'r--')
119 legend('Instant Power','Mean Value')
120
121 M4=mean(Power1+Power2+Power3;
122 figure(4)
123 plot(time-500,Power1+Power2+Power3)
124 title('Produced Power of All WECs of SFC');
125 xlabel('Time [s]')
126 ylabel('Produced Power , All WECs [kW]')
127 hold on
128 plot([time(1)-500 time(end)-500],[M4 M4],'r--')
129 legend('Instant Power','Mean value')
130
131 MM=mean(angle1*180/pi);
132 h2=figure(5);
133 plot(time,angle1*180/pi);
134 title('Relative Roll Motion between Semi-submersible and WEC1');
135 xlabel('Time [s]');
136 ylabel('Roll [deg]');
137 hold on;
138 plot(time,MM,'r--');
139 legend('','Mean Position');
140 legend('Instant Position','Mean Position');
141 saveTightFigure(h2,'RelativeRollofSFC');
142 saveas(h2,'RelativeRollofSFC','pdf');
143
144 figure(6)
145 plot(time,angle2*180/pi);
146 title('Rotation of WEC2');
```

```
147 xlabel('Time [s]');
148 ylabel('\theta [deg]');
149 saveas(figure(6),'Rotation WEC2','fig');
150
151 figure(7)
152 plot(time,angle3*180/pi);
153 title('Rotation of WEC3');
154 xlabel('Time [s]');
155 ylabel('\theta [deg]');
156 saveas(figure(7),'Rotation WEC3','fig');
157
158 %=========================================================================
159 % Pick out the max power and the average power, max rotation angle
160
161 max_p=[0 0 0];
162 ave_p=[0 0 0 0];
163 max_theta=[0 0 0];
164
165 max_p(1)=max(Power1);
166 max_p(2)=max(Power2);
167 max_p(3)=max(Power3);
168 ave_p(1)=mean(Power1);
169 ave_p(2)=mean(Power2);
170 ave_p(3)=mean(Power3);
171 ave_p(4)=mean(Power1+Power2+Power3);
172 max_theta(1)=max(angle1);
173 max_theta(2)=max(angle2);
174 max_theta(3)=max(angle3);
175 max_theta=max_theta*180/pi;
176 %=========================================================================
177 res=[ave_p  max_p max_theta];
```

Appendix B

Maximum Utility Factor Figures

This appendix displays all the figures of MUFs for both WECs of SFC and the BFWEC in all simulated sea states in this thesis.

B.1 WECs of SFC

B.1.1 MUF Figures in Opearational Sea State

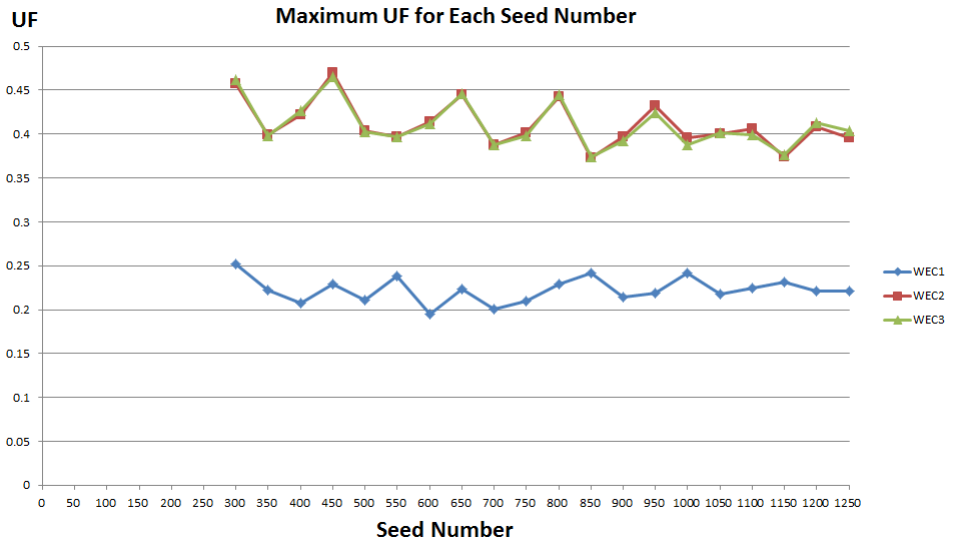

Figure B.1: Maximum utility factor for each seed number when $Hs = 6m, Tz = 12.6s, V = 8m/s, \theta = 0^0$.

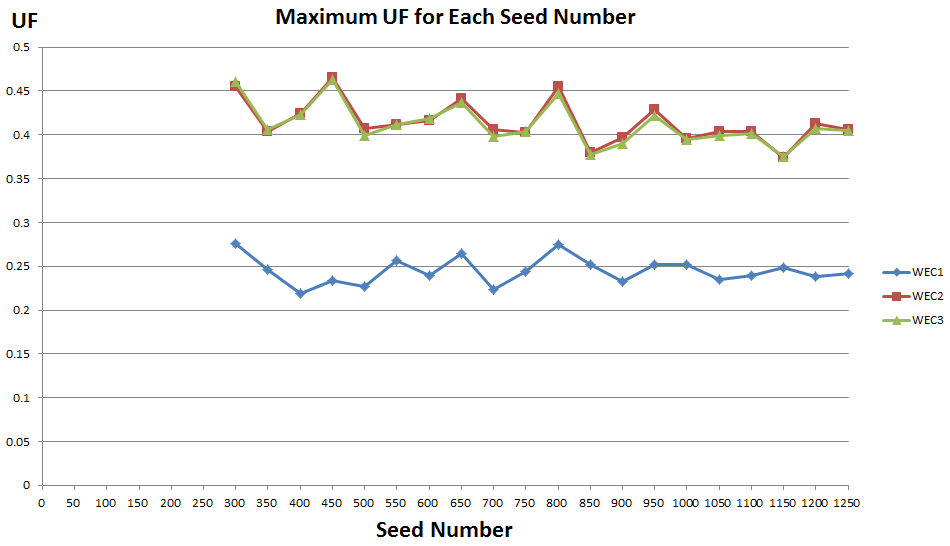

Figure B.2: Maximum utility factor for each seed number when $Hs = 6m, Tz = 12.6s, V = 11.4m/s, \theta = 0^0$.

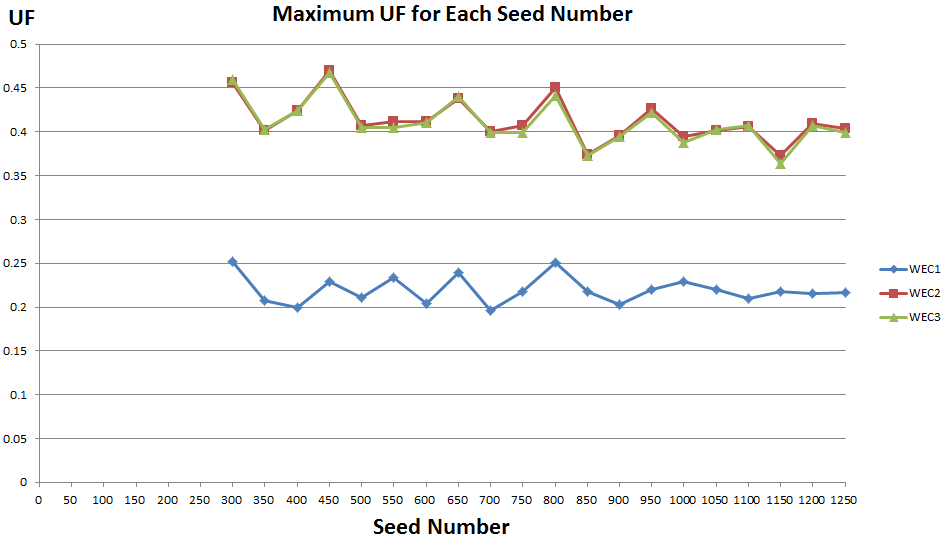

Figure B.3: Maximum utility factor for each seed number when $Hs = 6m, Tz = 12.6s, V = 18m/s, \theta = 0^0$.

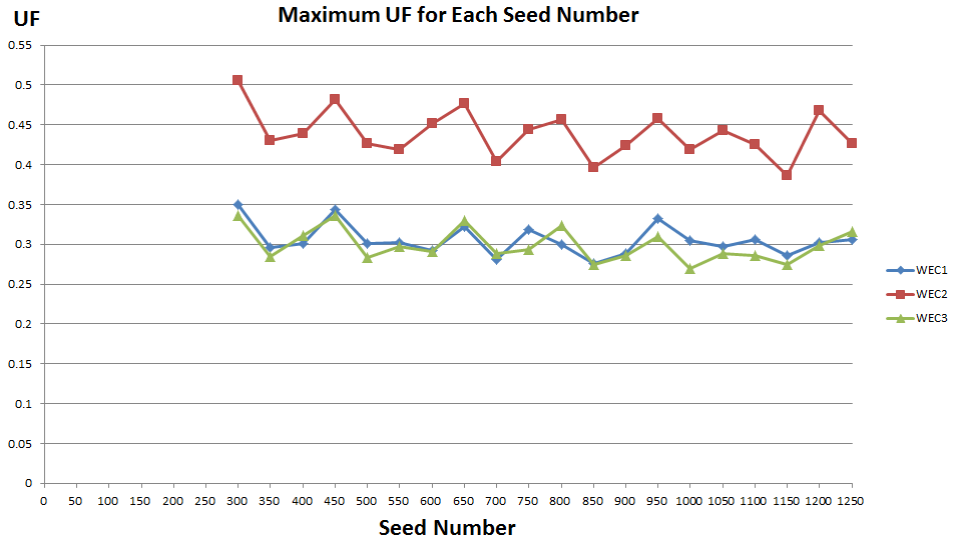

Figure B.4: Maximum utility factor for each seed number when $Hs = 6m, Tz = 12.6s, V = 8m/s, \theta = 30^0$.

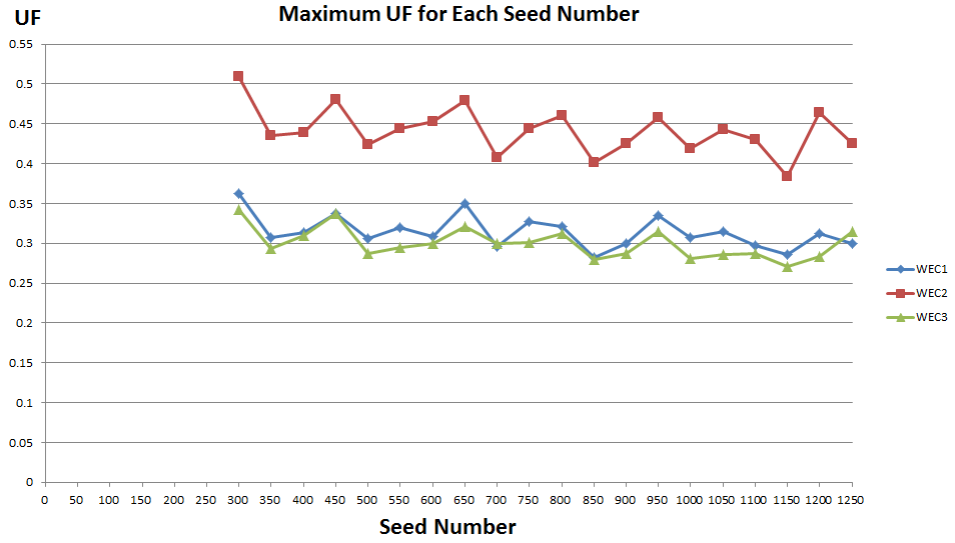

Figure B.5: Maximum utility factor for each seed number when $Hs = 6m, Tz = 12.6s, V = 11.4m/s, \theta = 30^0$.

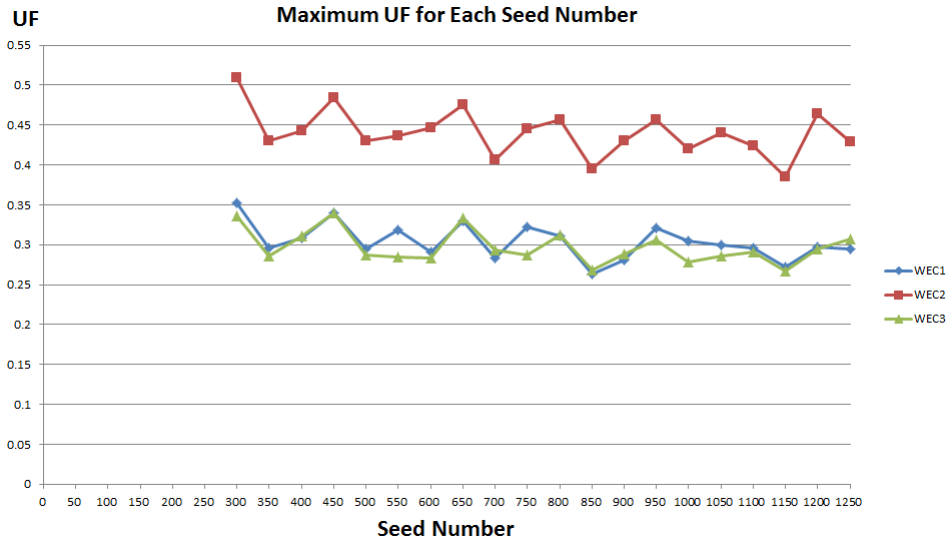

Figure B.6: Maximum utility factor for each seed number when $Hs = 6m, Tz = 12.6s, V = 18m/s, \theta = 30^0$.

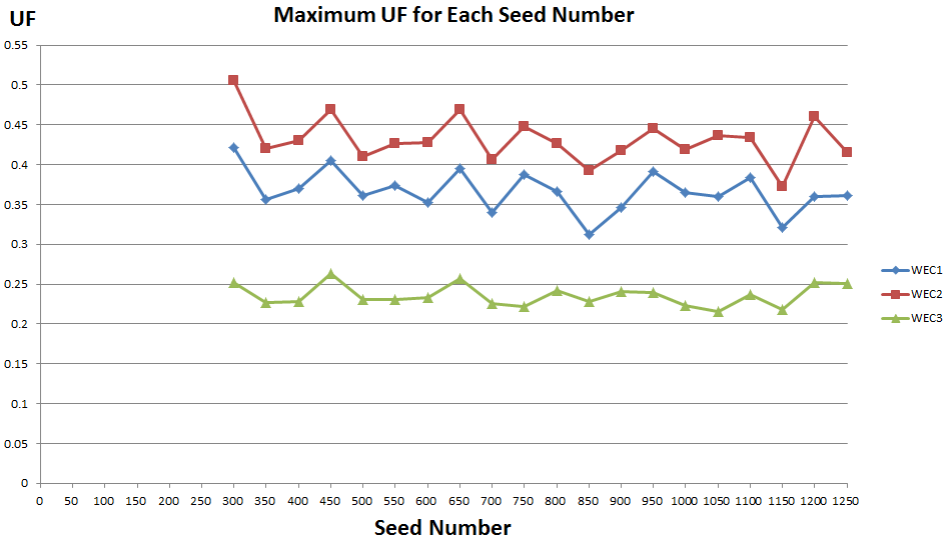

Figure B.7: Maximum utility factor for each seed number when $Hs = 6m, Tz = 12.6s, V = 8m/s, \theta = 45^0$.

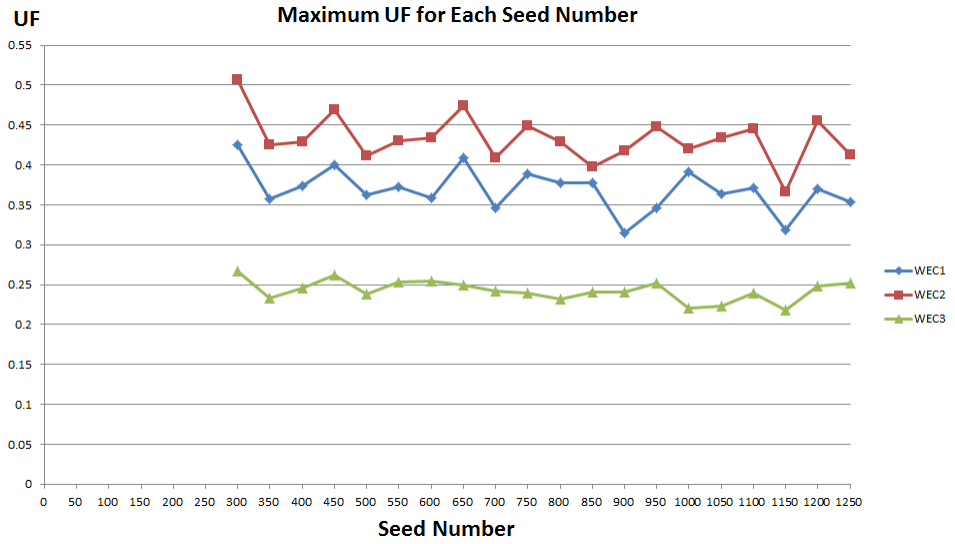

Figure B.8: Maximum utility factor for each seed number when $Hs = 6m, Tz = 12.6s, V = 11.4m/s, \theta = 45^0$.

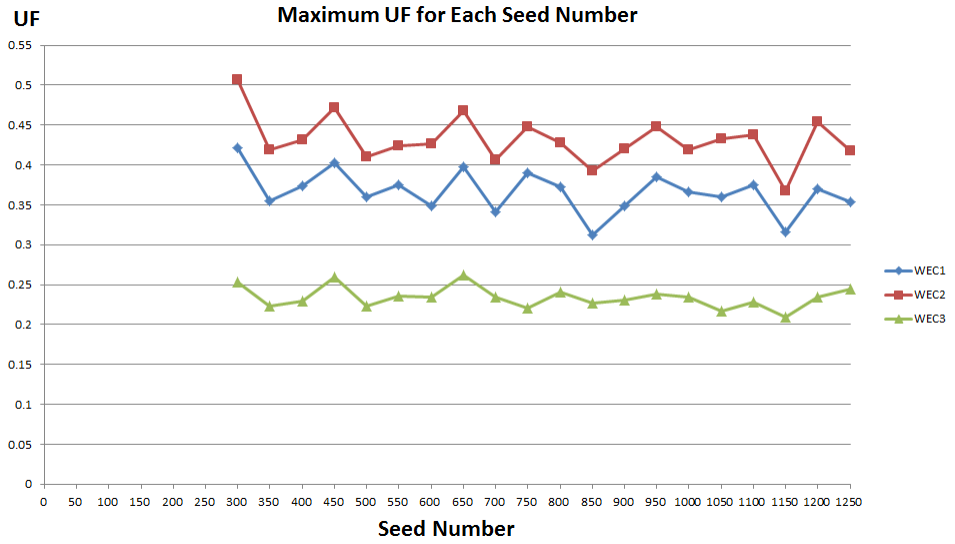

Figure B.9: Maximum utility factor for each seed number when $Hs = 6m, Tz = 12.6s, V = 18m/s, \theta = 45^0$.

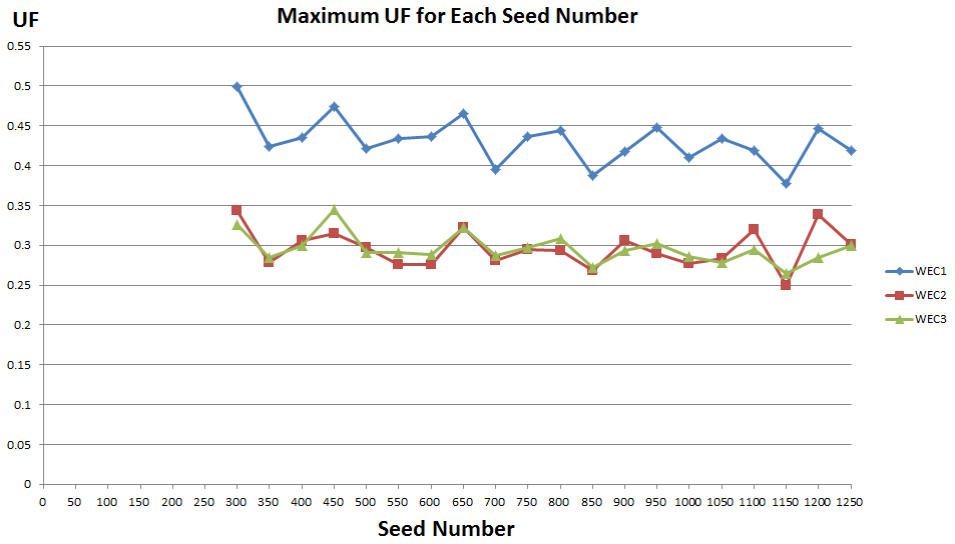

Figure B.10: Maximum utility factor for each seed number when $Hs = 6m, Tz = 12.6s, V = 8m/s, \theta = 90^0$.

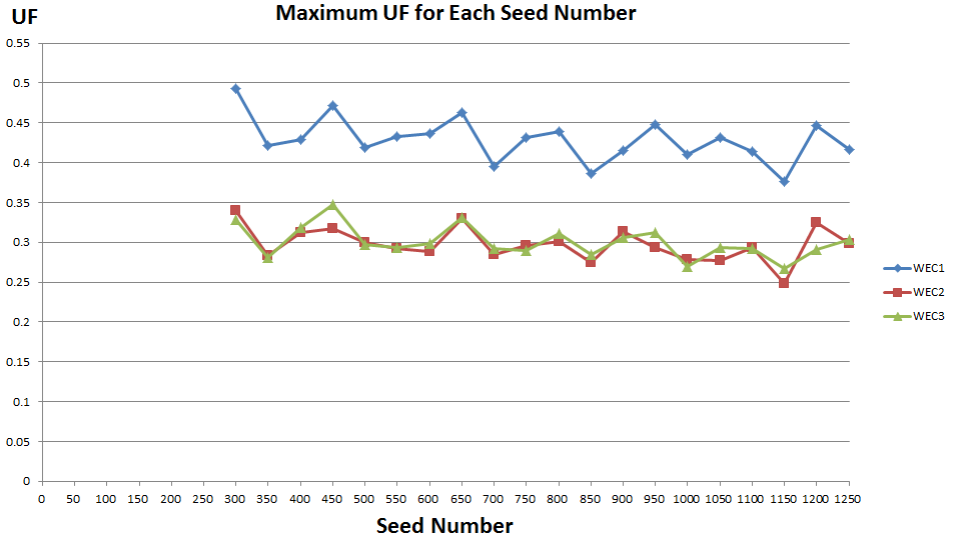

Figure B.11: Maximum utility factor for each seed number when $Hs = 6m, Tz = 12.6s, V = 11.4m/s, \theta = 90^0$.

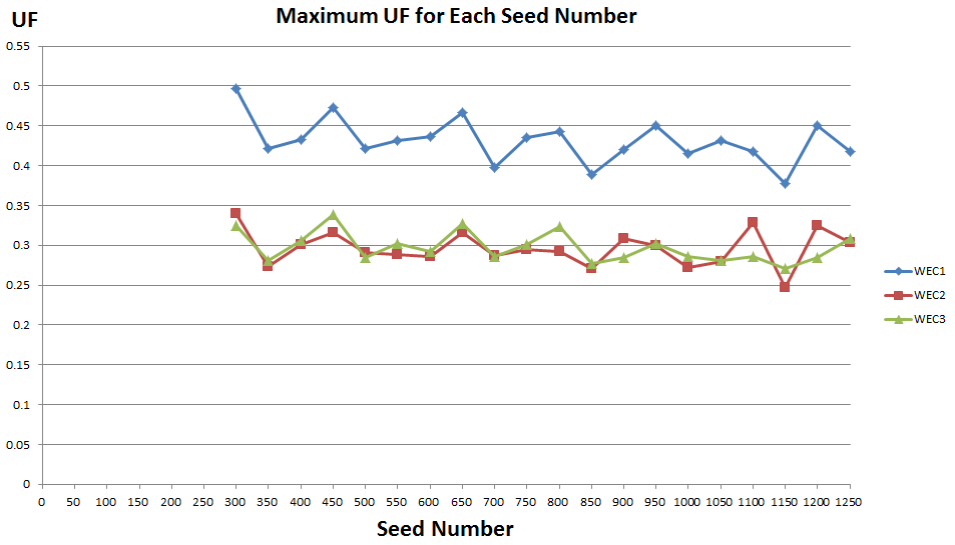

Figure B.12: Maximum utility factor for each seed number when $Hs = 6m, Tz = 12.6s, V = 18m/s, \theta = 90^0$.

B.1.2 MUF Figures in Survival Sea State

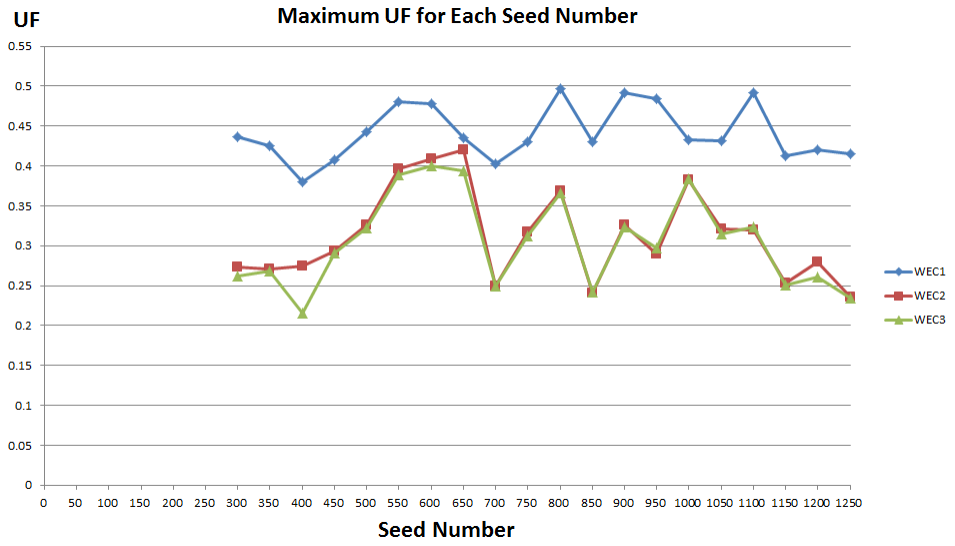

Figure B.13: Maximum utility factor for each seed number when $Hs = 15.6m, Tz = 14.5s, V = 8m/s, \theta = 0^0$.

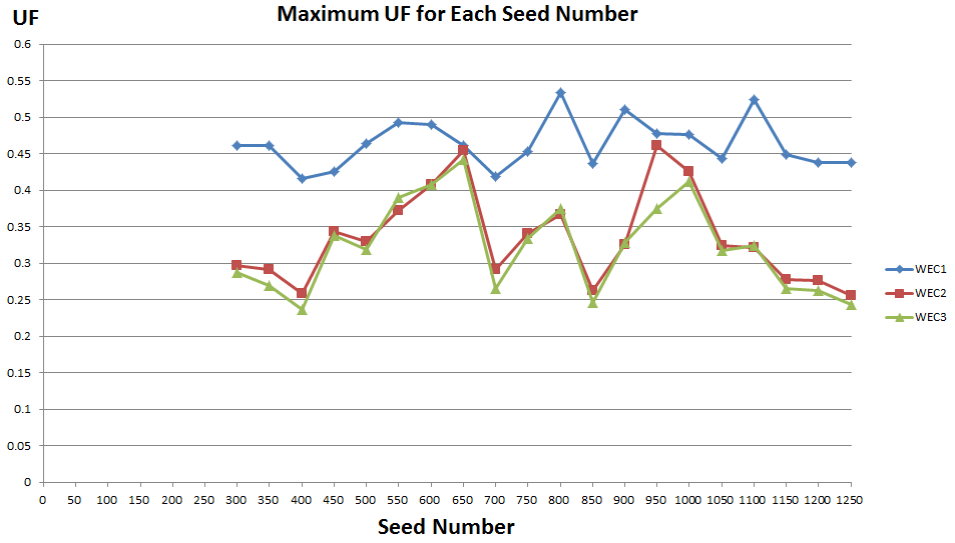

Figure B.14: Maximum utility factor for each seed number when $Hs = 15.6m, Tz = 14.5s, V = 11.4m/s, \theta = 0^0$.

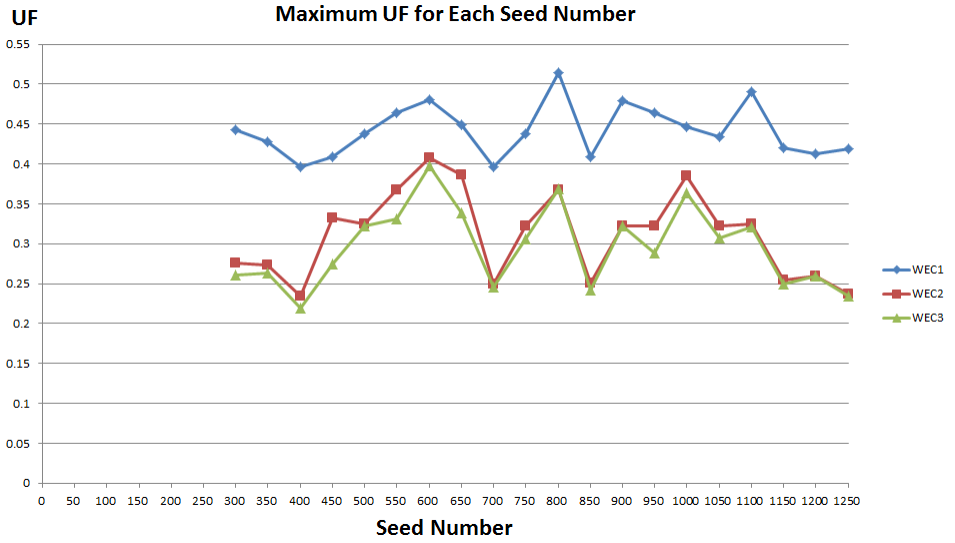

Figure B.15: Maximum utility factor for each seed number when $Hs = 15.6m, Tz = 14.5s, V = 18m/s, \theta = 0^0$.

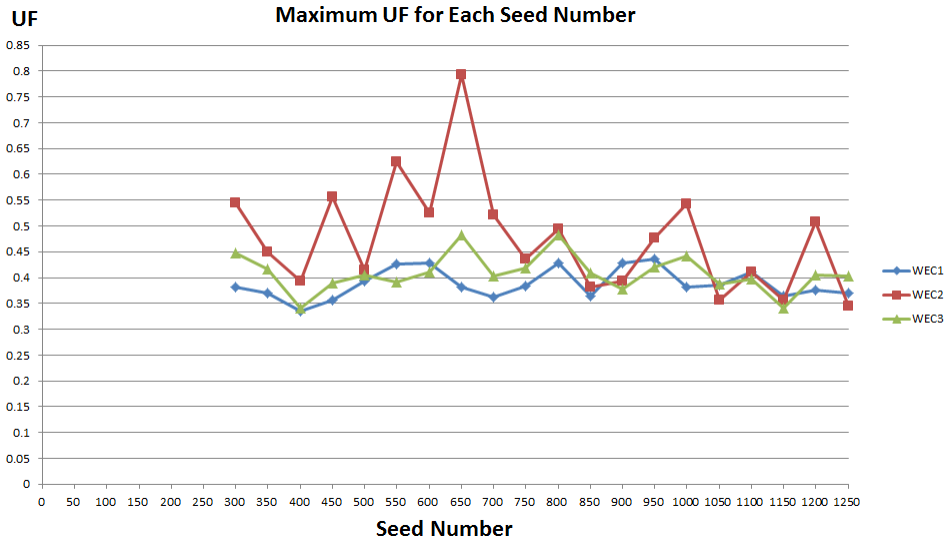

Figure B.16: Maximum utility factor for each seed number when $Hs = 15.6m, Tz = 14.5s, V = 8m/s, \theta = 30^0$.

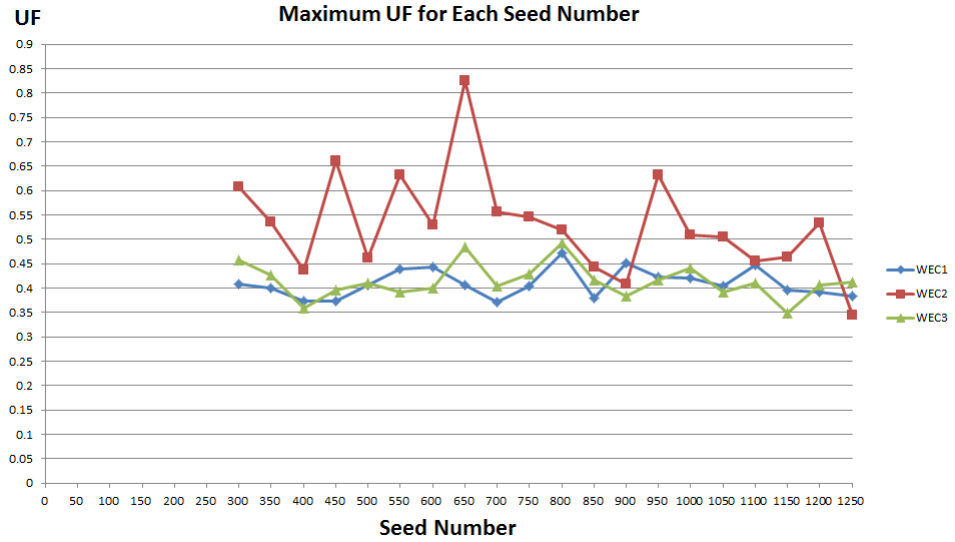

Figure B.17: Maximum utility factor for each seed number when $Hs = 15.6m, Tz = 14.5s, V = 11.4m/s, \theta = 30^0$.

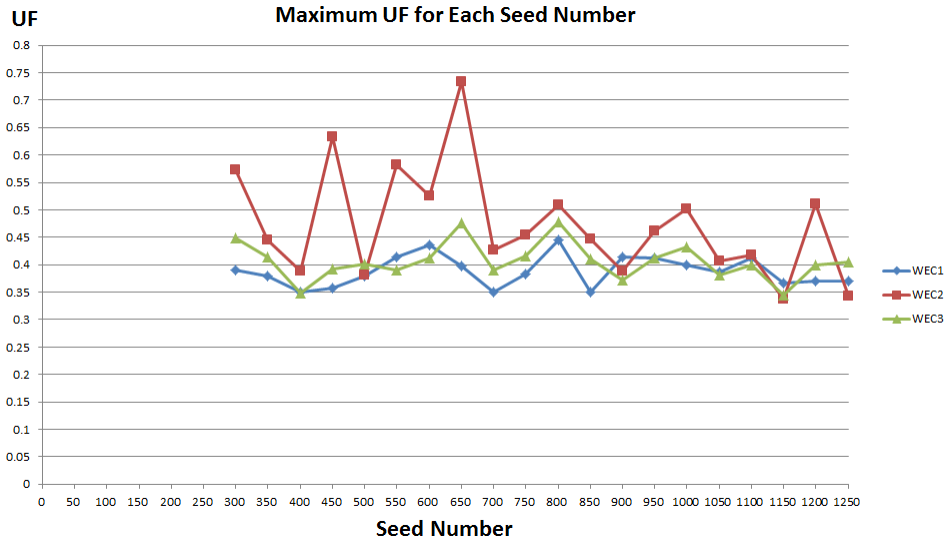

Figure B.18: Maximum utility factor for each seed number when $Hs = 15.6m, Tz = 14.5s, V = 18m/s, \theta = 30^0$.

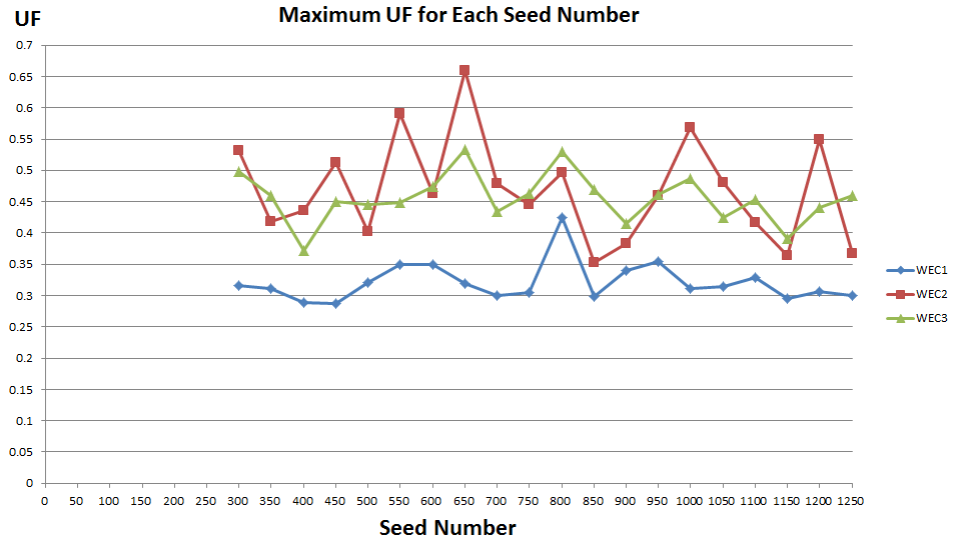

Figure B.19: Maximum utility factor for each seed number when $Hs = 15.6m, Tz = 14.5s, V = 8m/s, \theta = 45^0$.

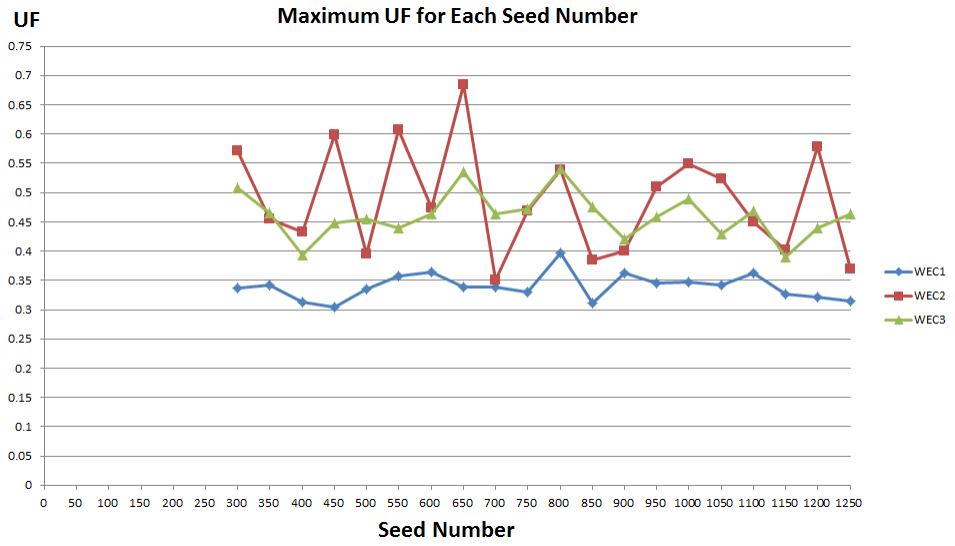

Figure B.20: Maximum utility factor for each seed number when $Hs = 15.6m, Tz = 14.5s, V = 11.4m/s, \theta = 45^0$.

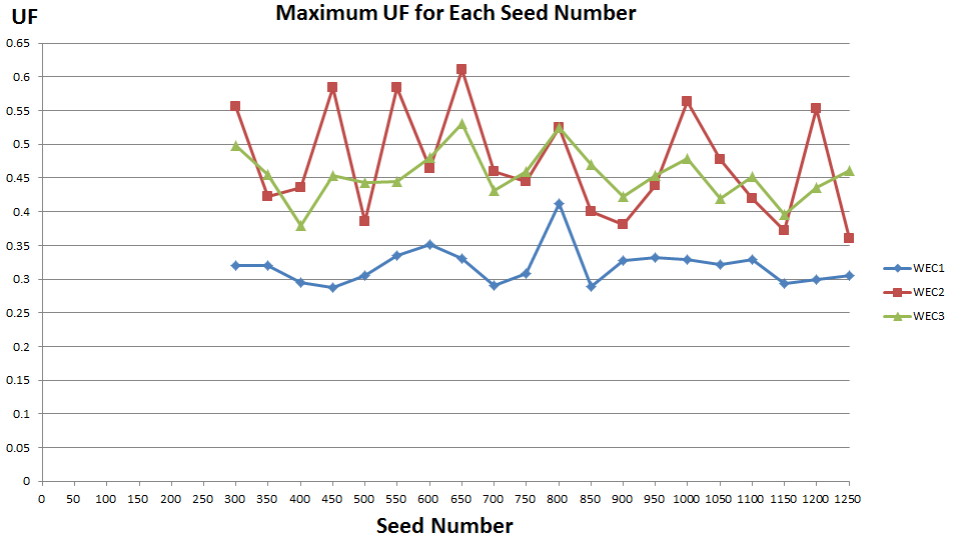

Figure B.21: Maximum utility factor for each seed number when $Hs = 15.6m, Tz = 14.5s, V = 18m/s, \theta = 45^0$.

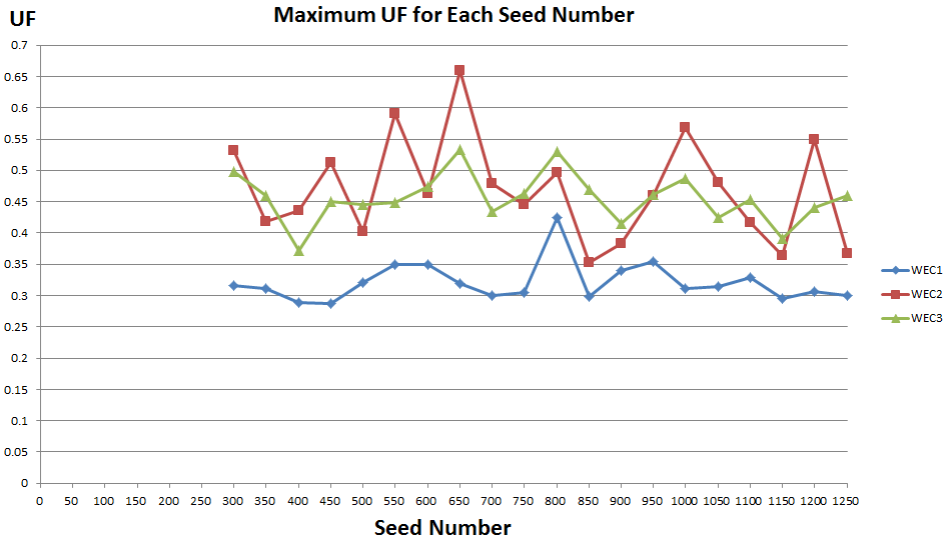

Figure B.22: Maximum utility factor for each seed number when $Hs = 15.6m, Tz = 14.5s, V = 8m/s, \theta = 90^0$.

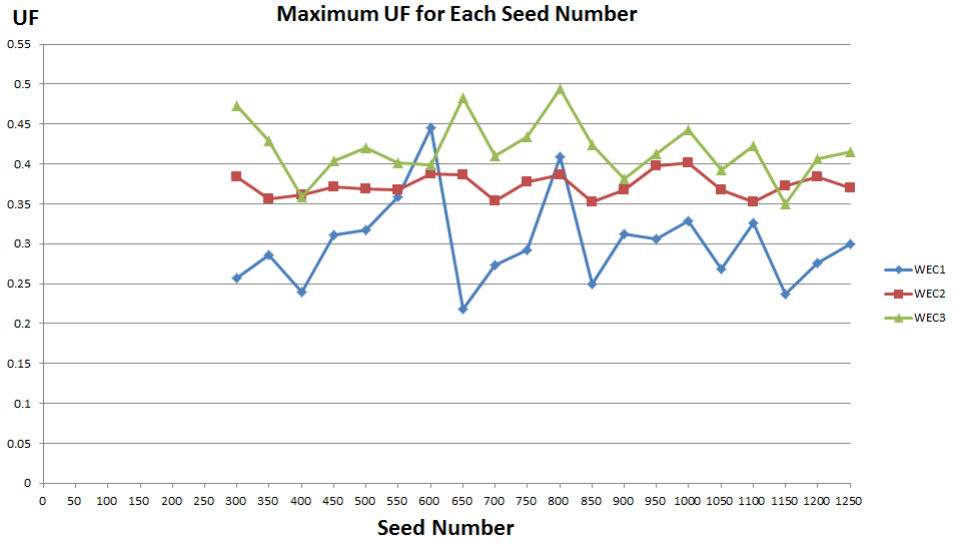

Figure B.23: Maximum utility factor for each seed number when $Hs = 15.6m, Tz = 14.5s, V = 11.4m/s, \theta = 90^0$.

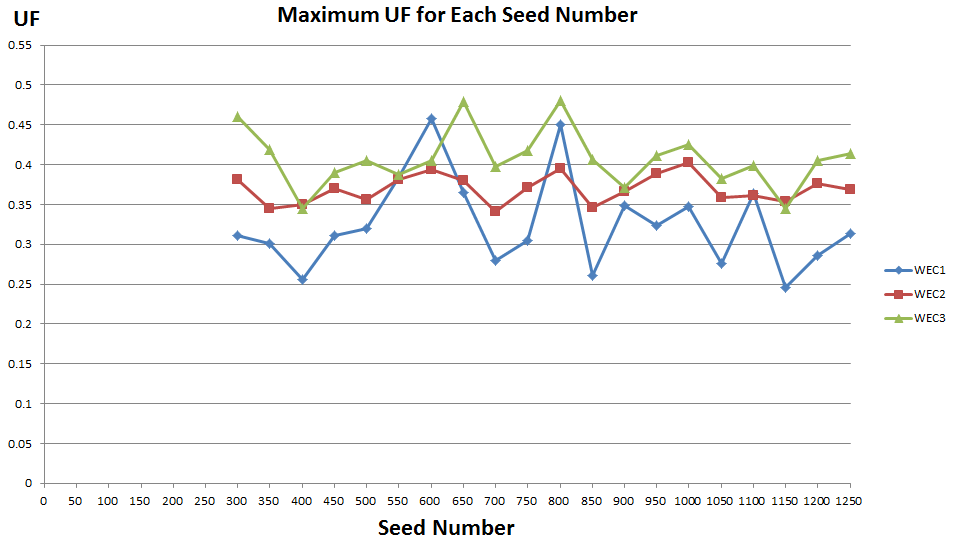

Figure B.24: Maximum utility factor for each seed number when $Hs = 15.6m, Tz = 14.5s, V = 18m/s, \theta = 90^0$.

B.2 Bottom-Fixed Wave Energy Converter

B.2.1 MUF Figures in Opearational Sea State

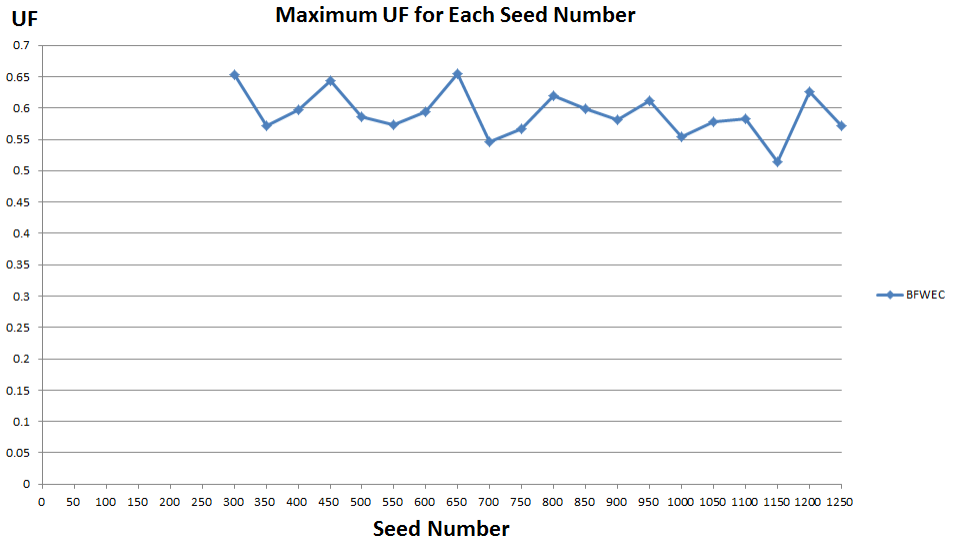

Figure B.25: Maximum utility factor for each seed number when $Hs = 6m, Tz = 12.6s, \theta = 0^0$.

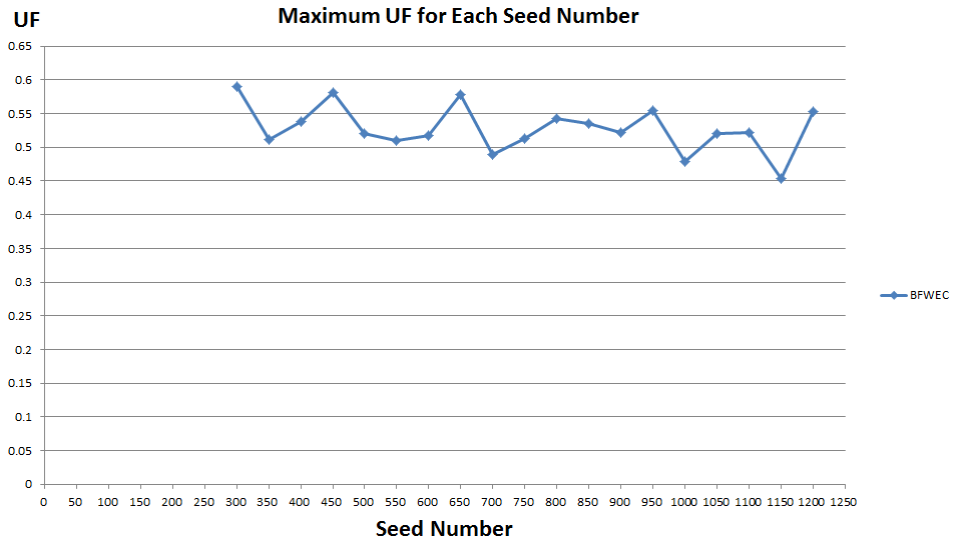

Figure B.26: Maximum utility factor for each seed number when $Hs = 6m, Tz = 12.6s, \theta = 30^0$.

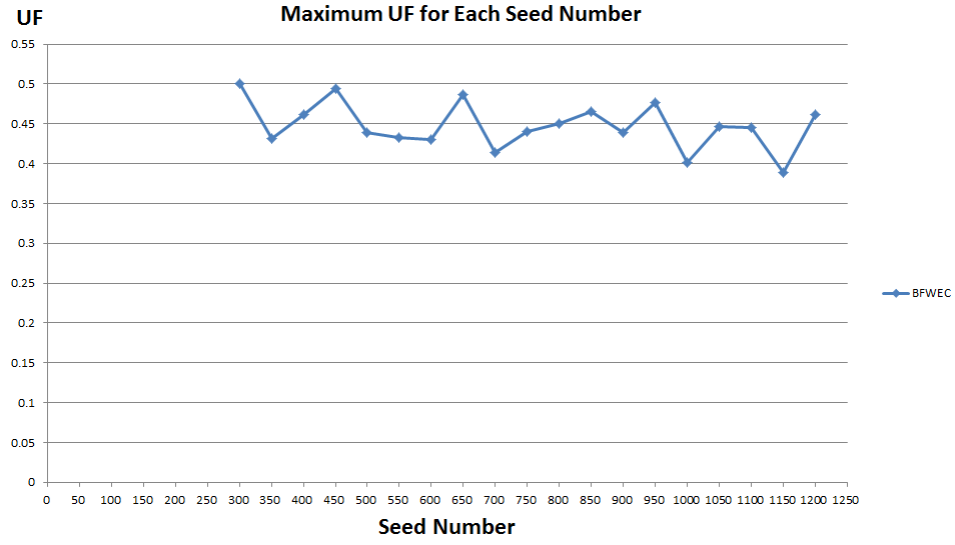

Figure B.27: Maximum utility factor for each seed number when $Hs = 6m, Tz = 12.6s, \theta = 45^0$.

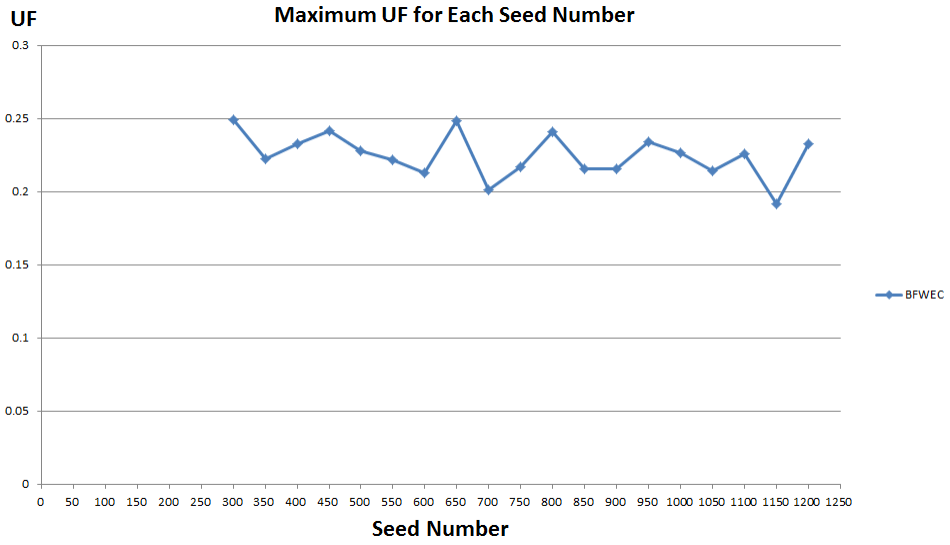

Figure B.28: Maximum utility factor for each seed number when $Hs = 6m, Tz = 12.6s, \theta = 90^0$.

B.2.2 MUF Figures in Survival Sea State

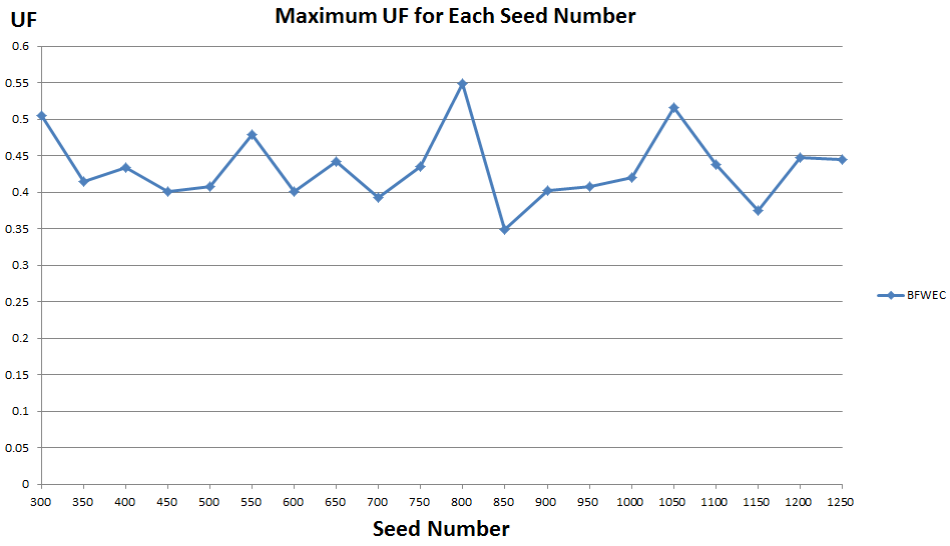

Figure B.29: Maximum utility factor for each seed number when $Hs = 15.6m, Tz = 14.5s, \theta = 0^0$.

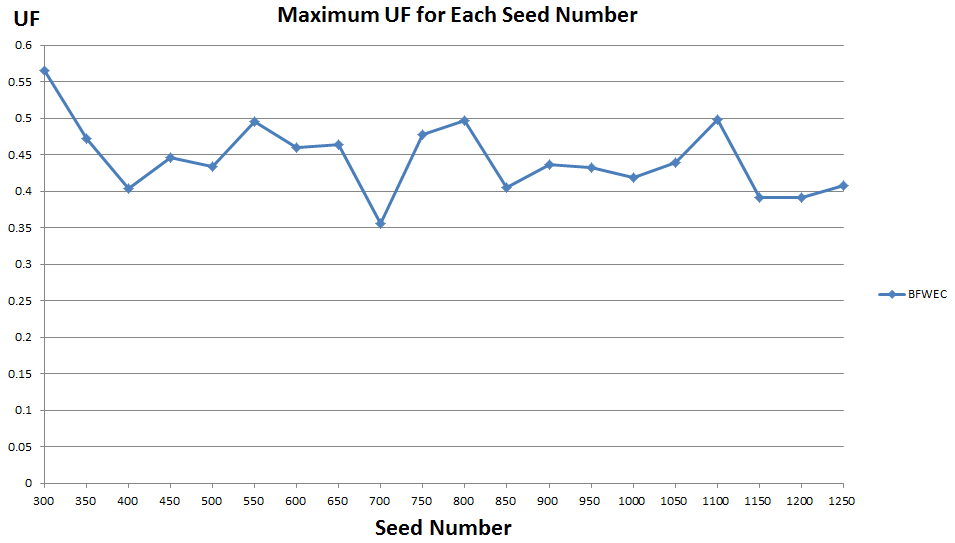

Figure B.30: Maximum utility factor for each seed number when $Hs = 15.6m, Tz = 14.5s, \theta = 30^0$.

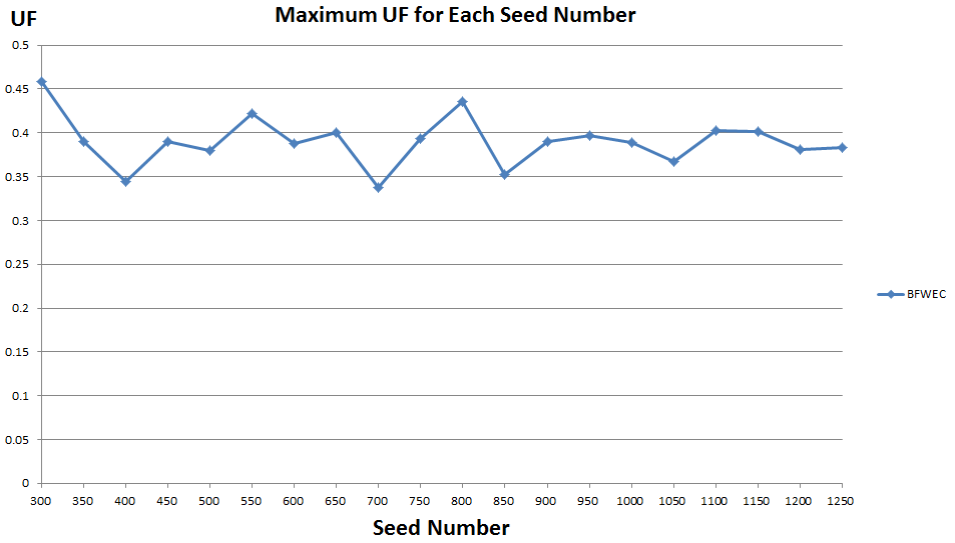

Figure B.31: Maximum utility factor for each seed number when $Hs = 15.6m, Tz = 14.5s, \theta = 45^0$.

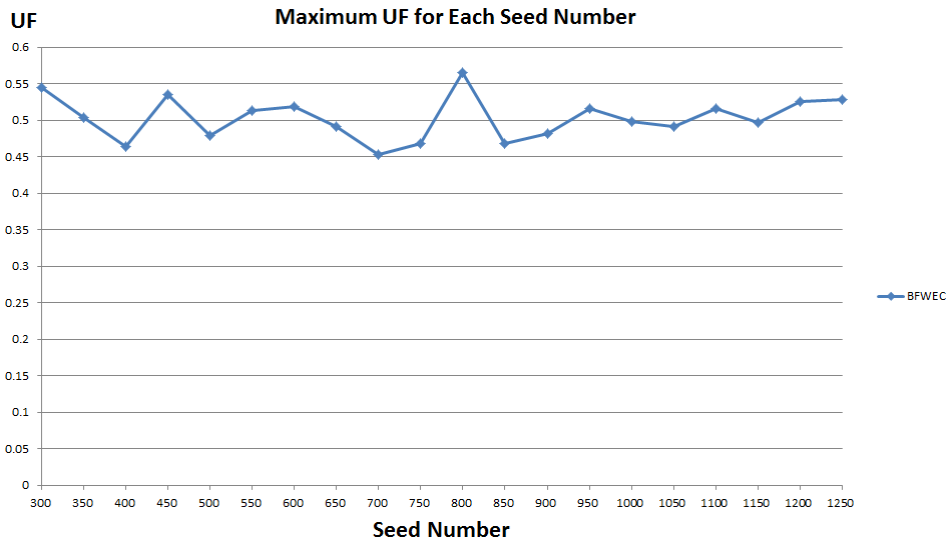

Figure B.32: Maximum utility factor for each seed number when $Hs = 15.6m, Tz = 14.5s, \theta = 90^0$.

Appendix C

Produced Power Figures

This appendix displays all the figures of produced power for both WECs of SFC and the BFWEC in all simulations of operational sea state in this thesis.

C.1 Power Produced by WECs of SFC

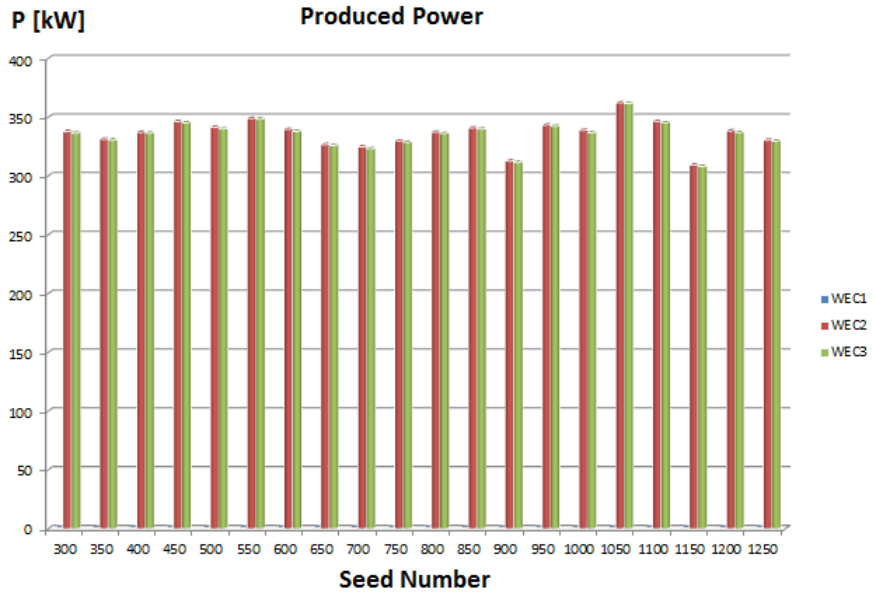

Figure C.1: Produced Power by WECs when $Hs = 6m, Tz = 12.6s, V = 8m/s, \theta = 0^0$.

C.2 Power Produced by BFWEC

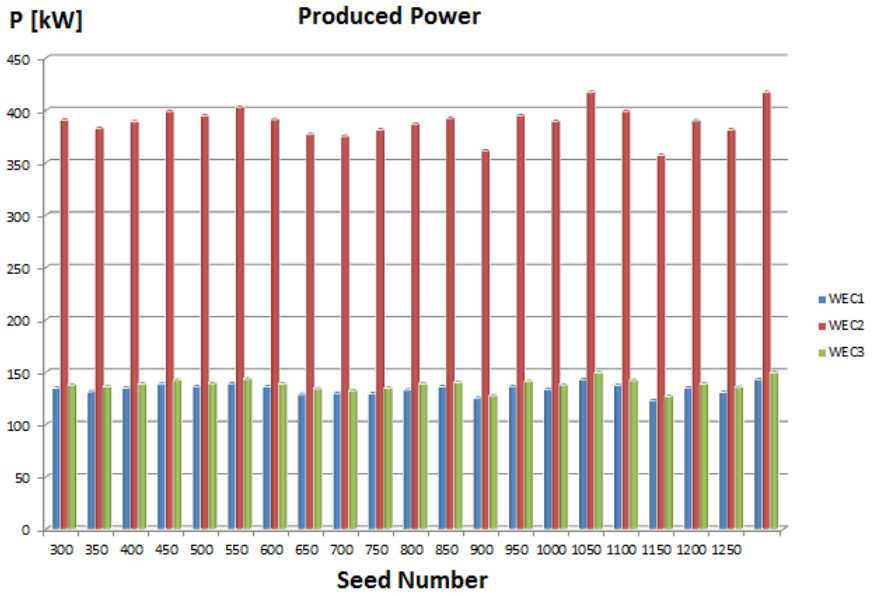

Figure C.2: Produced Power by WECs when $Hs = 6m, Tz = 12.6s, V = 8m/s, \theta = 30^0$.

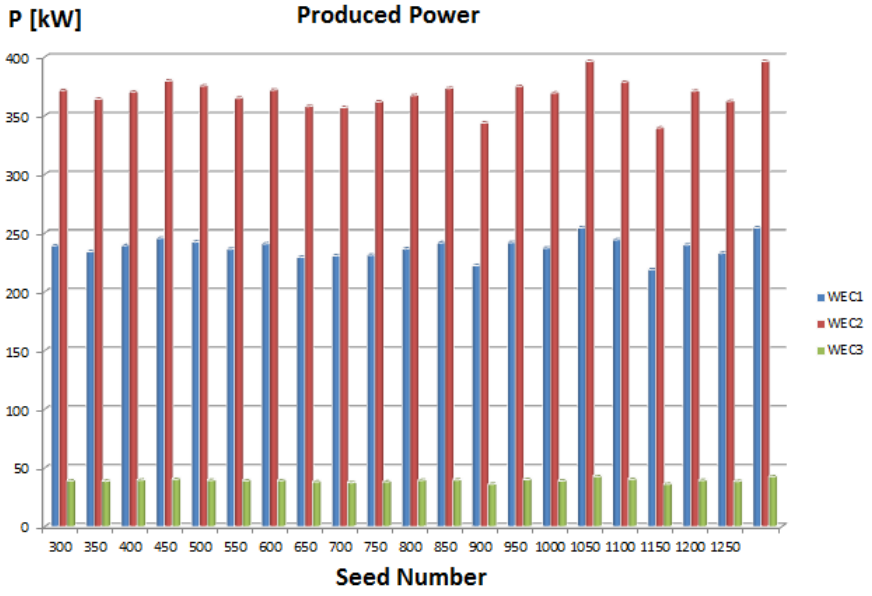

Figure C.3: Produced Power by WECs when $Hs = 6m, Tz = 12.6s, V = 8m/s, \theta = 45^0$.

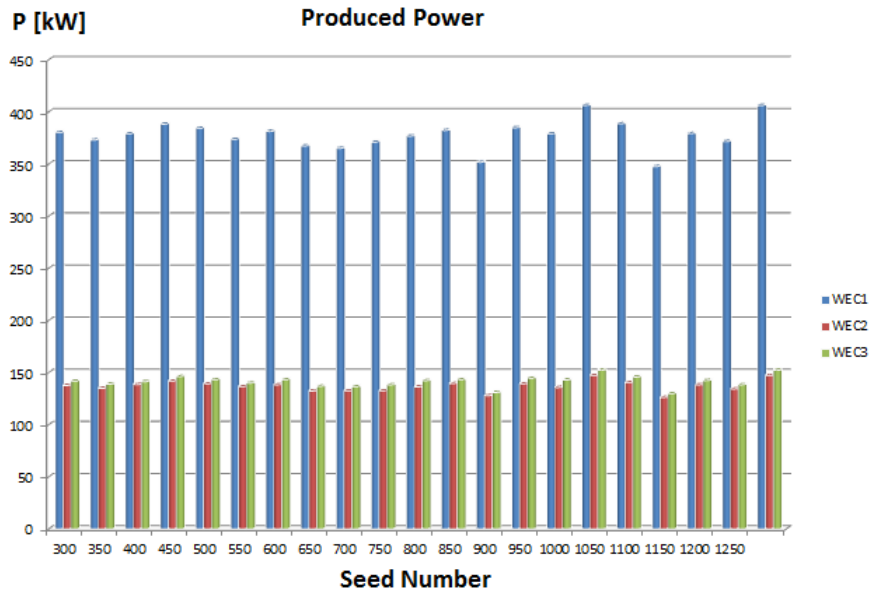

Figure C.4: Produced Power by WECs when $Hs = 6m, Tz = 12.6s, V = 8m/s, \theta = 90^0$.

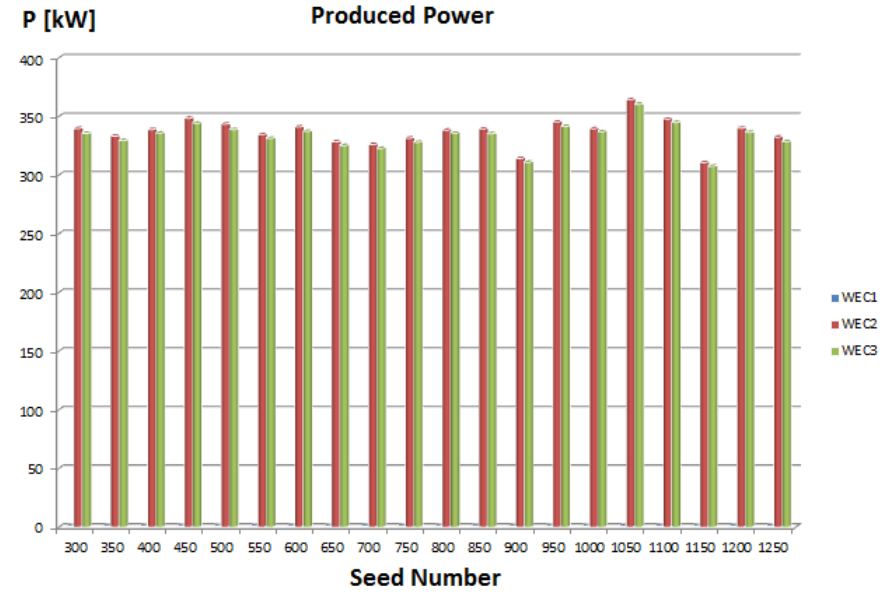

Figure C.5: Produced Power by WECs when $Hs = 6m, Tz = 12.6s, V = 11.4m/s, \theta = 0^0$.

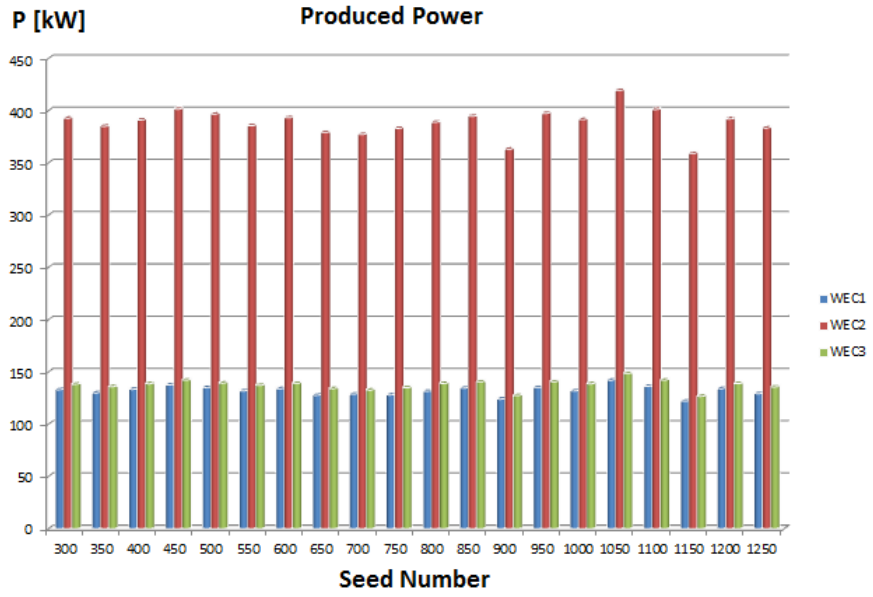

Figure C.6: Produced Power by WECs when $Hs = 6m, Tz = 12.6s, V = 11.4m/s, \theta = 30^0$.

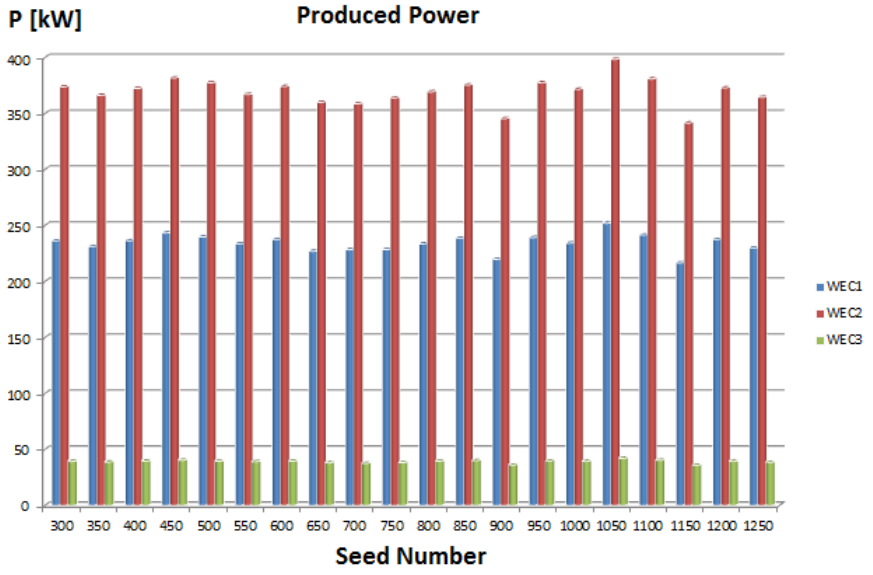

Figure C.7: Produced Power by WECs when $Hs = 6m, Tz = 12.6s, V = 11.4m/s, \theta = 45^0$.

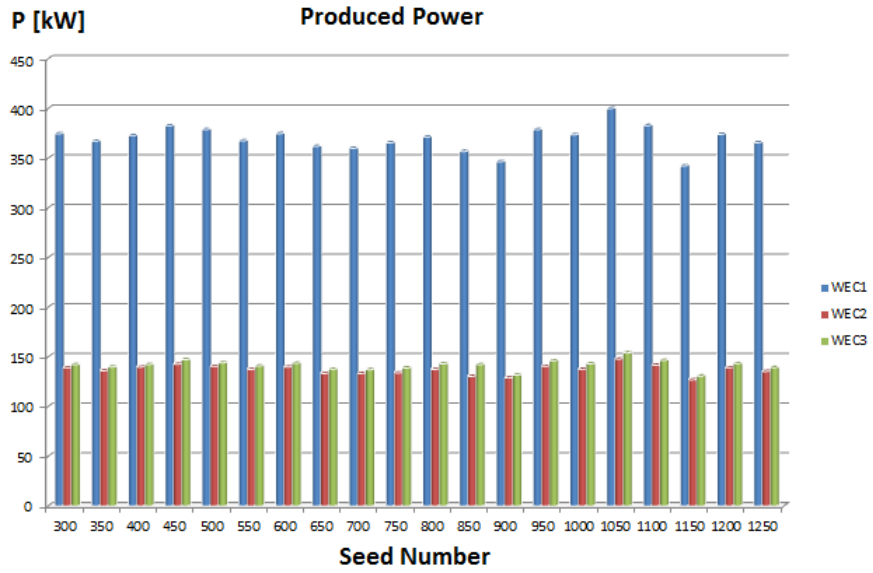

Figure C.8: Produced Power by WECs when $Hs = 6m, Tz = 12.6s, V = 11.4m/s, \theta = 90^0$.

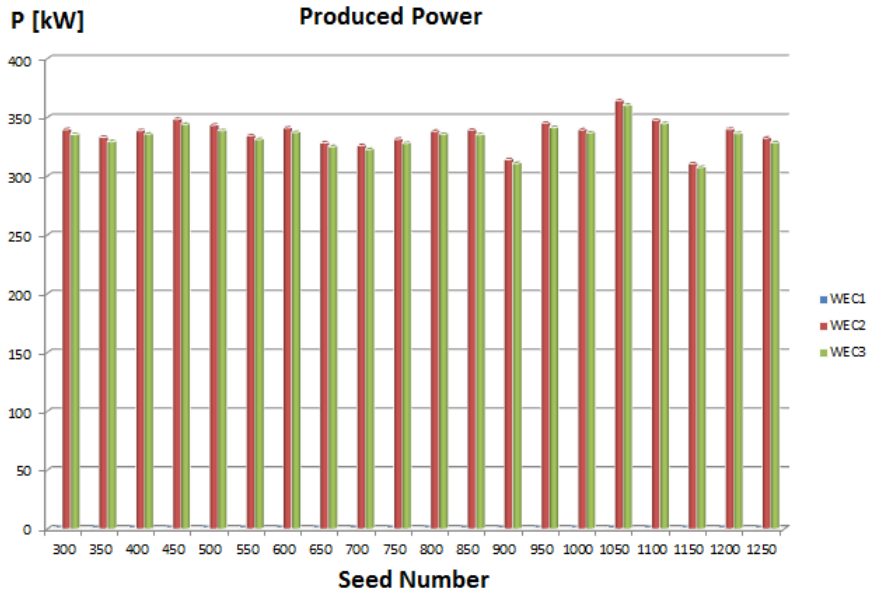

Figure C.9: Produced Power by WECs when $Hs = 6m, Tz = 12.6s, V = 18m/s, \theta = 0^0$.

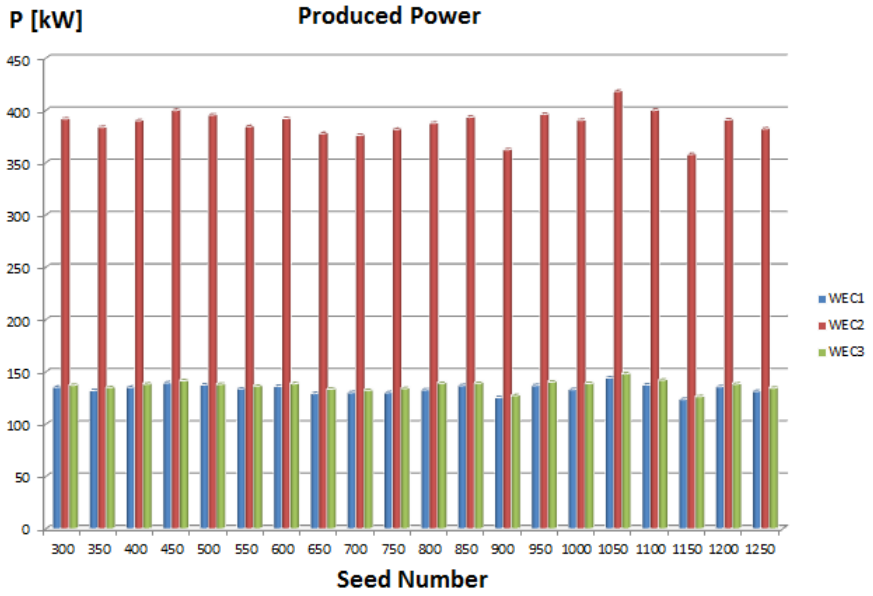

Figure C.10: Produced Power by WECs when $Hs = 6m, Tz = 12.6s, V = 18m/s, \theta = 30^0$.

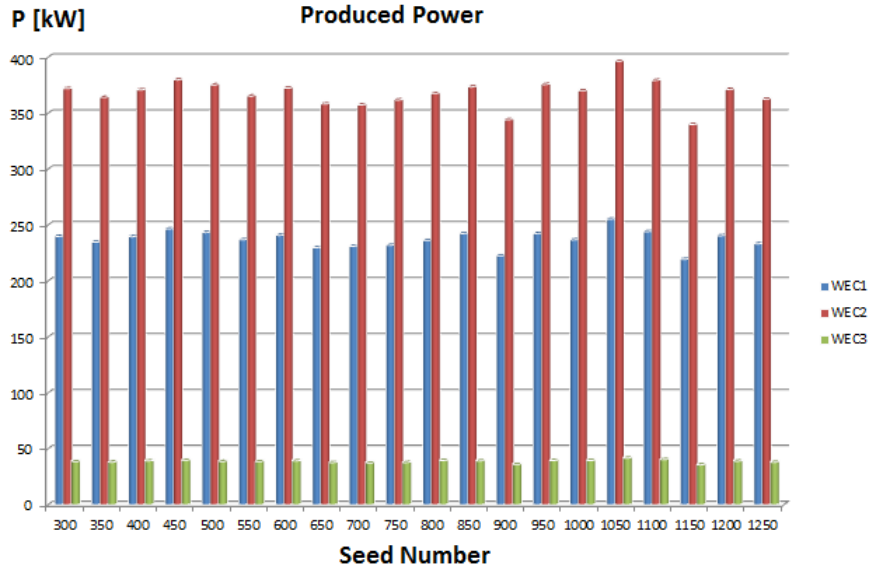

Figure C.11: Produced Power by WECs when $Hs = 6m, Tz = 12.6s, V = 18m/s, \theta = 45^0$.

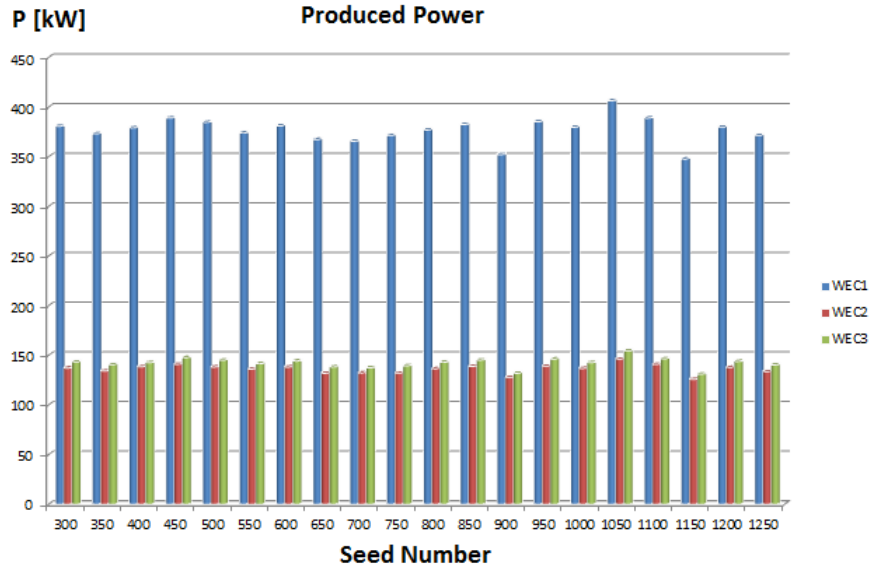

Figure C.12: Produced Power by WECs when $Hs = 6m, Tz = 12.6s, V = 18m/s, \theta = 90^0$.

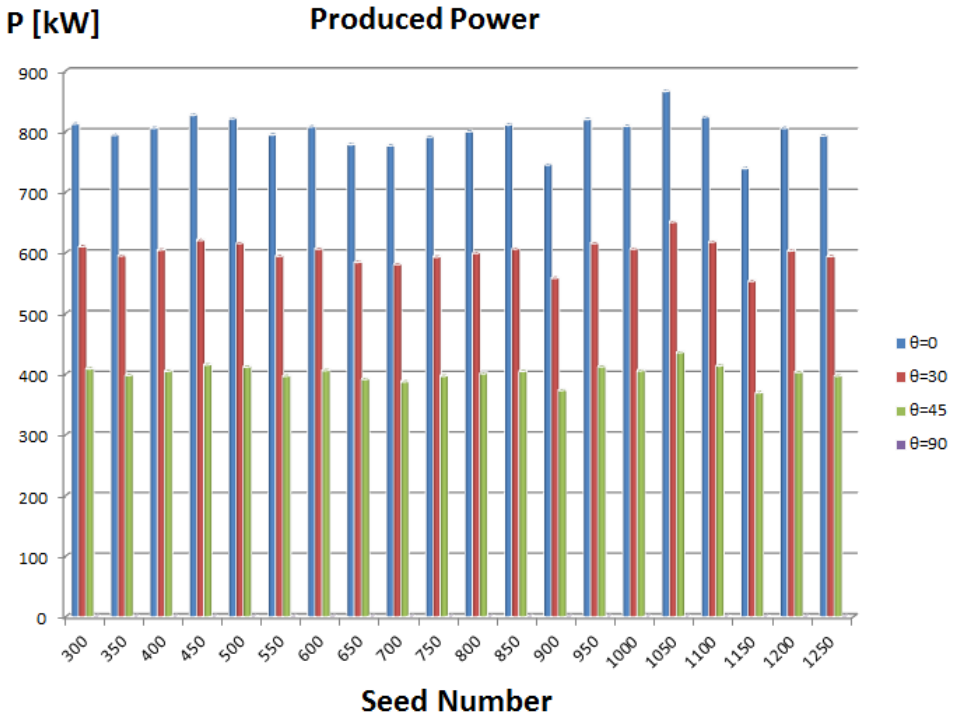

Figure C.13: Produced Power by BFWEC when $Hs = 6m, Tz = 12.6s$.

Bibliography

Babarit, A., Hals, J., Muliawan, M., Kurniawan, A., Moan, T., and Krokstad, J. (2012). Numerical benchmarking study of a selection of wave energy converters. *Renewable Energy*, 41:44–63.

Bønke, K. and Ambli, N. (1986). Prototype wave power stations in norway. In *Utilization of Ocean Waves—Wave to Energy Conversion*, pages 34–45. ASCE.

Bott, A. W., Hailey, J., and Hunter, P. (1978). The mauritius wave energy project research results and proposed outline design. In *International Symposium on Wave and Tidal Energy*.

Budal, K., Falnes, J., Iversen, L. C., Lillebekken, P. M., Oltedal, G., Hals, T., Onshus, T., and Høy, A. (1982). The norwegian wave-power buoy project.

Budar, K. and Falnes, J. (1975). A resonant point absorber of ocean-wave power. *Nature*, 256(5517):478–479.

Clément, A., McCullen, P., Falcão, A., Fiorentino, A., Gardner, F., Hammarlund, K., Lemonis, G., Lewis, T., Nielsen, K., Petroncini, n., et al. (2002). Wave energy in europe: current status and perspectives. *Renewable and sustainable energy reviews*, 6(5):405–431.

Clough, R. W. and Penzien, J. (1993). Dynamics of structures, chapter 2. third edition.

Count, B. and Evans, D. (1984). The influence of projecting sidewalls on the hydrodynamic performance of wave-energy devices. *Journal of Fluid Mechanics*, 145:361–376.

David J. Laino and A. Craig Hansen (2002). Aerodyn user's guide. *available electronically at http://wind/designcodes/simulators/aerodyn/AeroDyn. pd f.*

Det Norske Veritas (2010). Sesam user's manual: Wadam. *Det Norske Veritas SESAM as*.

Falcão, A. F. d. O. (2010). Wave energy utilization: A review of the technologies. *Renewable and sustainable energy reviews*, 14(3):899–918.

Falnes, J. (1999). Wave-energy conversion through relative motion between two single-mode oscillating bodies. *Journal of Offshore Mechanics and Arctic Engineering*, 121(1):32–38.

Faltinsen, O. M. (1993). *Sea loads on ships and offshore structures*, volume 1. Cambridge university press.

Fylling, I., Larsen, C., Sødahl, N., Ormberg, H., Engseth, A., Passano, E., and Holthe, K. (1995). Riflex theory manual. *SINTEF report no. STF70 F*, 95219:53.

Fylling, I., Larsen, C., Sødahl, N., Passano, E., Bech, A., Engseth, A., Lie, H., and Ormberg, H. (2008). Riflex user's manual 3.6. *MARINTEK, Trondheim, Norway*.

H. Ormberg, H. Lie and F. Meling (2007). Simo user's guide.

Hals, J., Falnes, J., and Moan, T. (2011). A comparison of selected strategies for adaptive control of wave energy converters. *Journal of Offshore Mechanics and Arctic Engineering-Transactions of The Asme*.

Jefferys, E. (1984). Simulation of wave power devices. *Applied Ocean Research*, 6(1):31–39.

Jonkman, J. and Matha, D. (2011). Dynamics of offshore floating wind turbines—analysis of three concepts. *Wind Energy*, 14(4):557–569.

Jonkman, J. M. (2010). *Definition of the Floating System for Phase IV of OC3*. National Renewable Energy Laboratory.

Jonkman, J. M., Butterfield, S., Musial, W., and Scott, G. (2009). *Definition of a 5-MW reference wind turbine for offshore system development*. National Renewable Energy Laboratory Golden, CO.

Kofoed, J. P., Frigaard, P., Friis-Madsen, E., and Sørensen, H. C. (2006). Prototype testing of the wave energy converter wave dragon. *Renewable energy*, 31(2):181–189.

Kurniawan, A., Pedersen, E., and Moan, T. (2012). Bond graph modelling of a wave energy conversion system with hydraulic power take-off. *Renewable energy*, 38(1):234–244.

Kurniawan,A. and Moan,T. (2012). Characteristics of a pitching wave absorber with rotatable flap. *Energy Procedia*, 20:134–147.

Kurniawan,A. and Moan,T. (2013). Optimal geometries for wave absorbers oscillating about a fixed axis. *Oceanic Engineering, IEEE Journal of*, 38(1):117–130.

Li, L., Gao, Z., and Moan, T. (2013). Joint environmental data at five european offshore sites for design of combined wind and wave energy devices. In *ASME 2013 32nd International Conference on Ocean, Offshore and Arctic Engineering*, pages V008T09A006–V008T09A006. American Society of Mechanical Engineers.

Lopes, M. F. P., Hals, J., Gomes, R. P. F., Moan, T., Gato, L. M. C., and Falcao, A. F. d. O. (2009). Experimental and numerical investigation of non-predictive phase-control strategies for a point-absorbing wave energy converter. *Ocean Engineering*, 36(5):386–402. The article is reprinted with kind permission from Elsevier, sciencedirect.com.

Luan, C., Gao, Z., and Moan, T. (2014a). Conceptual designs of a 5-mw and a 10-mw semi-submersible wind turbine with emphasis on the design procedure. *Journal of Offshore Mechanics and Arctic Engineering*.

Luan, C., Michailides, C., Gao, Z., and Moan, T. (2014b). Modeling and analysis of a 5mw semi-submersible wind turbine combined with three flap-type wave energy converters. In *ASME 2014 33rd International Conference on Ocean, Offshore and Arctic Engineering*.

Luxcey, N., Ormberg, H., and Passano, E. (2011). Global analysis of a floating wind turbine using an aero-hydro-elastic numerical model: Part 2—benchmark study. In *ASME 2011 30th International Conference on Ocean, Offshore and Arctic Engineering*, pages 819–827. American Society of Mechanical Engineers.

Margheritini, L., Vicinanza, D., and Frigaard, P. (2009). Ssg wave energy converter: Design, reliability and hydraulic performance of an innovative overtopping device. *Renewable Energy*, 34(5):1371–1380.

Masuda, Y. (1972). Study of wave activated generator and future view as an island power source. In *2nd International Ocean Development Conference, Preprints*, volume 2.

Masuda, Y. and McCormick, M. E. (1986). Experiences in pneumatic wave energy conversion in japan. In *Utilization of Ocean Waves—Wave to Energy Conversion*, pages 1–33. ASCE.

Mehlum, E. (1986). Tapchan. In *Hydrodynamics of Ocean Wave-Energy Utilization*, pages 51–55. Springer.

Michailides, C., Luan, C.and Gao, Z., and Moan, T. (2014). Effect of flap type wave energy converters on the response of a semi-submersible wind turbine in operational conditins. In *ASME 2014 33rd International Conference on Ocean, Offshore and Arctic Engineering*.

Nielsen, F. G., Hanson, T. D., and Skaare, B. (2006). Integrated dynamic analysis of floating offshore wind turbines. In *25th International Conference on Offshore Mechanics and Arctic Engineering*, pages 671–679. American Society of Mechanical Engineers.

Ormberg, H., Passano, E., and Luxcey, N. (2011). Global analysis of a floating wind turbine using an aero-hydro-elastic model: Part 1—code development and case study. In *ASME 2011 30th International Conference on Ocean, Offshore and Arctic Engineering*, pages 837–847. American Society of Mechanical Engineers.

Palme, A. (1920). Wave motion turbine. *Power*, 52(18):200–201.

Patrick J. Moriarty and A. Craig Hansen (2005). *AeroDyn theory manual*. National Renewable Energy Laboratory Golden, Colorado, USA.

Pitt, D. M. and Peters, D. A. (1981). Theoretical prediction of dynamic-inflow derivatives. *Vertica*, 5(1):21–34.

Robertson, A., Jonkman, J., Masciola, M., Song, H., Goupee, A., Coulling, A., and Luan, C. (2012). Definition of the semisubmersible floating system for phase ii of oc4. *IEA OC4 Report*.

Roddier, D., Peiffer, A., Aubault, A., and Weinstein, J. (2011). A generic 5 mw windfloat for numerical tool validation & comparison against a generic spar.

Salter, S. (1974). Wave power. *Nature*, 249(5459):720–724.

Salter, S. (1992). The swinging mace. In *Proceedings of Workshop Wave Energy R&D, Cork, Ireland*, pages 197–206.

Salter, S., Taylor, J., and Caldwell, N. (2002). Power conversion mechanisms for wave energy. *Proceedings of the Institution of Mechanical Engineers, Part M: Journal of Engineering for the Maritime Environment*, 216(1):1–27.

Scott, K. (1965). Electricity from the wave. *Sea Frontiers*, 11(4).

Standards Norway (2004). Norsok standard n004:design of steel structures.

Taghipour, R., Arswendy, A., Devergez, M. J. A., and Moan, T. (2008). Structural analysis of a multi-body wave energy converter in the frequency domain by interfacing wamit and abaqus. *The International Journal of Offshore Mechanics and Arctic Engineering, (Presented at the 28th International Conference on Offshore Mechanics and Arctic Engineering, 2008, Estoril, Portugal)*.

WWEA (2014). World Wind Energy Association: World Wind Energy Report 2013.

Yang, L., Hals, J., and Moan, T. (2010). Analysis of dynamic effects relevant for the wear damage in hydraulic machines for wave energy conversion. *Ocean Engineering*, 37(13):1089–1102. The article is reprinted with kind permission from Elsevier, sciencedirect.com.